POLITECNICO DI TORINO

Commission of Mechanical, Aerospace, Automotive and Production Engineering

Master's Degree in Automotive Engineering

Master's Degree Thesis

Development and validation of a lead-acid battery model

Supervisor:

Paolo Stefano Crovetti

Candidate:

Francesco Pittau

February 2019

Table of contents

List of figures

List of tables

Abstract

This research concerns the design, parametrization and validation of a lead-acid battery model for automotive application. The developed model will be implemented in a model of the complete vehicle electric system, comprising alternator, battery and loads. The complete model is used by FCA to perform simulations of energetic balance for different vehicles in different markets, which influence the reference temperature and driving cycles. The aim of this kind of simulations is to validate the choice of the alternator size, before starting with the consequent on-vehicle testing phase. The goodness of the choice is considered observing whether the alternator is or is not able to maintain the battery's state of charge (SoC) above a certain threshold when tested in critical reference driving cycles.

Chapter 1
Introduction

1.1 The vehicle electric system

In a vehicle based on a thermal engine, the electric system is made by several components with the functions of power generation, storage and distribution in order to provide electric energy to the many electric and electronic components.

The complete system is composed by an *alternator*, which is a rotary electric machine that converts part of the mechanical power generated by the thermal engine in electrical power, a *battery of lead accumulators*, which has the function to store electrical energy, the electrical *power distribution network* and a *starter electric motor*, which converts part of the energy stored in the battery in mechanical form to power the starter motor and start the thermal engine. The vehicle electric architecture is shown in figure 1.1, in which the starter motor can be considered as one of the loads.

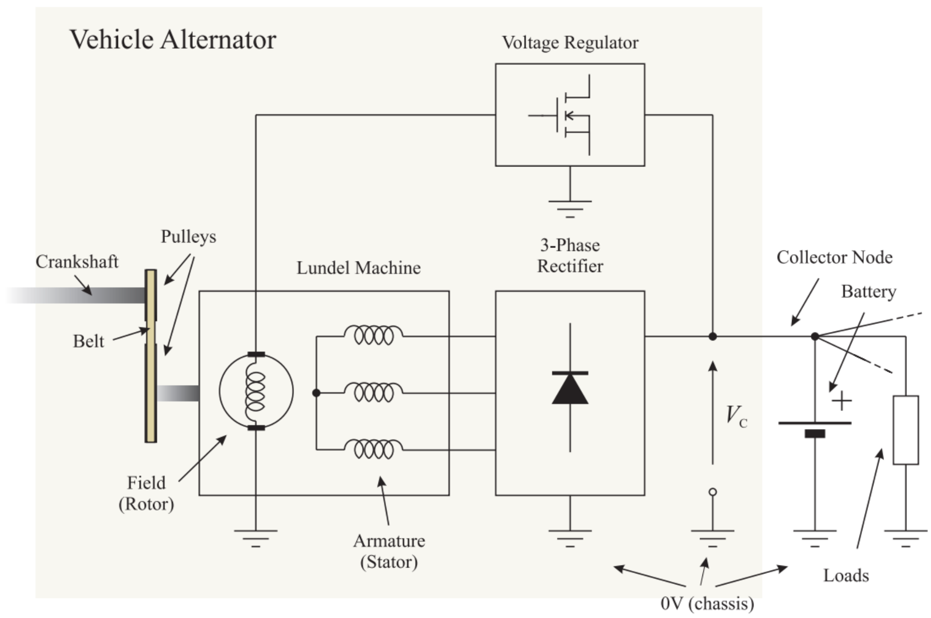

Figure 1.1. Diagram of the vehicle electric system [5]

The alternator is made by several sub-components: a *Lundel machine*, driven by the engine crankshaft, that delivers an AC current depending on its rotation speed, as shown in figure 1.2, a *3-phase rectifier* which converts the output current from AC to DC, and a *voltage regulator* that maintain the voltage at the terminals of the alternator almost constant independently from the alternator speed and the electrical loads connected. This voltage is distributed to the electrical loads and to the battery by the power distribution network.

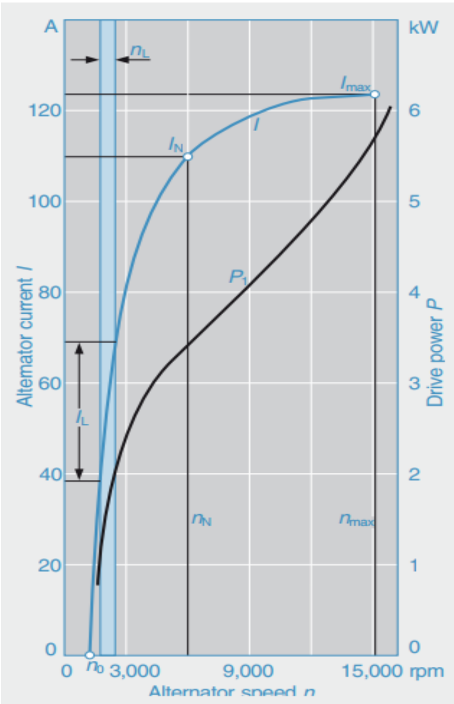

Figure 1.2. Speed-current characteristic of a car alternator [4]

The battery can be described as a passive component. When the current delivered by the alternator is larger than the total current required by the loads, the battery get recharged. However, when the alternator is not able to deliver the current required by loads, part of the energy stored in the battery is used to sustain all the connected loads. Moreover, to start the thermal engine, the starter motor is powered by the car battery.

When designing the vehicle electric system, the choice of the alternator and the battery is fundamental. The alternator must be able to maintain the battery charged even during critical driving cycles, while the battery must be able to power the starter motor during cranking in every condition. For what concerns the choice of the battery, the most critical condition is at low temperature and thus, validation tests and battery choice are based mainly on this condition. Also, the cheapness of lead-acid battery allows to oversize the battery capacity, assuring a larger safety margin for the cranking. On the contrary, the choice of the alternator is far more delicate and is based on *energy balance simulations*.

An energy balance simulation is the calculation of the expected generated and consumed electric power during the vehicle different working conditions. In figure 1.3, the equivalent circuit of the electric layout of a vehicle is shown. When both the switches are open, it describes the *parked car* condition during which the battery is slowly discharged by off-key loads. When the switches are closed, it respectively describes the *cranking* and the *running vehicle* condition. During cranking, the battery is quickly discharged to power the starter motor, and thus, this phase is the most important in the definition of the battery size. When the vehicle is running all types of load are connected to the system and the alternator generates an electric power dependent on engine rotational speed, making this working condition fundamental to evaluate the balance between generated and consumed electrical energy and thus to dimension the alternator.

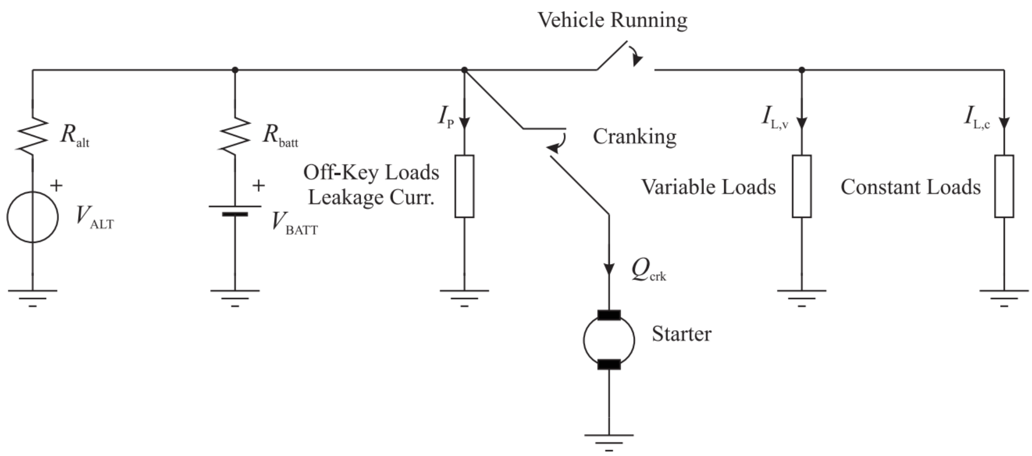

Figure 1.3. Equivalent circuit of the vehicle electric plant [5]

1.2 Thesis objective

In FCA, energy balance simulations are performed considering only the running vehicle condition. A model of the complete vehicle electric system is used to simulate some specific driving cycles dependent on the market. The objective of these simulations is to verify whether the chosen alternator can maintain the state of charge of the battery above a certain level. The most critical condition is simulated, which is given by cycles at low alternator rotational speeds and with most of the electric loads connected.

The objective of this thesis is the development of a mathematical model of the battery that will be implemented in the complete model of the vehicle electric system. This is used to draw energy balance simulations and thus validate the alternator choice. Models of order superior to the first and physical models will not be considered to avoid excessive complexity and assure faster simulation times. For this thesis, it will be used a functional model of the first order that will be parametrized to best reproduce the behavior of EFB batteries (Enhanced Flooded Battery), which is the most common type currently employed on FCA vehicles.

1.3 Organization of the thesis

This thesis is organized into seven chapters.

Chapter 2 is a brief introduction about lead-acid batteries in which their theory, their construction and the main technical definitions are described.

In chapter 3, the considerations made to choose the equivalent circuit are presented.

Chapter 4 shows the implementation of the model in Simulink.

Chapter 5 presents the methodology and the approach used for the parametrization of the model.

In chapter 6, both the parametrization and validation testing procedures are presented, and the results are shown.

In chapter 7, the results of the validation process are showed, and some considerations about the goodness of the model are made.

Chapter 8 presents the achievements of this thesis, the main limitations of the model and proposes future improvements.

Chapter 2

Conceptual analysis

In this first chapter the chemical principles and the constructional features of lead-acid batteries are described, with a more detailed analysis on batteries for SLI application. Moreover, the definitions of the main variables used when talking about batteries and their performance are given to the reader.

Lead-acid batteries in ICE vehicles have the function to accumulate and deliver the energy requested by the starter motor during cranking and to feed all the electric loads of the car whenever the alternator is not able to. The technology of lead-acid batteries has evolved during last decades with the introduction of EFB and AGM types and it is still the most widely adopted solution, thanks to its cost, safety and performance.

In figure 2.1 a basic representation of a lead-acid cell is shown, in which is possible to see the main components: two electrodes, one positive and one negative, and a sulfuric acid water solution.

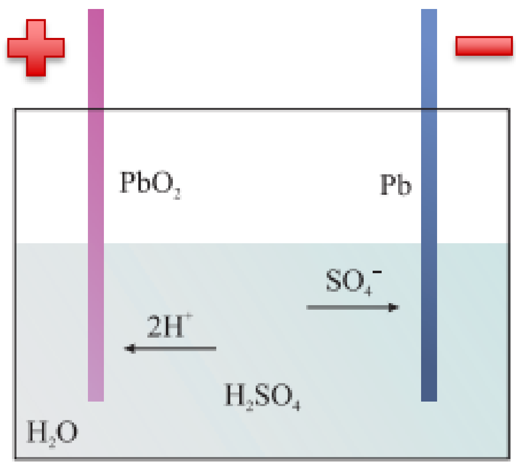

Figure 2.1. Lead-acid cell representation [5]

2.1 Chemical Characteristics

Lead acid batteries use large surface porous structures as electrodes with lead dioxide PbO_2 as positive active material and metallic lead Pb as negative active material. These two plates are immersed in a sulfuric acid H_2SO_4 solution which is the electrolyte. The usual value of specific gravity (relative density of the solute with respect to the solvent, which is water) is ~1.28.

The reactions occurring at the electrodes are:

- Negative Electrode

$$Pb \Longleftrightarrow Pb^{2+} + 2e$$

$$Pb^{2+} + {SO_4}^{2-} \Longleftrightarrow PbSO_4$$

- Positive Electrode

$$PbO_2 + 4H^+ + 2e \Longleftrightarrow Pb^{2+} + 2H_2O$$

$$Pb^{2+} + {SO_4}^{2-} \Longleftrightarrow PbSO_4$$

- Overall Reaction

$$Pb + PbO_2 + 2H_2SO_4 \Longleftrightarrow 2PbSO_4 + 2H_2O$$

As the cell approaches the full charge, almost all the lead sulfate $PbSO_4$ is already converted in metallic lead and lead dioxide, and the cell voltage become greater than the gassing voltage (~2.39V). This phenomenon is called *gassing* and causes the production of hydrogen and oxygen with the consequent loss of water:

- Negative Electrode

$$2H^+ + 2e \Longleftrightarrow H_2$$

- Positive Electrode

$$H_2O - 2e \Longleftrightarrow \frac{1}{2}O_2 + 2H^+$$

- Overall Reaction

$$H_2O \Longleftrightarrow H_2 + \frac{1}{2}O_2$$

To minimize this reaction, it is possible to use sealed lead-acid batteries, in which the gasses recombine into water, which is thus restored.

General characteristics of a lead-acid battery under charge and discharge conditions are shown in figure 2.2. When discharging the battery at a constant current, the voltage decreases smoothly down to the cutoff voltage due to the depletion of active material, internal resistance losses and polarization, and the specific gravity of the solution decreases linearly with the amount of charge released.

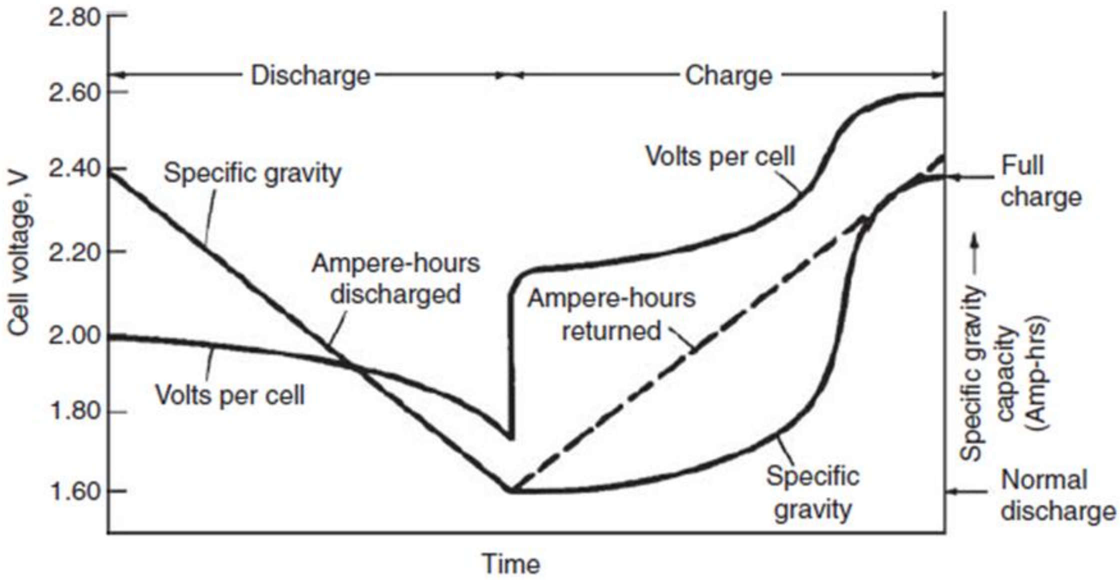

Figure 2.2. Typical performance characteristic of a lead-acid battery [3]

The voltage of a single cell is 2 V, nominally. The open circuit voltage is proportional to the solution concentration and goes from 2.125V for specific gravity equal to 1.28 to 2.05V for specific gravity 1.21. The cutoff voltage corresponding to a fully discharged cell is 1.75 V.

The specific gravity depends on battery application and service requirements. The electrolyte concentration should be high enough to offer good conductivity, but not so high to cause the deterioration of the separators or the corrosion of other components.

During discharge, the sulfuric acid concentration decreases proportionally to the charge delivered by the battery; for this reason, the concentration is an index of the battery state of charge as shown in table 2.1, where the letters indicate batteries for different applications.

	Specific gravity			
State of charge	*A*	*B*	*C*	*D*
100% (full charge)	1.330	1.280	1.265	1.225
75%	1.300	1.250	1.225	1.185
50%	1.270	1.220	1.190	1.150
25%	1.240	1.190	1.155	1.115
Discharged	1.210	1.160	1.120	1.0

Table 2.1. State of charge-specific gravity relation for different application batteries [3]

The open circuit voltage can be approximated by the Nernst equation:

$$OCV = 2.047 + \frac{RT}{F}\ln\left(\frac{\alpha H_2SO_4}{\alpha H_2O}\right)$$

where R is the universal gas constant, T is the absolute temperature, F is the Faraday constant and finally αH_2O and αH_2SO_4 are the electrolyte components concentrations. It is important to remark that the open circuit voltage depends on the temperature and the specific gravity of the solution. In figure 2.3, the almost linear relation between the open circuit voltage and the specific gravity at 25°C is shown.

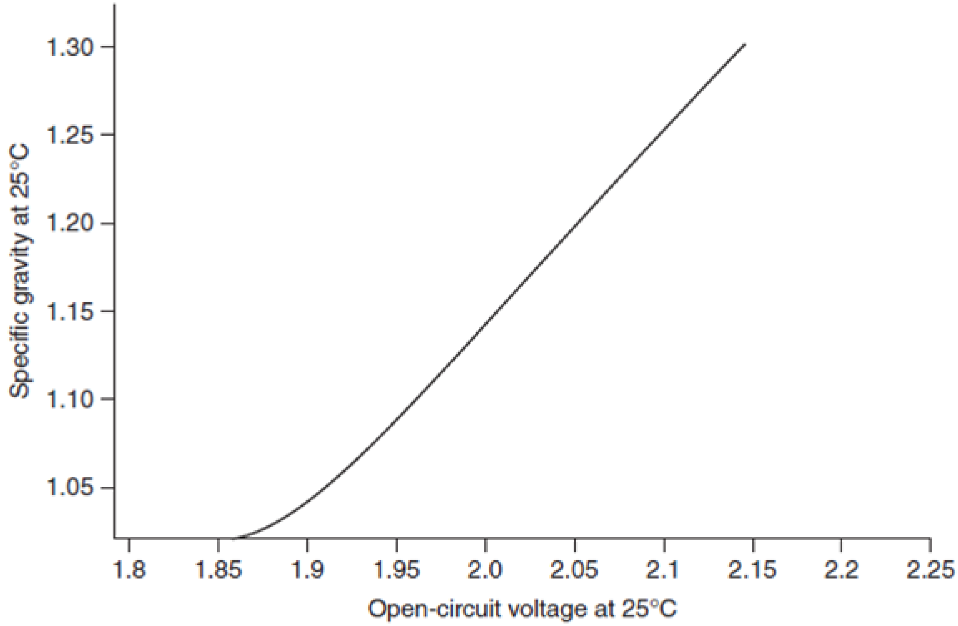

Figure 2.3. Open circuit voltage-specific gravity curve at 25 °C [3]

When a current is flowing through the battery, the voltage is different with respect to the open circuit voltage at the same specific gravity. This is due to internal resistive losses and polarization.

There are two types of polarization: activation polarization and concentration polarization. Activation polarization is due to the accumulation of lead sulfate crystals on electrodes plates during discharge. Lead sulfate is not an active material and then reduces the surface available for chemical reaction between electrode plate and electrolyte. Concentration polarization is due to non-homogeneous specific gravity reduction in the electrolyte. The sulfur acid is consumed at electrode interface and its diffusion in the solution is not fast enough to maintain the solution concentration homogeneous.

The equilibrium of the electrode reactions is in the discharge direction. This causes to have a rate of self-discharge in open circuit. The main cause of self-discharge is the instability of metallic lead and lead dioxide in sulfuric acid solutions. In fact in open circuit they still react with the electrolyte:

$$PbO_2 + H_2SO_4 \Longleftrightarrow PbSO_4 + H_2O + \frac{1}{2}O_2$$

$$Pb + H_2SO_4 \Longleftrightarrow PbSO_4 + H_2$$

The self-discharge at the negative electrode is generally more rapid and the effect is increased by the presence of catalytic metallic ions. Antimony lost at the positive electrode, for example, can diffuse to the negative electrode and increase self-discharge rate. To reduce this effect low-antimony or Ca-Pb (not containing any antimony) are used. Because the presence of antimony has other beneficial effects, low-antimony grids are a good compromise. In figure 2.4, the self-discharge rates of batteries with different grid type is shown. Considering that, in general, higher the temperature faster the reaction rate it's important to choose the correct storing temperature.

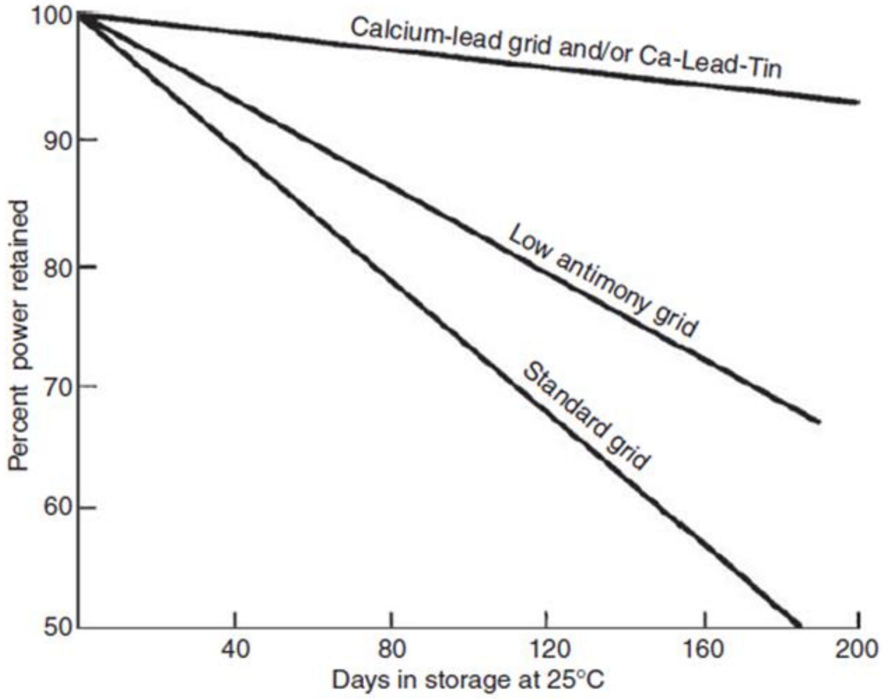

Figure 2.4. Self-discharge behavior of batteries with different alloy grids [3]

In figure 2.5 the self-discharge dependence on temperature for a battery with 6% antimonial lead grids is shown. As visible, batteries should be stored between 5 and 15°C to reduce the loss of charge.

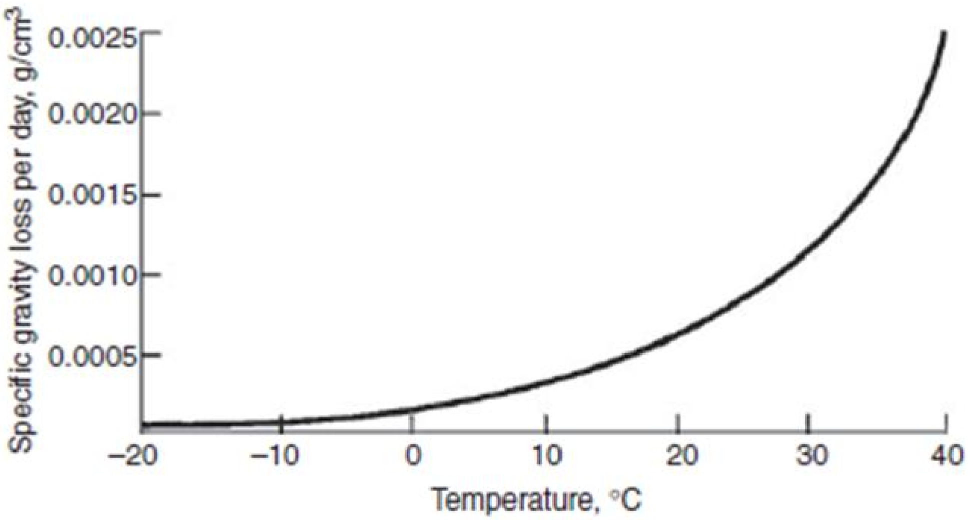

Figure 2.5. Self-discharge dependence on temperature [3]

2.2 Battery construction

A typical lead-acid battery is shown in figure 2.6. It's made by 6 cells connected in series, each of them with a 2V nominal voltage. Each cell is made by two sets of alternated grids, one positive (10) and one negative (11). Each positive grid is inserted in a porous envelope separator, as visible in figure 2.7, which has the functions of avoiding contact with adjacent grids, while allowing the passage of the electrolyte. They are then inserted in a rigid plastic container (8), filled with the electrolyte. The plastic plates (4) separate different cells. First and last cell are connected to battery terminals (5).

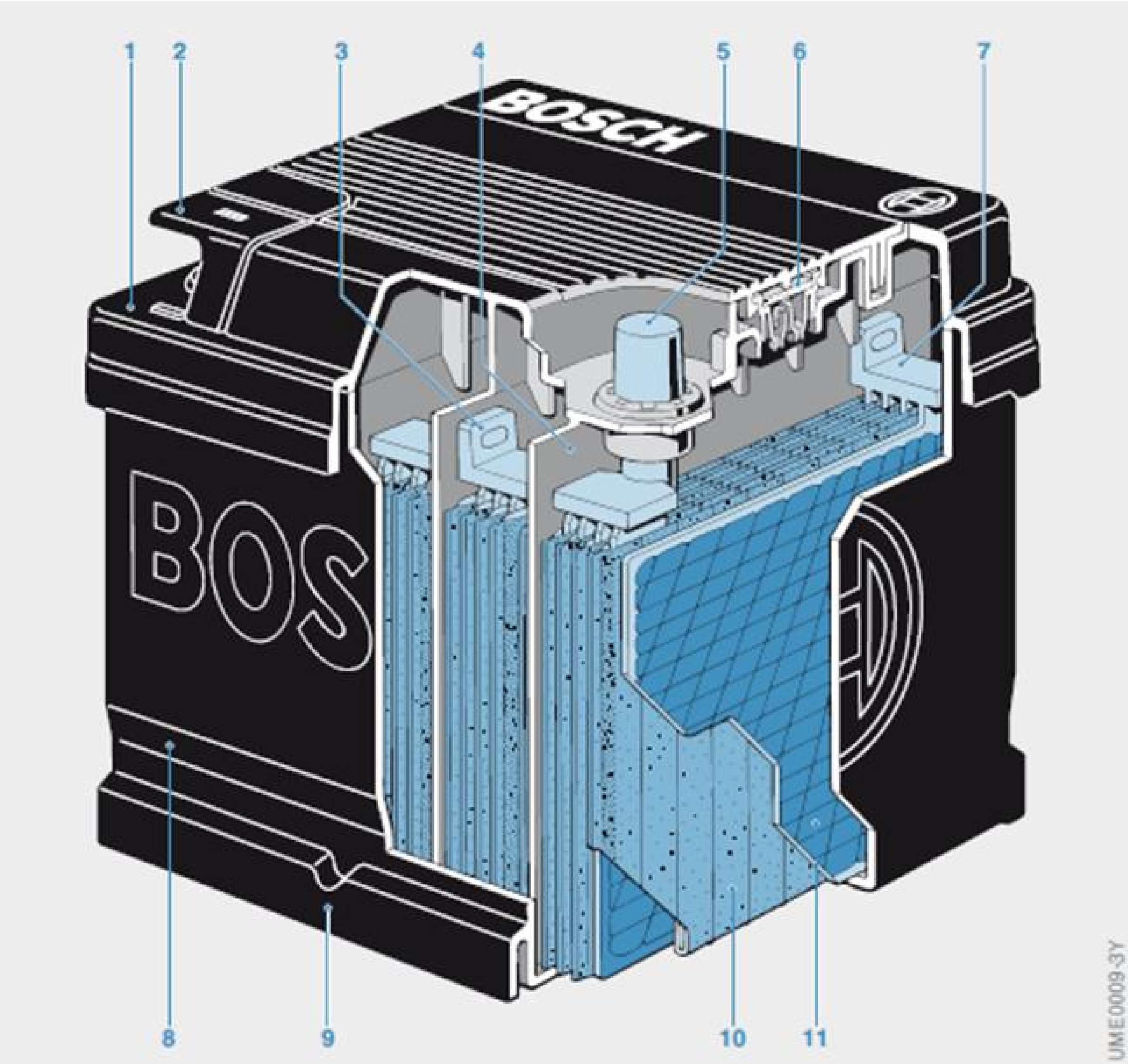

Figure 2.6. Typical lead-acid SLI battery [4]

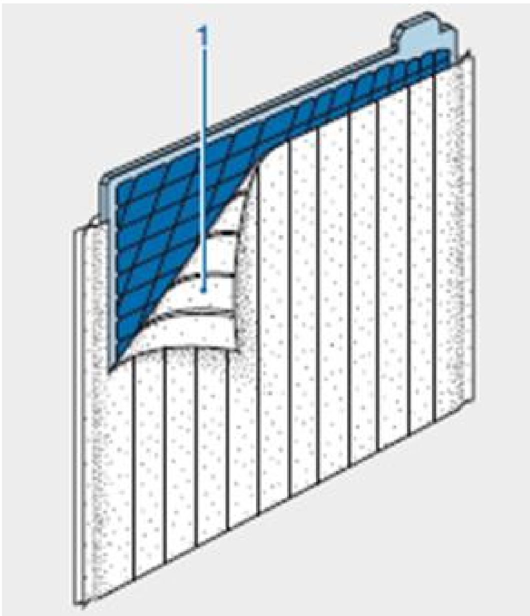

Figure 2.7. Positive plate inserted in envelope-type separator [4]

The grids have the function of mechanically supporting the active material and conduct electricity to cell terminals. They can be made of different lead alloys:

- Antimony alloys. Classic alloy Pb-Sb in which the antimony is used to harden the grid with respect to the pure lead solution. The tendency nowadays is to keep a very low percentage of antimony, about 1.5÷2% in order to reduce the self-discharge effects.
- Calcium alloys. To harden the alloy, calcium is used in the range of 0.03÷0.05%, not over to avoid the occurrence of corrosion phenomena. Usually ternary alloys Pb-Ca-Sn are used, adding a percentage of tin between 0.25-2%.

The grid design influences the capability of conducting electricity. In general, grids are rectangular structures made by an external thicker frame and a thinner internal structure of horizontal and vertical bars. An advance in grid design is the radial grid, in which the internal vertical bars ore oriented to the tab, improving electricity conductibility. Both designs are visible in figure 2.8.

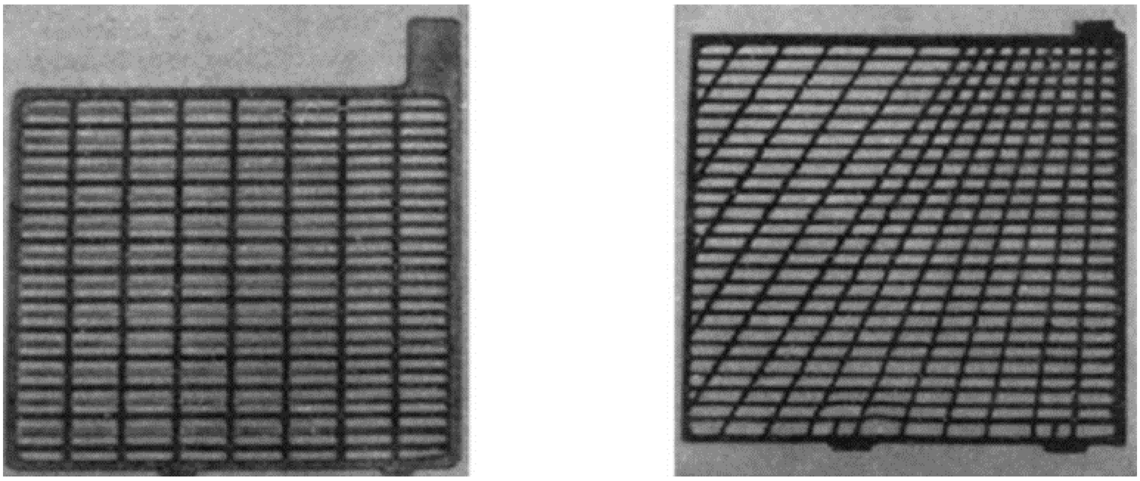

Figure 2.8. Different types of grids [3]

The actual electrode plates are made assembling the active material on grids. This is done converting the lead oxide in a paste, which is then applied on the grids. The application process is called pasting and is basically made by pressing the lead oxide on both side of the grid at the same time filling the internal grid cavities.

2.3 SLI Batteries

SLI stands for Starting, Lightning and Ignition and identifies the typical automotive battery type. In a car the main job of the battery is to feed the starter motor, and for this reason SLI batteries are designed to deliver a very high current for a short period of time. However, they are not intended for deep discharge application and in fact repeated full discharges may compromise the life expectancy of the battery. For the objectives of this thesis, it is important to define some characteristics of the battery.

2.3.1 Nominal voltage, open circuit voltage and terminal voltage

The nominal voltage is defined by the normative and is 12 V for automotive batteries. The open circuit voltage (OCV) is the voltage measured when no load is connected to the terminals. This voltage is of particular importance in steady state conditions, because when the battery is fully stable (it may take up to several days to completely “relax” a battery after usage) this measure is directly proportional to the electrolyte temperature and density. The electrolyte density is the most accurate index of the real SoC of the battery.

The terminal voltage is the difference of potential between the battery poles, and it is dependent on two components: an open circuit voltage and a voltage drop due to the internal resistance of the battery. Both these components are dependent on several factors, as the electrolyte temperature, the state of charge, the state of health and the charge/discharge current intensity.

2.3.2 Nominal capacity and available capacity

The nominal capacity C_{20} is the rated electrical charge of the battery and is expressed in ampere hours $[Ah]$. The normative (EN 50342-1:2015, 3.4.2) states that, considering for example a 60 Ah model, the battery must be able to deliver its nominal current $I_{20} = C_{20}/(20h) = 3\ A$ for at least 20 hours without going below the threshold voltage of 10.5V.

The available capacity is the deliverable electric charge under specific conditions. The main influencing variables are the discharge current level, the state of charge, the electrolyte temperature, and the battery state of health. In figure 2.9 the available capacity as a function of temperature and discharge current is shown, and in figure 2.10 the available capacity as a function of the discharge current level is shown, with the relative time of discharge before reaching 10.5 V. The available capacity is well approximated by the *Peukert's law*, when considering a constant temperature:

$$C_{available} = C_{20}\left(\frac{I}{I_{20}}\right)^{\alpha}$$

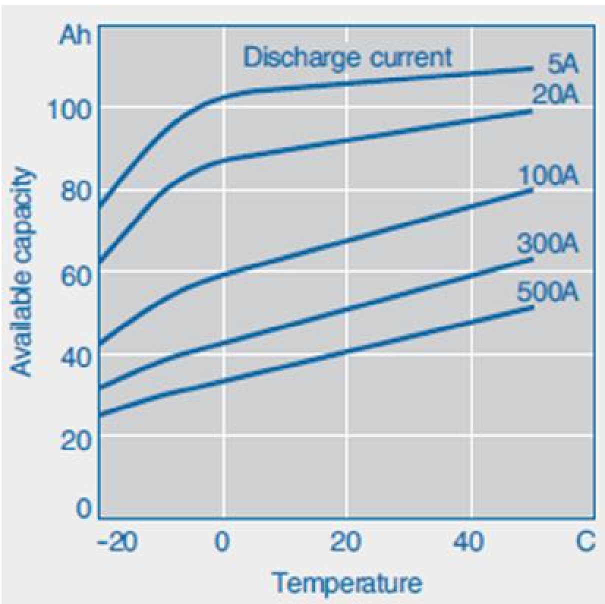

Figure 2.9. Available battery capacity depending on temperature and discharge current [4]

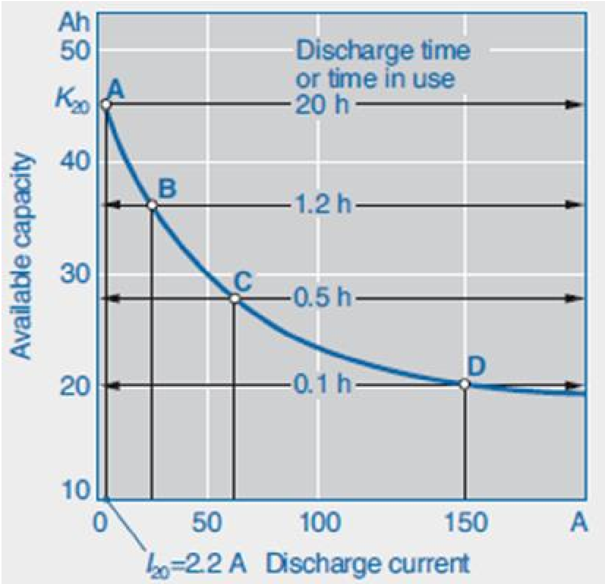

Figure 2.10. Available capacity versus discharge current [4]

2.3.3 Low temperature test current

The low temperature test current I_{cc} indicates the current output capability of the battery at low temperatures. The normative (EN 50342-1:2015, 3.4.1) states that, a battery kept at -18 °C and discharged for 10 seconds at I_{cc}, must mantain a final terminal voltage above 7.5 V. For car batteries this rated value is extremely important, considering that the main job of the battery is to feed the starter motor even in the most critical condition.

2.4 State of charge estimation

The state of charge estimation is one of the main criticalities for lead-acid batteries due to the high tolerance of the estimations in steady state conditions and no reliable methods during dynamic conditions. Two main methods are used in this thesis:

- Estimation from open circuit voltage. As already stated, in steady state conditions and considering a fully relaxed battery, the SoC is directly proportional to the electrolyte temperature and density. Thus, if it is not possible to physically measure the electrolyte density, the better way to estimate it is to measure the OCV. Thus, it can be stated that, for a battery completely relaxed, the OCV is a direct measure of the battery state of charge. The tables and/or graphs showing this relationship, which is almost linear, can be obtained directly by the battery manufacturer.

- Ampere hours counting. During normal battery operation, the easier way to estimate the SoC is to integrate over time the current delivered and drained by the battery.

$$\Delta SoC = \frac{\int_{t_0}^{t} I_{batt} dt}{C_{20}}$$

In conclusion, the first method is considered reliable, but usable only in particular conditions, while the second method is applicable in normal battery conditions but is not reliable enough. Thus, the best approach is to rely on Ah counting and adjust with the SoC estimation from the OCV when it is possible to.

Chapter 3

Equivalent circuit

The modelling of lead-acid batteries is almost always done by black-box and equivalent circuit models. Physical models, in which all the electrochemical phenomena are specifically described, are unusual and also too complex to be efficiently implemented. Thus, equivalent electric circuits are normally used to describe the lead-acid battery behavior.

In this chapter, some typical equivalent circuits found in literature and the model currently used by FCA will be presented. From these, a proper equivalent circuit will be chosen to develop the final model.

3.1 Battery equivalent circuits in literature

Two typical battery equivalent circuits can be found in literature [1] [5].

The circuit shown in figure 3.1 is static. It is made by an ideal voltage source representing the open circuit voltage and a resistor. The resistance of the resistor changes depending on the charge/discharge current, the temperature and the SoC. The open circuit value, as already stated in paragraph 1.1, changes depending on the SoC and the temperature.

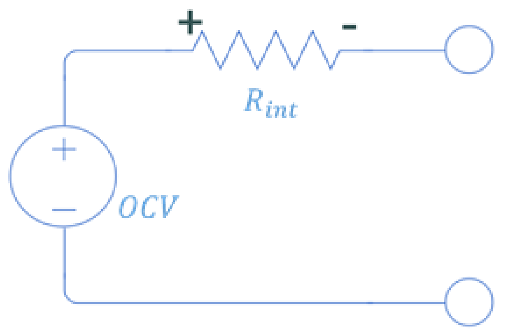

Figure 3.1. Static equivalent circuit [5]

In figure 3.2 a complete dynamic equivalent circuit is shown. It is made by a main branch including a RC parallel with a second resistor in series and a second branch accountable for parasitic current absorption. The parasitic current is relevant only during the recharge phase when the SoC is near 100%. Modern car alternators manage the recharge of the battery in order to keep the state of charge below the 80%. For this reason, it is possible to neglect the parasitic branch considering a simpler model, as the circuit shown in figure 3.3.

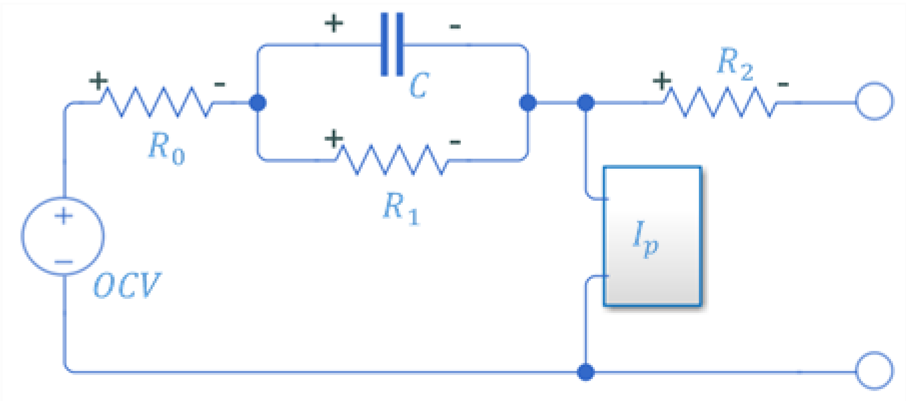

Figure 3.2. Complete dynamic equivalent circuit [1]

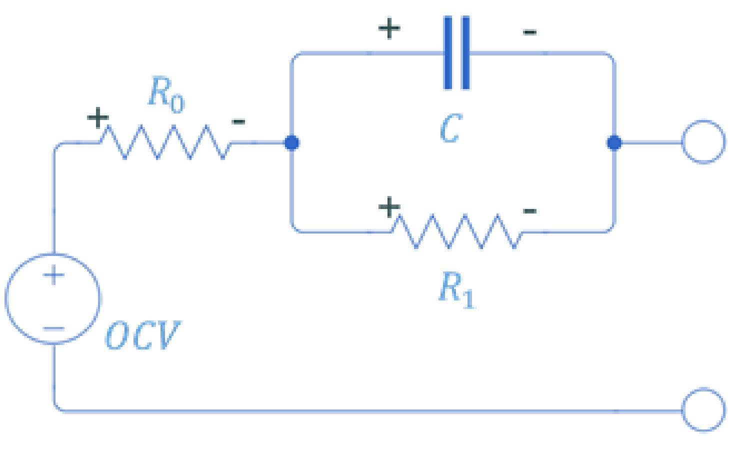

Figure 3.3. Simplified dynamic equivalent circuit [2]

3.2 Battery equivalent circuit used by FCA

The battery model currently used in FCA is based on the equivalent circuit shown in figure 3.4. It is made by a voltage generator representing the open circuit voltage and an RC series with a second resistance in parallel.

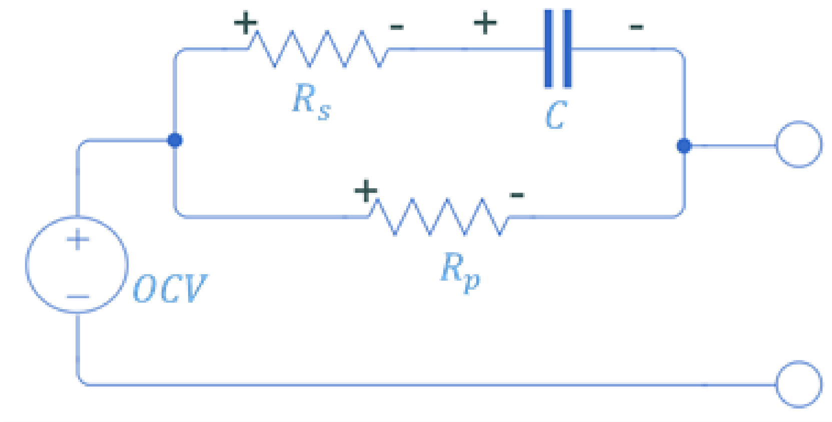

Figure 3.4. FCA equivalent circuit

The expressions of R_p and OCV are:

$$OCV = \begin{cases} A_{10} + A_{20}T_{batt} + A_{30}SoC, & I_{batt} \geq 0 \\ A_1(1 + A_2T_{batt})(1 - A_3(1 - SoC) + A_4(1 - SoC)^2), & I_{batt} < 0 \end{cases}$$

$$R_p = \begin{cases} \dfrac{14.5 - OCV}{f_1 f_2 C_{20}}, & I_{batt} \geq 0 \\ \dfrac{2.4}{I_{cc}}\left(a_T + b_T e^{\frac{T_{batt}}{c_T}}\right)(a_{SoD} + b_{SoD}(1 - SoC) + (1 - SoC)^3), & I_{batt} < 0 \end{cases}$$

where:

$$f_1 = \begin{cases} a_p T_{batt}^2 + k_p e^{h_p} T_{batt} + e^{h_p}, & T_{batt} \geq 0 \\ e^{k_p T_{batt} + h_p}, & T_{batt} < 0 \end{cases}$$

$$f_2 = \theta_f \left(\beta_f + \sqrt{\left(1 - \alpha_f\right)^2 + \beta_f^2 + (1 - SoC)^2}\right).$$

Finally, R_s depends on R_p and C on R_s:

$$R_s = \begin{cases} k_c R_p, & I_{batt} \geq 0 \\ k_d R_p, & I_{batt} < 0 \end{cases}$$

$$C = \begin{cases} \dfrac{\tau_c}{R_s}, & I_{batt} \geq 0 \\ \dfrac{\tau_d}{R_s}, & I_{batt} < 0 \end{cases}.$$

Some issues were found in the implementation of this model.

- The model describes R_p and OCV with complex expressions, defining their dependence on the SoC and the temperature. A total of about thirty parameters are present in these expressions and almost no documentation about them is available, so it is not possible to understand their influence and whether they have or do not have a physical meaning.
- The expressions of R_p and OCV in charge and discharge are derived by two different static models. The model for the charging phase has been designed by a FIAT's consultant in the early '90s and the model for discharge has been made by Bosch for validation activities on starter motors. Thus, for the charge model, it is easy to understand how it has been validated on old batteries with different construction methodologies and different performances with respect to modern ones. For what concerns the discharge model, the main issue is that it has been designed for very high current levels (reached by batteries only during cranking), which are not representative of the operating conditions considered to draw the vehicle energy balance.
- No dependency on the current level is present in both the charge and discharge models, while this dependency is fundamental as stated in the literature [1] [2] [5].
- The way the dynamics has been described by the introduction of a second resistance and a capacitor is unusual, as visible by the comparison between figure 3.3 and figure 3.4.

3.3 Choice of the equivalent circuit

Due to the reasons previously presented, the development of a new model has been preferred. An equivalent circuit as in figure 3.5 will be used for this thesis.

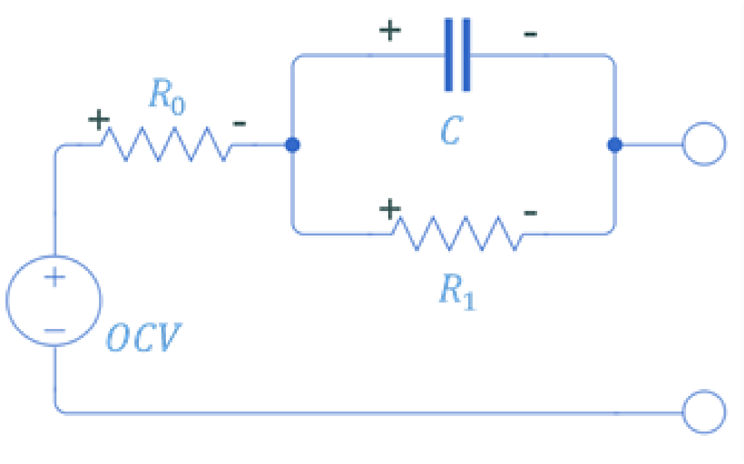

Figure 3.5. Equivalent circuit of the battery adopted

The dynamics of such circuit is described by the first-order differential equation:

$$\frac{dV_c}{dt} = -\frac{V_c}{R_1 C} + \frac{I_{batt}}{C}$$

where I_{batt} is considered as an input. From V_c, which is the solution of this differential equation, is possible to find the voltage at the terminals of the battery V_{batt} as:

$$V_{batt} = \mathrm{OCV} + R_0 I_{batt} + V_c.$$

This voltage is the final output of the model.

The values of R_0, R_1 and C are obtained from look-up tables depending on the SoC and the charge/discharge current intensity. The process of parametrization used to find the values of these three parameters as a function of SoC and current will be described in chapter 3. The open circuit voltage component is obtained from the manufacturer SoC-OCV curve, shown in figure 3.6.

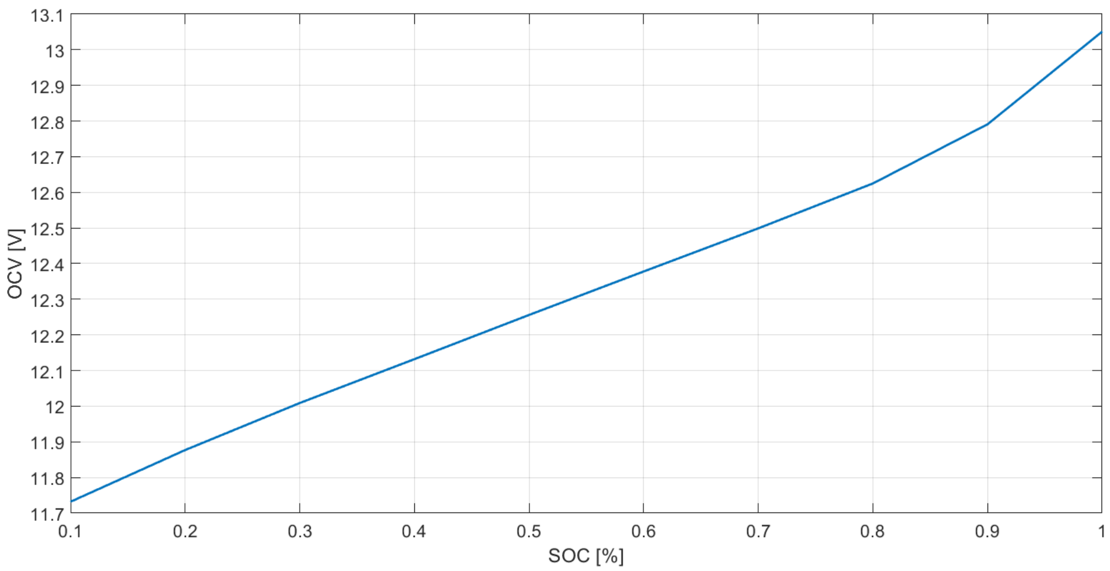

Figure 3.6. Manufacturer experimental SoC-OCV curve

In figure 3.7, the final implementation of the model in Simulink is shown and will be discussed in detail in chapter 4.

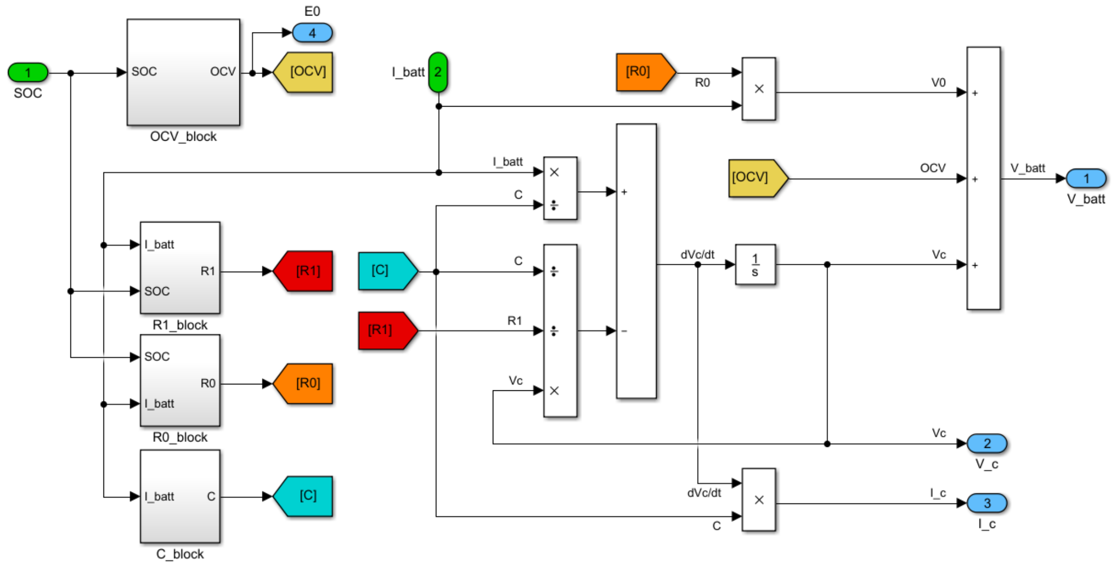

Figure 3.7. Simulink implementation of the battery model

Chapter 4
Simulink implementation

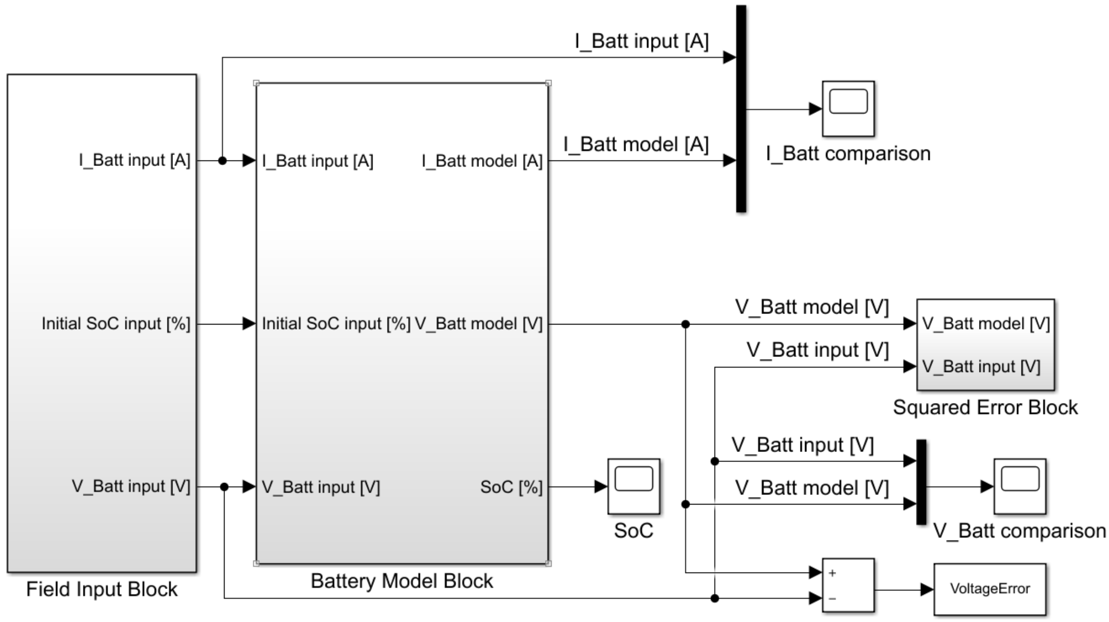

Figure 4.1. Simulink implementation of the complete model

The final implementation of the complete model on Simulink is shown in figure 4.1.

Two main blocks are present, the *field input block* and the *battery model block*.

4.1 Field input block

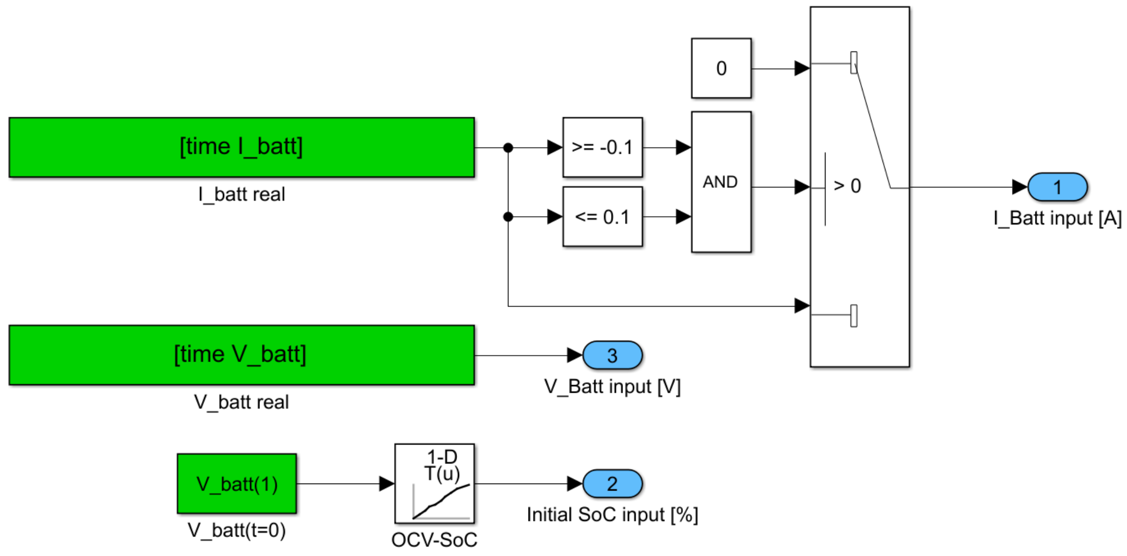

Figure 4.2. Field input block

The field input block is shown in detail in figure 4.2. In this block the three inputs of the complete Simulink model are defined from the experimental data. The voltage is taken as it is, and in case the signal is too noisy, it gets previously filtered in the Matlab script. For the current, the same approach is adopted, but to avoid discontinuities when the current oscillates around the zero (due to the switching between the charge and discharge parameters), a switch is implemented imposing the condition:

$$I_{batt,imput} = 0, \quad for - 0.1 < I_{batt,real} < 0.1.$$

The initial SoC is found from the initial value of OCV using the OCV-SoC look-up table.

4.2 Battery model block

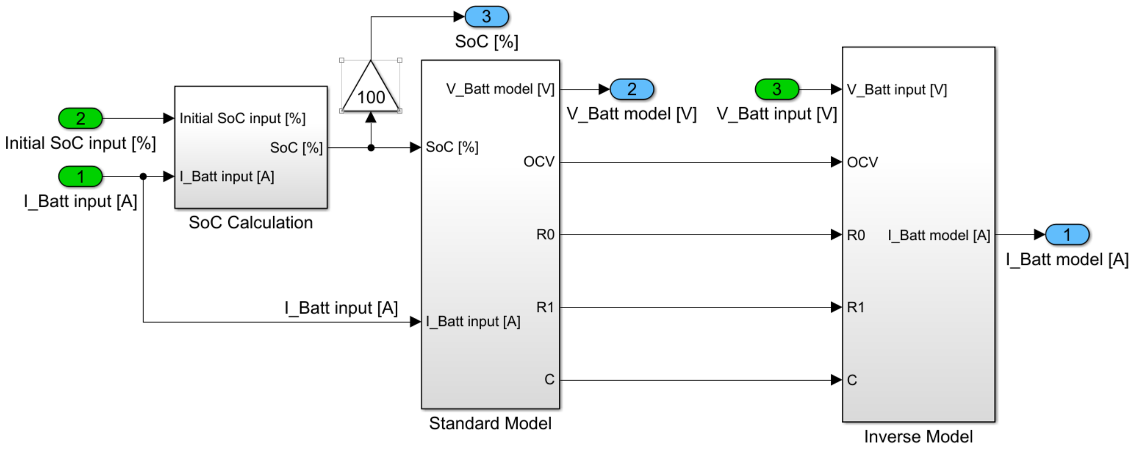

Figure 4.3. Battery model block

The battery model block is shown in figure 4.3. It is composed by three blocks: the *SoC calculation block*, the *standard model block* and the *inverse model block*. Inside the SoC calculation block, the integration of the current over time is performed, from which the instantaneous SoC of the battery is calculated. The standard model block contains the battery model working with the real current as an input and the voltage as an output. In opposition, the inverse model block contains the battery model that simulate the current profile using the real terminal voltage as an input.

4.2.1 SoC calculation block

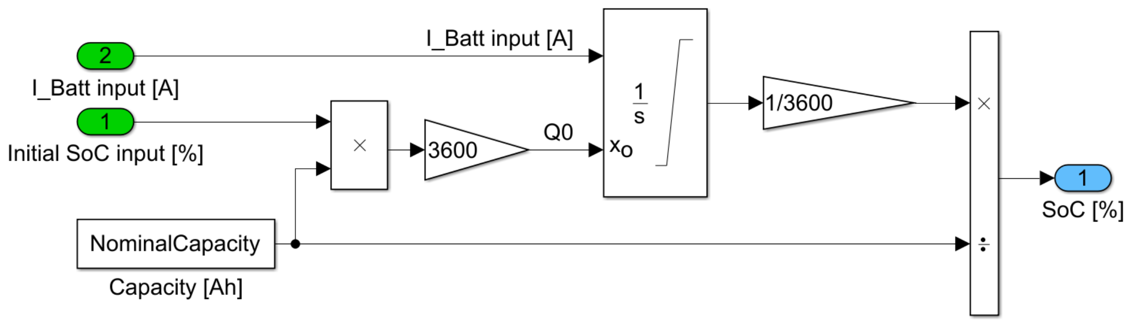

Figure 4.4. SoC calculation block

The instantaneous SoC is found as:

$$SoC = \frac{\int_{Q_0} I_{batt,input} dt}{C_{20} \cdot 3600}$$

where Q_0 is the initial electric charge stored in the battery and is found as:

$$Q_0 = C_{20} \cdot SoC_{initial} \cdot 3600.$$

4.2.2 Standard model block

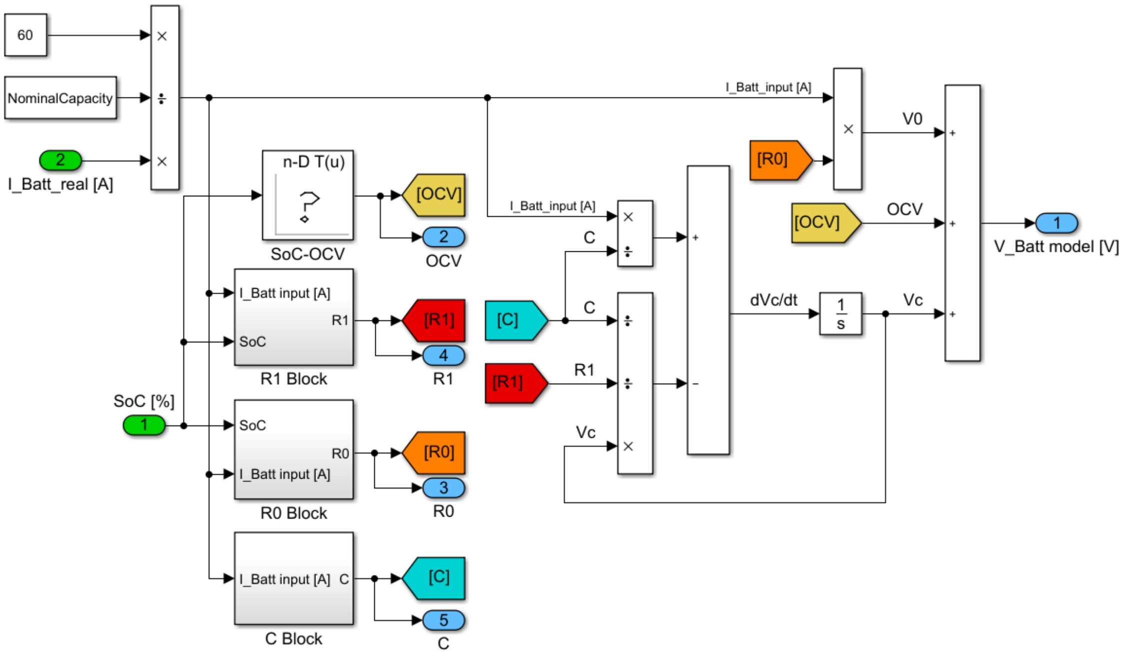

Figure 4.5. Standard model block

In figure 4.5 the implementation of the standard battery model contained in the standard model block is shown. The terminal voltage, which is the final output, is expressed as:

$$V_{batt,model} = R_0 \left(\frac{60}{C_{20}} I_{batt,real} \right) + OCV + V_c$$

where the OCV component is found from the SoC-OCV look-up table and V_c is the solution of the differential equation:

$$\frac{dV_c}{dt} = \frac{\left(\frac{60}{C_{20}} I_{batt,real}\right)}{C} - \frac{V_c}{R_1 C}.$$

As already stated in paragraph 5.2, $\frac{60}{C_{20}} I_{batt,real}$ is used instead of $I_{batt,real}$ to extend the model application to batteries of different size with respect to the Exide 60Ah600A on which the model has been parametrized.

The values of R_0, R_1 and C are obtained inside the R_0 *block*, the R_1 *block* and the C *block*, which are shown from figure 4.6 to figure 4.8. These blocks are a simple implementation of the values presented in table 6.5 and table 6.6.

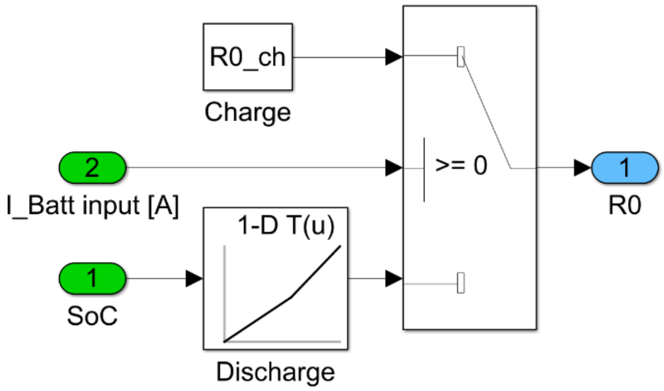

Figure 4.6. R_0 block

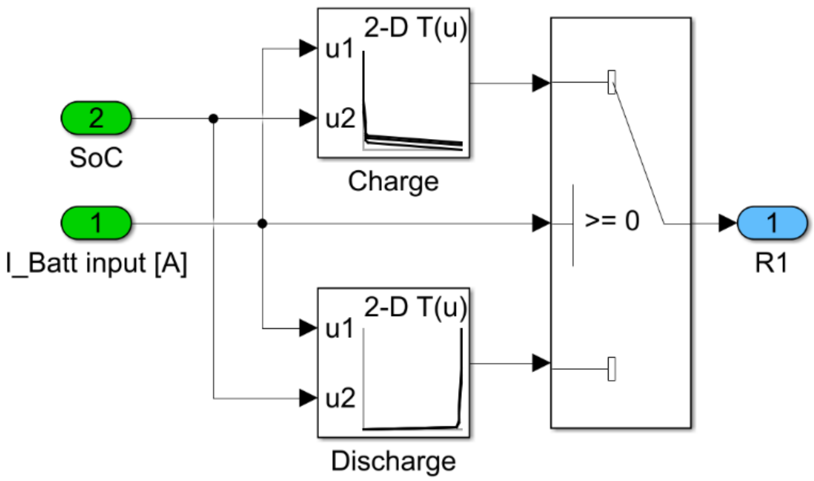

Figure 4.7. R_1 block

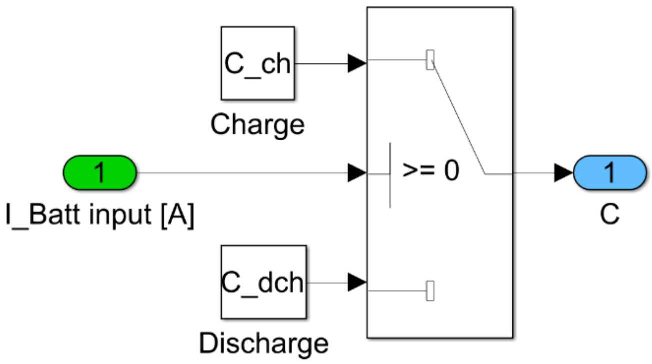

Figure 4.8. C block

4.2.3 Inverse model block

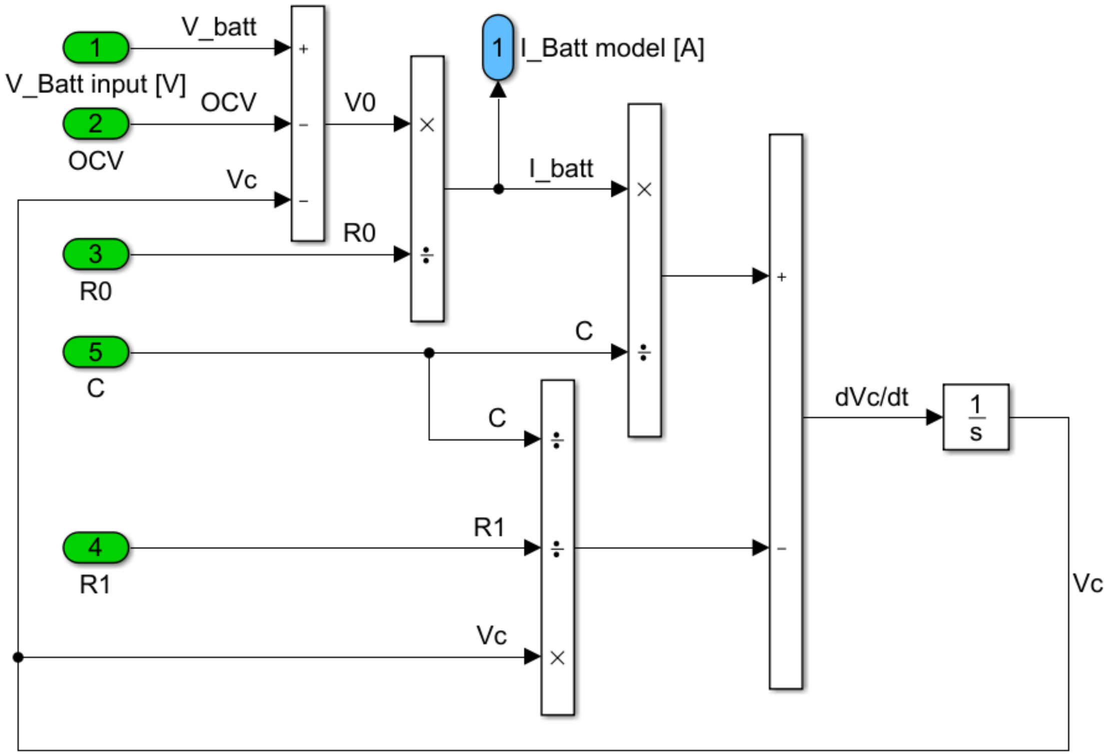

Figure 4.9. Inverse model block

In figure 4.9 the inverse model is shown. It has been called inverse because it is based on the same equations as the standard model, but the input and the output are inverted. The only purpose of this block is to give a different perspective to analyze the results of the validation tests. The current is found as:

$$I_{batt,model} = \frac{V_{batt,real} - OCV - V_c}{R_0}$$

where V_c is the solution of the differential equation:

$$\frac{dV_c}{dt} = \frac{I_{batt,model}}{C} - \frac{V_c}{R_1 C}.$$

In this case is not possible to find directly the values of OCV, R_0, R_1 and C, because they are all dependent on the current, which in this case is the output of the model, not the input. For this reason, the values of OCV, R_0, R_1 and C obtained inside the standard model are used.

Chapter 5

Model parametrization

In this chapter the procedure used to find the pattern of R_0, R_1 and C (shown in figure 3.5) depending on the SoC and the current intensity is described, for both the charge and discharge phases. The parametrization of the model has been performed through a process of *curve fitting* of some charge/discharge impulses data obtained from a set of laboratory experiments.

The chapter is divided in two parts. In the first paragraph, the assumptions made for the comparison between the real data and the model output are presented. In the second paragraph, the algorithm developed for the curve fitting is explained.

5.1 Conceptual approach

In figure 5.1, a typical curve of the battery voltage during a discharge at constant current is shown.

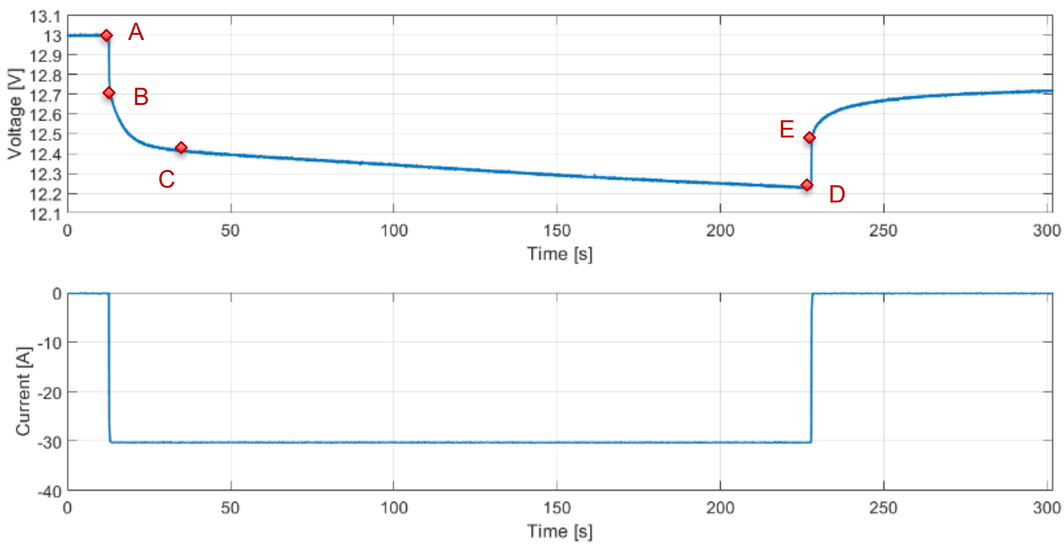

Figure 5.1. Typical lead-acid battery's discharge impulse behavior

A qualitative description of this curve can be made. In the point A, the current goes from 0 to -30A (discharge) and the voltage drops almost instantly to V_B. From point B to point C, the voltage keeps decreasing following a curve similar to an exponential. From point C to point D, the voltage decreases maintaining a slope almost constant. Finally, in point D, the current goes back to 0 and the voltage rises almost instantly to V_E. After the point E, the voltage slowly reaches the steady-state open circuit voltage of the battery (it could take up to a couple of days).

As shown in figure 5.2, this behavior can be well reproduced by the model.

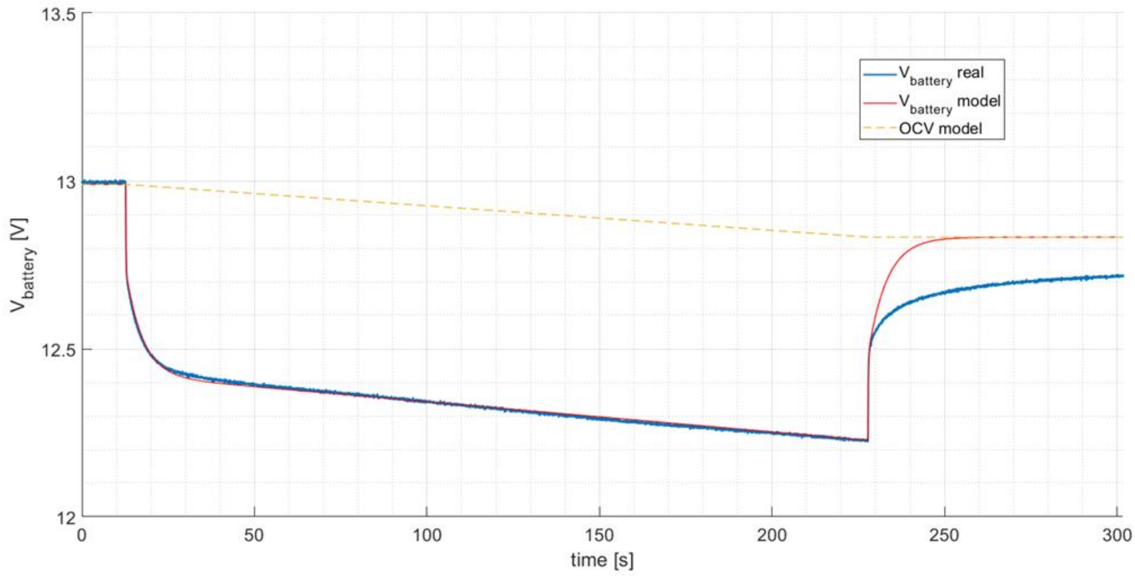

Figure 5.2. Comparison between acquisition data and model output for a single discharge impulse

Anyway, it is necessary to make some assumptions regarding the different voltage components present in the model. Following, the equation of the output of the model, during each phase, is presented.

- Before point A, the current is 0 and thus, no voltage drop across resistors is present. The only component is the open circuit voltage, which is directly proportional to the SoC.

$$V_{model} = OCV$$

- From point A to point B, the current rises almost instantly to -30A. In this initial phase, the capacitor behaves as a short-circuit and then the terminal voltage can be considered as:

$$V_{model} = OCV + R_0 I_{batt} \quad where\ I_{batt} < 0\ (discharge)$$

- From point B to point C, the voltage exponential shape is described by the charging transient of the equivalent circuit capacitor. During this phase, the model terminal voltage is made by:

$$V_{model} = OCV + R_0 I_{batt} + R_1 I_{batt} \left(1 - e^{-\frac{t}{\tau}}\right) \quad where\ \tau = R_1 C$$

  It is important to remark that, the asymptotical value of the capacitor voltage is assumed to be reached at point C.

- Due to the last assumption, from point C to point D, the model is assumed to be in quasi-steady state, which means that the capacitor is acting as an open circuit and no variation of the voltage across the capacitor is present. For this reason, the constant-rate decrease from point C to point D cannot be represented by the equivalent circuit dynamic behavior. In fact, this decrease is well reproduced by the decrease of the OCV component as the SoC goes down. In fact, in figure 5.2, it is possible to highlight that during the constant discharge impulse the OCV component and the real voltage are almost parallel.
  During this phase the model voltage is composed by:

$$V_{model} = OCV(SoC) + (R_0 + R_1) I_{batt}$$

  where the OCV value changes with the state of charge.

- From point D to point E, the current goes back to zero and the capacitor is still fully charged. Thus, in point E the voltage is equal to:

$$V_{model} = OCV + V_c(final) \quad where\ V_c(final) = -R_1 I_{batt}$$

- After point E, the capacitor starts discharging and the voltage goes back to the OCV value correspondent to the final SoC. Because in this thesis a first-order model has been used and the time constant has been found considering the transient from point B to point C, it is not possible to represent the voltage behavior of this phase. A second-order model with a second, much higher, time constant would be needed.

5.2 Curve fitting algorithm

The complete algorithm used for the curve fitting process is presented in appendix A. The algorithm has as an input the experimental test current and find the R_0, R_1 and C values that best fit the real voltage curve. It works on a single charge/discharge impulse, for which the initial state of charge is estimated in two ways:

- From the level of the OCV before the impulse, using the manufacturer SoC-OCV curve.
- From the Ah counting performed on the previous impulses of the test sequence. Thus, the initial SoC of the impulse is the final SoC of the previous one.

In figure 5.3, a flowchart explaining the algorithm logic is shown. The calculation of the different parameters is made in different points of the real voltage curve and is now explained more in detail.

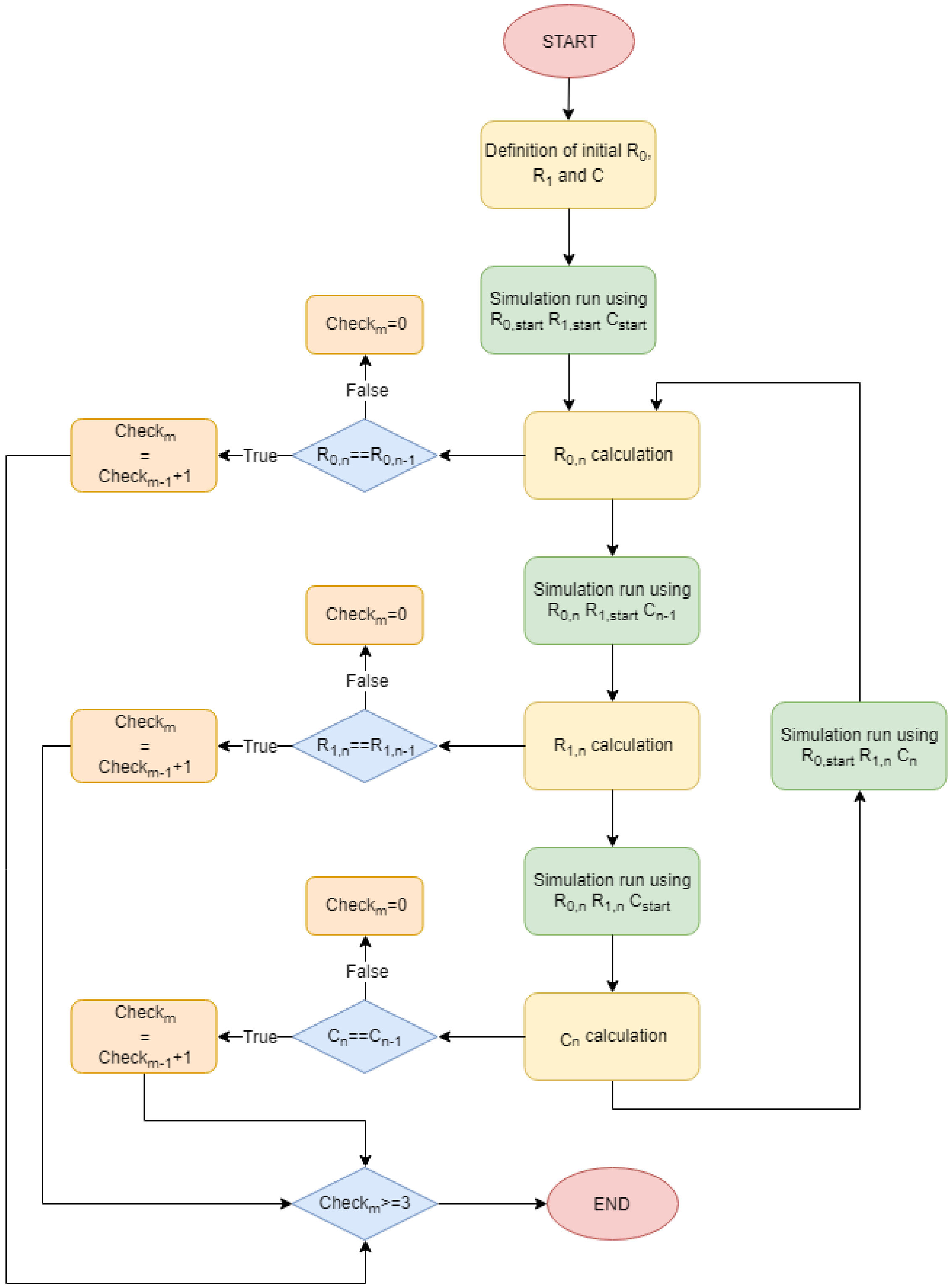

Figure 5.3. Flowchart of parametrization algorithm functioning

The initial R_0, R_1 and C values are:

$$R_{0,start} = 0.001\ \Omega \qquad R_{1,start} = 0.001\ \Omega \qquad C_{start} = 10\ F$$

From these, the algorithm run a first simulation to plot the model terminal voltage. As previously stated, the instantaneous voltage drop from point A to point B (figure 5.1) is composed by the OCV component and the voltage drop across R_0. Thus in point B, knowing the OCV component from the SoC of the battery, and measuring the error between the real voltage and the model voltage, the value of R_0 is found as:

$$R_{0,n} = \frac{\Delta V(B)}{I_{batt}} + R_{0,start}$$

A new simulation, using as parameters $R_{0,n}$, $R_{1,start}$ and C_{start}, is run. As assumed in paragraph 3.1, from point C to point D the capacitor of the equivalent circuit is fully charged and behave as an open circuit. This means the model terminal voltage is composed by the OCV and the voltage drop across both resistors R_0 and R_1. Knowing the OCV component from the SoC and considering $R_0 = R_{0,n}$, by measuring the difference between the model and real voltages in point D (figure 5.1), it is possible to find $R_{1,n}$ as:

$$R_{1,n} = \frac{\Delta V(D)}{I_{batt}} + R_{1,start}$$

Finally, considering $R_0 = R_{0,n}$ and $R_1 = R_{1,n}$, the C value is calculated. The capacitor is the equivalent circuit component that directly influence the model dynamics. For this reason, the final chosen value is the one assuring the smallest errors possible between real and model voltages from point B to point C. Thus, the algorithm iterates a set of simulations, performed with increasing values of C. The iteration stops, when the value of C that minimize the sum of squared errors between real and model voltages is found.

The calculation of R_0, R_1 and C is inside a for-cycle that iterate this process until all the parameters values satisfy the condition:

$$R_{0,n} = R_{0,n-1} \qquad R_{1,n} = R_{1,n-1} \qquad C_n = C_{n-1}.$$

Chapter 6
Testing

Two different sets of tests have been performed. The first set has been designed for the model parametrization and used in the procedure described in chapter 3. The second set has been designed for the validation of the model, activity that will be seen more in detail in chapter 6. In the following, the considerations behind the tests design and their results will be presented.

6.1 Tests for parametrization

The tests for parametrization have the objective to find 24 distinctive sets of R_0, R_1 and C values (12 for discharge and 12 for charge), each of them valid for a specific current intensity-SoC combination. From these, the look-up tables implemented in the final model will be compiled.

6.1.1 Parametrization tests design

For this thesis, an Exide EFB 60Ah600A has been tested (an initial try test has been performed on an Exide EFB 60Ah500A). Due to constructional features, it is obvious that different manufacturer and/or different size batteries will behave differently, thus the parameters found from these tests are considered fully reliable only for the tested model of battery. However, for validation purposes, the reliability of the model on batteries of different size has been tested and will be presented in chapter 6.

The test procedure will cover specific levels of current and SoC. For this reason, the ideal ranges of application of the model are:

$$SoC \approx 60 \div 80\% \quad and \quad I_{batt} = 0 \div 50\ A$$

which are the typical conditions of automotive batteries during discharge.

The battery discharge has been tested with the following procedure:

1. Full charge.
2. 24-hour relaxation.
3. Discharge at constant current I_{20} till the voltage reaches 10.5 V. This is a typical C_{20} test, from which the measured Ah value can be considered as the actual capacity of the battery and used instead of the rated C_{20}.
4. Full charge followed by 4-hour relaxation.
5. Fast discharge to $SoC = 80\%$ considering Ah counting method.
6. 24-hour relaxation
7. Sequence of 4 discharge steps at different current level and variable length, each of them followed by a 2-hour relaxation. This sequence is visible in figure 6.1. The aim of this sequence is to have really small SoC variations between consecutive discharge impulses. The full sequence range of SoC is ~4%, which translates in a 0.06V OCV range. The OCV value correspondent to a certain SoC has an accuracy tolerance larger than ±0.05V. For these reasons, considering the full discharge sequence as it is at constant SoC has been considered a safe assumption. The constant SoC associated to this sequence has been evaluated from the starting value of OCV, considering it as a good estimation thanks to the prior 24-hour battery relaxation.
8. Fast discharge of a $\Delta SoC = 5\%$ considering Ah counting method.

9. Repetition of steps from 6 to 8 two more times. The initial SoC before any discharge sequence is always estimated from the measured OCV.

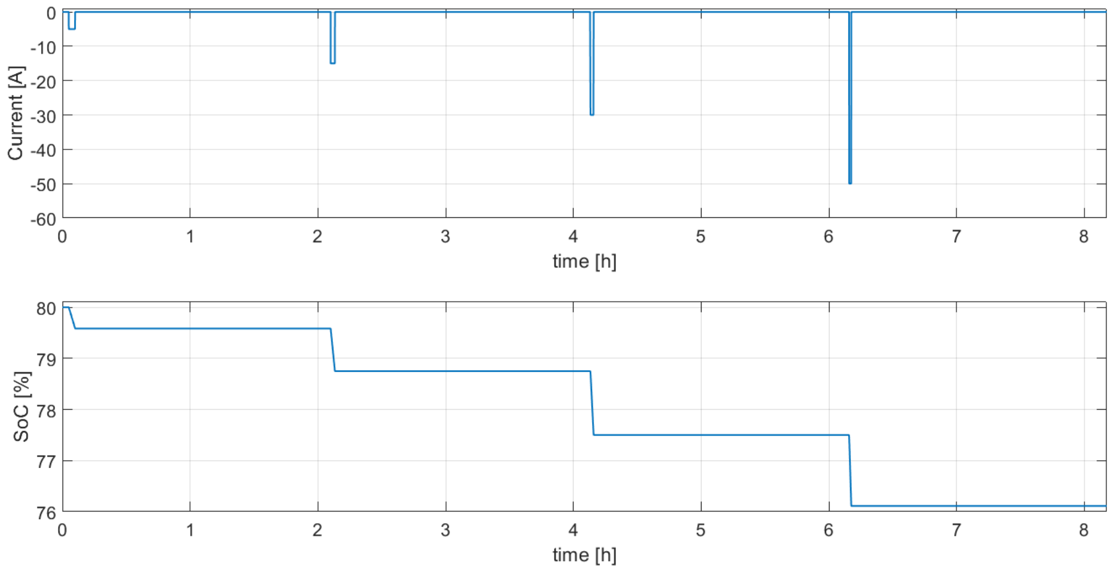

Figure 6.1. Discharge sequence used for parametrization

For what concerns the test of the battery under charging, a similar procedure has been adopted, but considering different current intensities. In this case, the ideal ranges of application of the model are:

$$SoC \approx 60 \div 80\% \quad and \quad I_{batt} = 0 \div 20\ A$$

The battery charge test procedure is composed by:

1. 24 hour relaxation. The starting condition is the end of the discharge tests and then, after this first relaxation, the initial SoC is defined by the measured OCV.

2. Sequence of 3 charge steps at different current level and variable length, each of them followed by a 2 hour relaxation. This sequence is shown in figure 6.2. The considerations behind this sequence are the same made for the step 7 of the discharge test procedure.

3. Fast charge of a $\Delta SoC = 5\%$ considering Ah counting method.

4. Repetition of steps from 1 to 3 two more times. The initial SoC before any charge sequence is always estimated from the measured OCV.

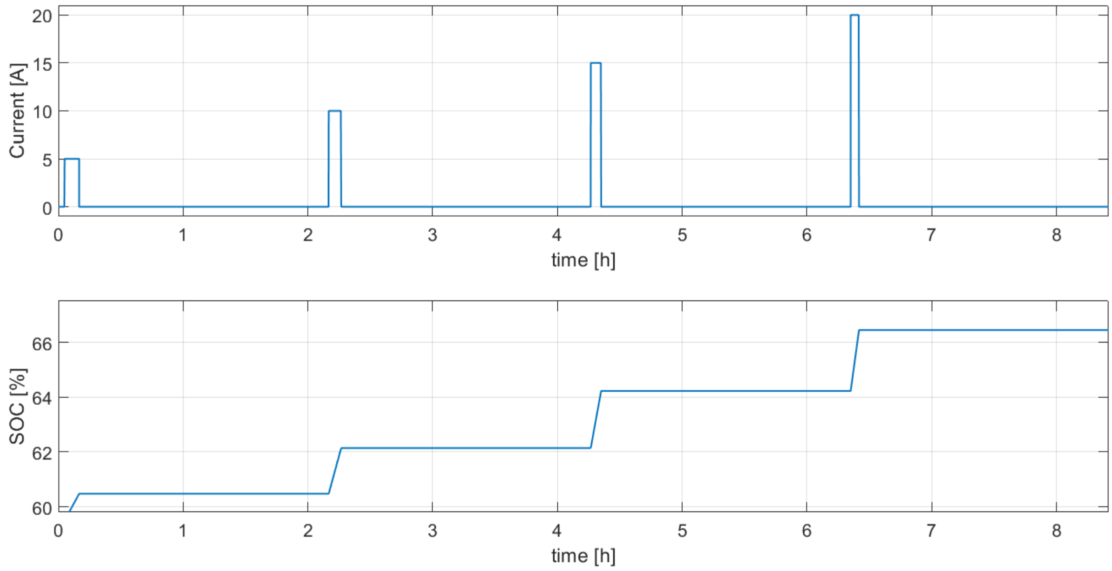

Figure 6.2. Charge sequence for parametrization

The goodness of the test procedure has been tested with a first discharge sequence performed on an Exide EFB 60Ah500A. In figure 6.3 the voltage profile during one of the discharge impulses is shown.

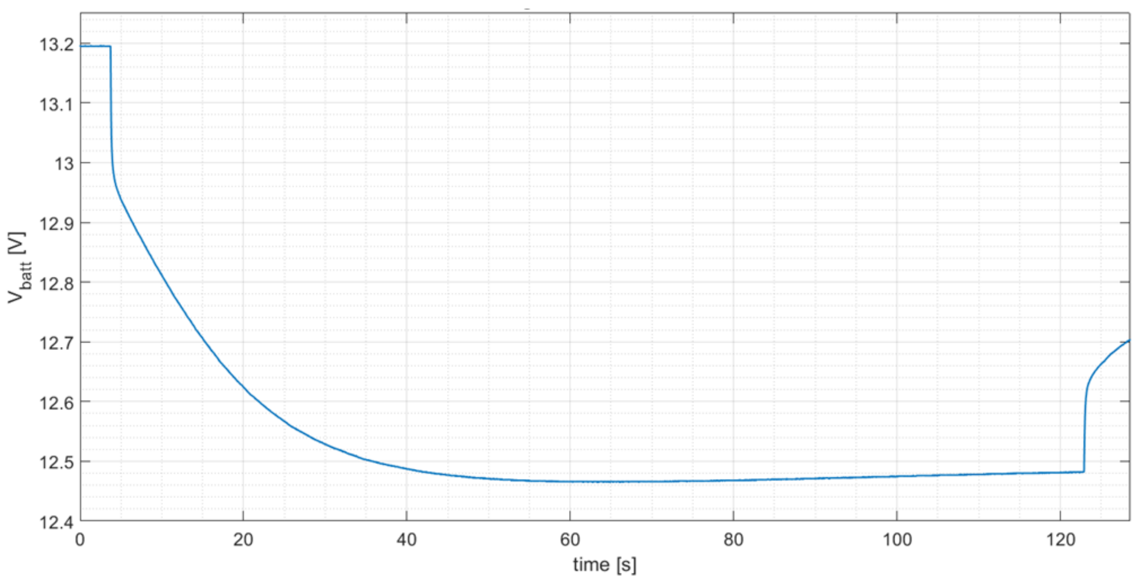

Figure 6.3. Discharge impulse of an Exide 60Ah-500A

Looking at this profile, several unexpected features can be observed.

The first unexpected characteristic is that the initial OCV is much higher than expected, especially considering that the battery comes from a 24h relaxation. The estimated SoC through Ah counting is 80%, which nominally would correspond to $OCV \approx 12.625\ V$. In the test, $OCV \approx 13.2\ V$, which is also out of range considering Exide OCV-SoC curve in figure 3.6. This unexpected level of OCV could be due to the high capacity measured with the C_{20} test. In fact, during the C_{20} test, the battery delivered ~72Ah, which is considered an unusual result, as confirmed by Exide engineers too. The root cause of the capacity and OCV levels is probably the electrolyte concentration above usual values in the production stock of the battery under test.

The second unexpected feature is the shape of the profile. In figure 6.4, the comparison between the behavior registered during test (plot on the left) and the expected profile (plot on the right) is shown. It is easy to notice that, after the first sharp decrease, the voltage starts to slowly increase. This particular behavior is called *coup de fouet*, and is described more in detail in appendix B.

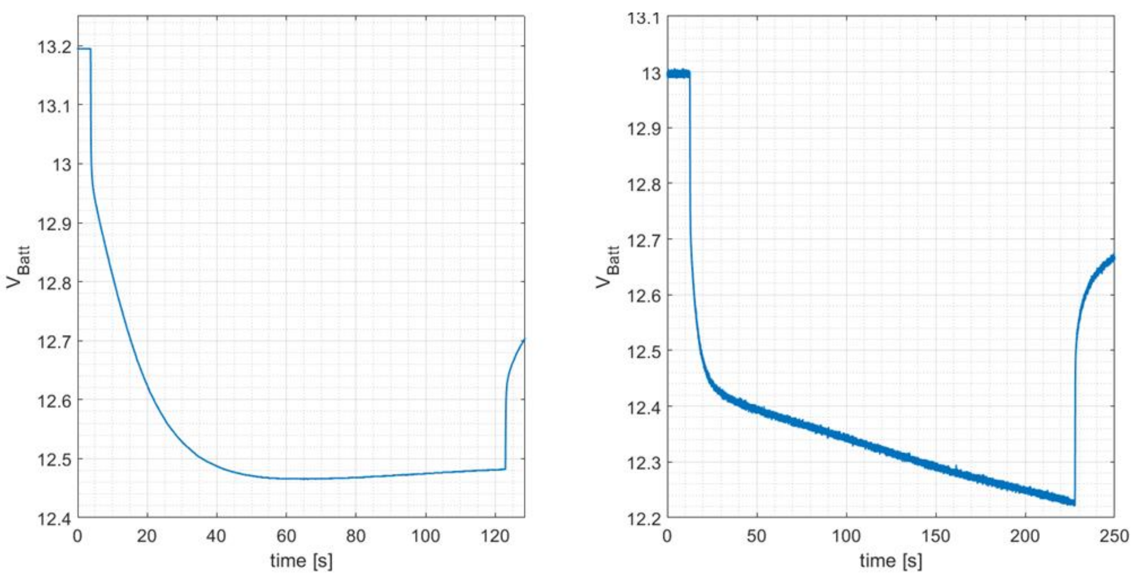

Figure 6.4. Comparison between discharge impulse with and without Coup de Fouet effect

Considering the result of this first test, some adjustments to the procedures previously described will be made.

The first modification is the removal of the C_{20} test. This is done, because a complete discharge could compromise the battery behavior due to the sulfation of the plates. This phenomenon occurs when the battery is discharged to a very low level of SoC. During a deep discharge, a thick layer of lead sulfate generates on the plates surface and is not fully absorbed during the next recharge, reducing the amount of active material and compromising plates conductivity. The effect is more severe the longer the battery is kept at a low SoC.

The second change is the battery model. From now on an Exide EFB 60Ah600A will be tested. This battery is presented by Exide as a simple update of the EFB 60Ah500A with no significant changes for what concerns constructional features and performance.

6.1.2 Parametrization tests results

From figure 6.5 to figure 6.8, the voltage profiles of the first test in discharge are shown.

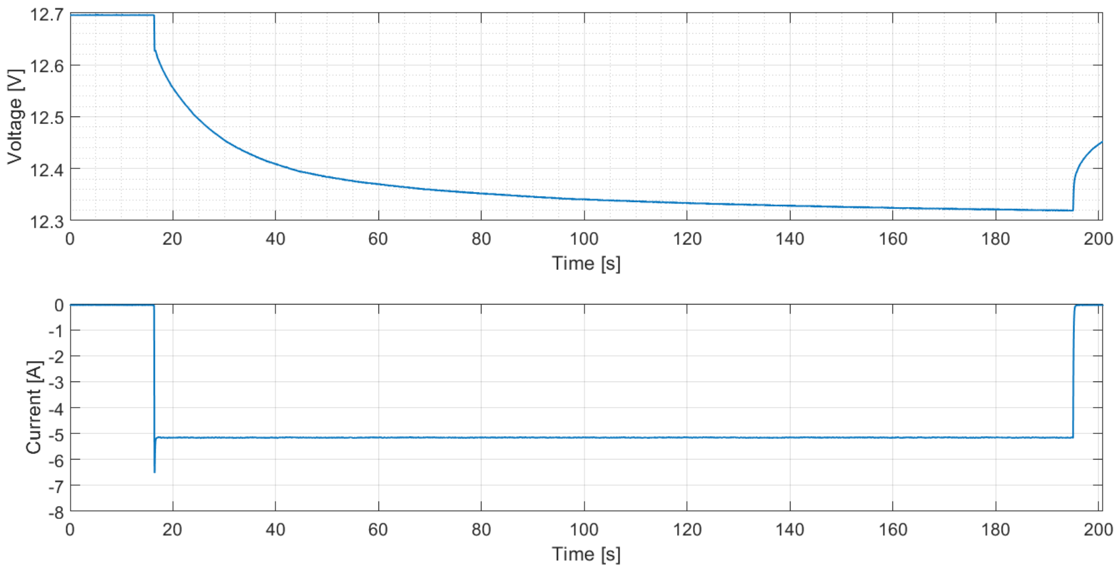

Figure 6.5. First discharge test – 5A impulse

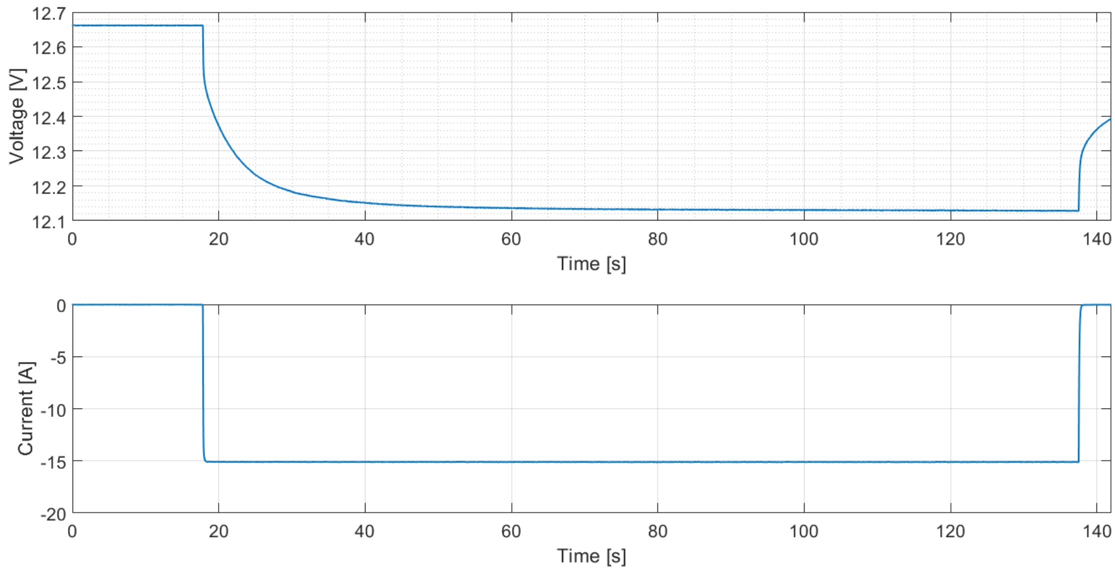

Figure 6.6. First discharge test – 15A impulse

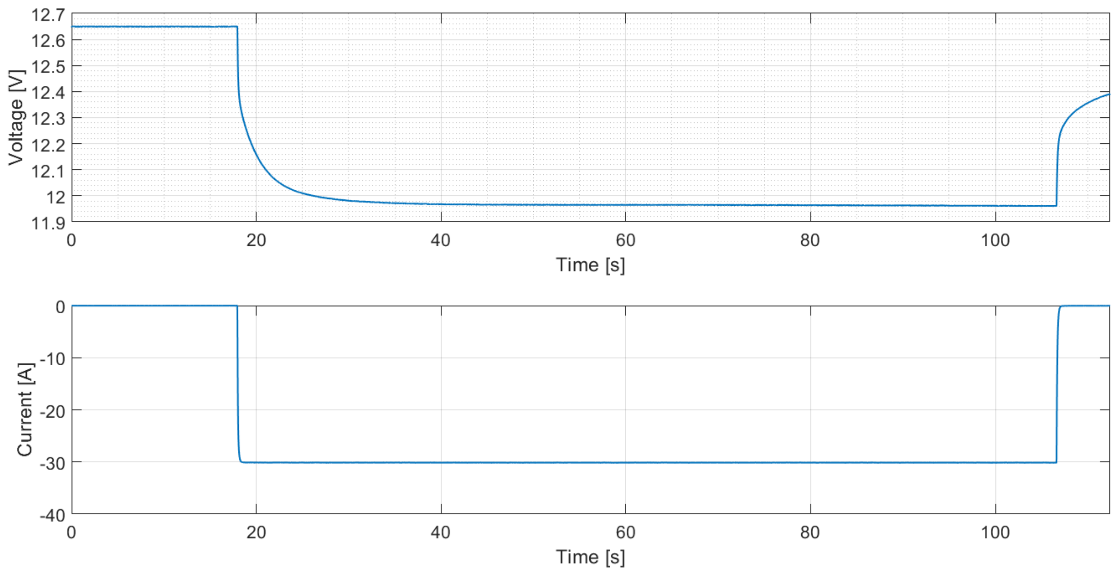

Figure 6.7. First discharge test – 30A impulse

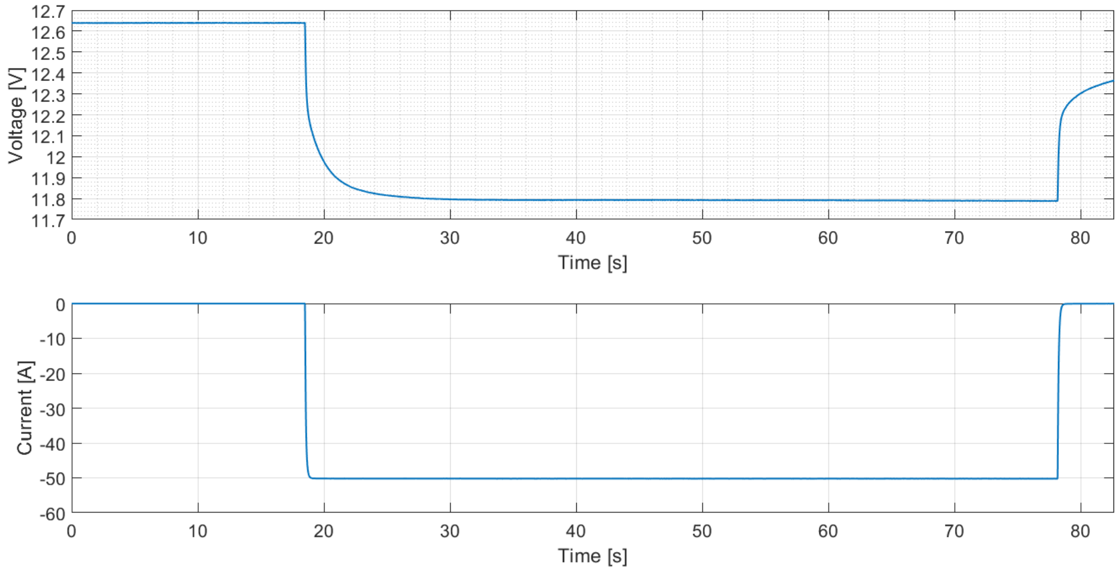

Figure 6.8. First discharge test – 50A impulse

The profile shape is the expected one and it does not seem to present the coup de fouet effect, or at least not so severe to compromise the results as happened for the case in figure 6.3. The other main requirement of this test procedure is to have all the impulses starting from a small range of OCV. For the first impulse the OCV is 12.69V and for the last impulse is 12.64V, resulting in a 0.05V range. In terms of SoC, it corresponds to a 3% range, which is considered as a satisfactory result. The other two discharge test and the set of three charge tests give similar results and can be efficiently used for the parametrization as well.

From these sets of acquisitions it is possible to proceed with the parametrization process, using the algorithm presented in paragraph 3.2. The several sets of R_0, R_1 and C values, obtained for different current-SoC combinations, are now presented.

a) Discharge parameters

The values in table 6.1 have been found estimating the initial SoC of each discharge impulse from the OCV. It is possible to notice that, the biggest variation in term of resistance is registered on R_1, both depending on state of charge and current intensity. The variation of R_0 is more or less 40%, while the variation of R_1 is about 600%. From figure 6.9 to figure 6.14, the values of the parameters are plotted as a function of current intensity and SoC. R_0 and R_1 show a clear monotonic pattern, both versus current and SoC, unlike C.

R_0 [ohm]		State of Charge [%]		
		83 %	74 %	63 %
Current [A]	5	0.01159	0.01021	0.00950
	15	0.00946	0.00882	0.00849
	30	0.00851	0.00832	0.00821
	50	0.00820	0.00803	0.00782
R_1 [ohm]		State of Charge [%]		
		83 %	74 %	63 %
Current [A]	5	0.06011	0.05215	0.04623
	15	0.02490	0.02177	0.02039
	30	0.01363	0.01197	0.01156
	50	0.00831	0.00750	0.00756
C [Farad]		State of Charge [%]		
		83 %	74 %	63 %
Current [A]	5	318.1	460.3	471.5
	15	210.8	230.7	235.7
	30	210.8	210.8	210.8
	50	210.8	210.8	174.1

Table 6.1. Parameters for discharge (SoC estimated from OCV)

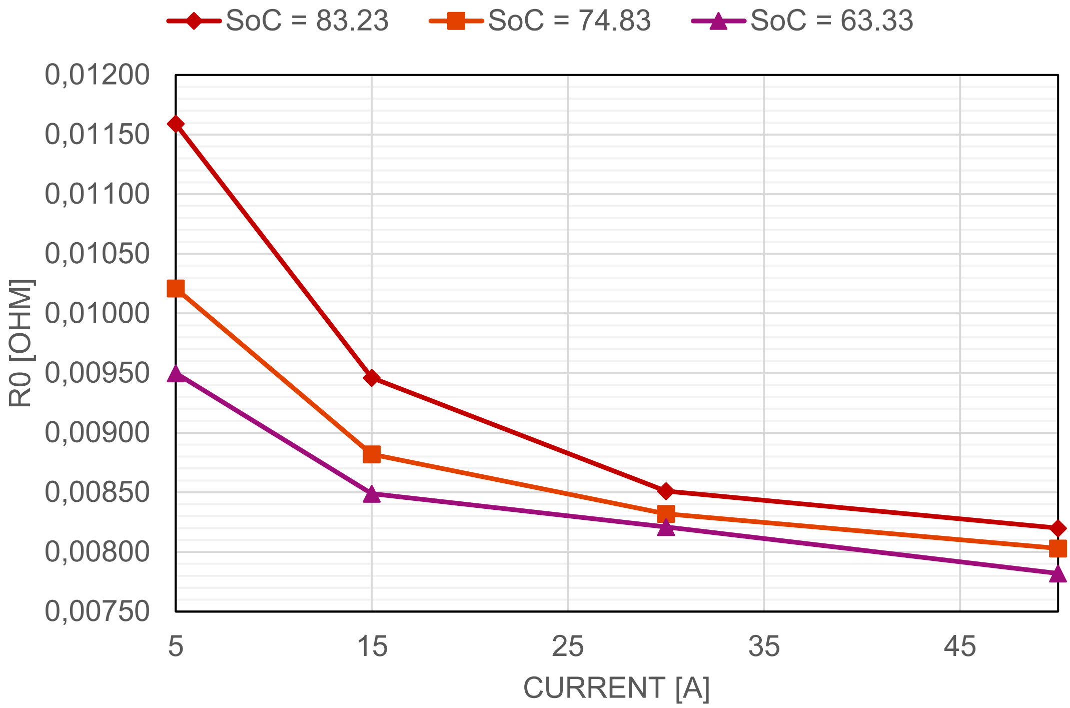

Figure 6.9. R_0 vs current for discharge (SoC estimated from OCV)

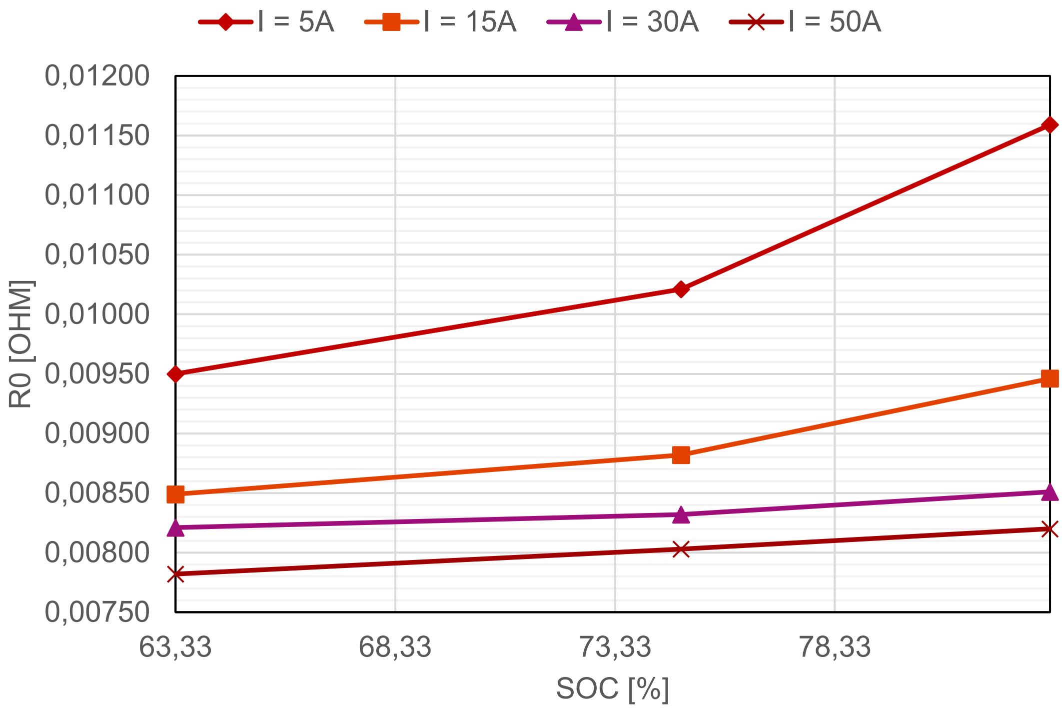

Figure 6.10. R_0 vs SoC for discharge (SoC estimated from OCV)

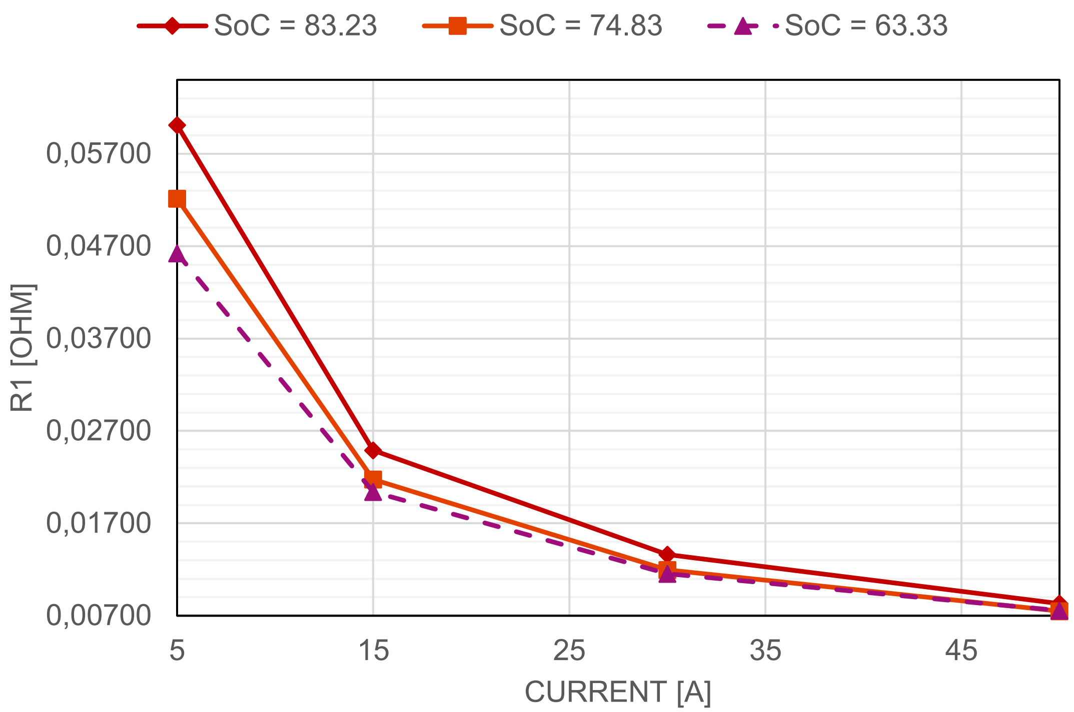

Figure 6.11. R_1 vs current for discharge (SoC estimated from OCV)

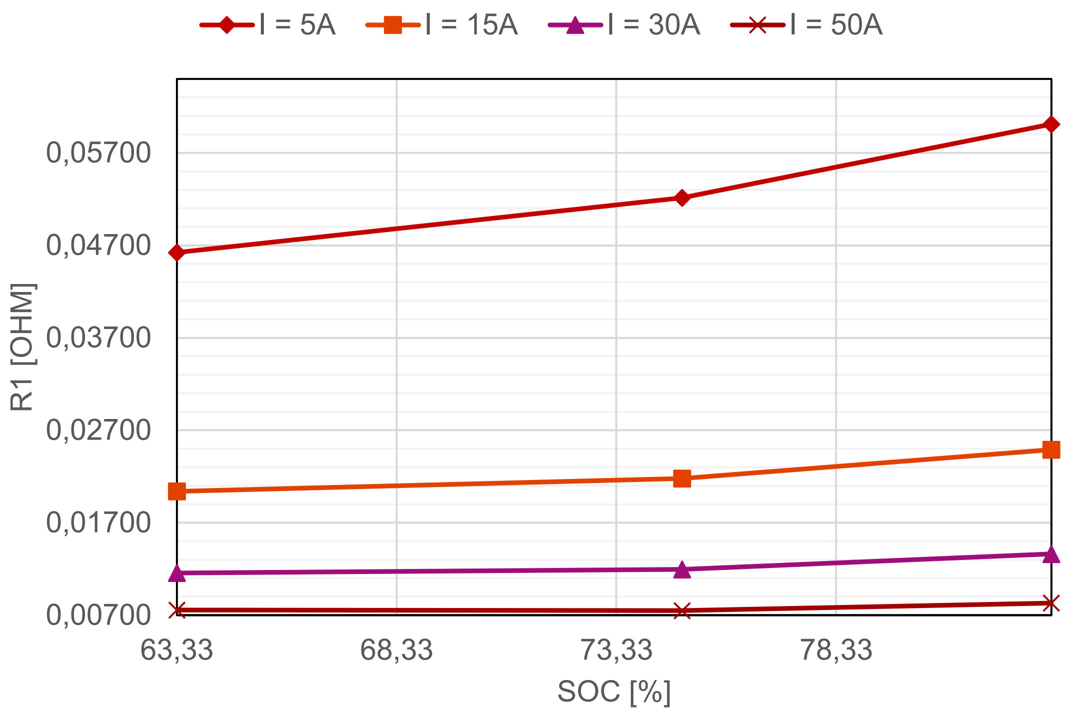

Figure 6.12. R_1 vs SoC for discharge (SoC estimated from OCV)

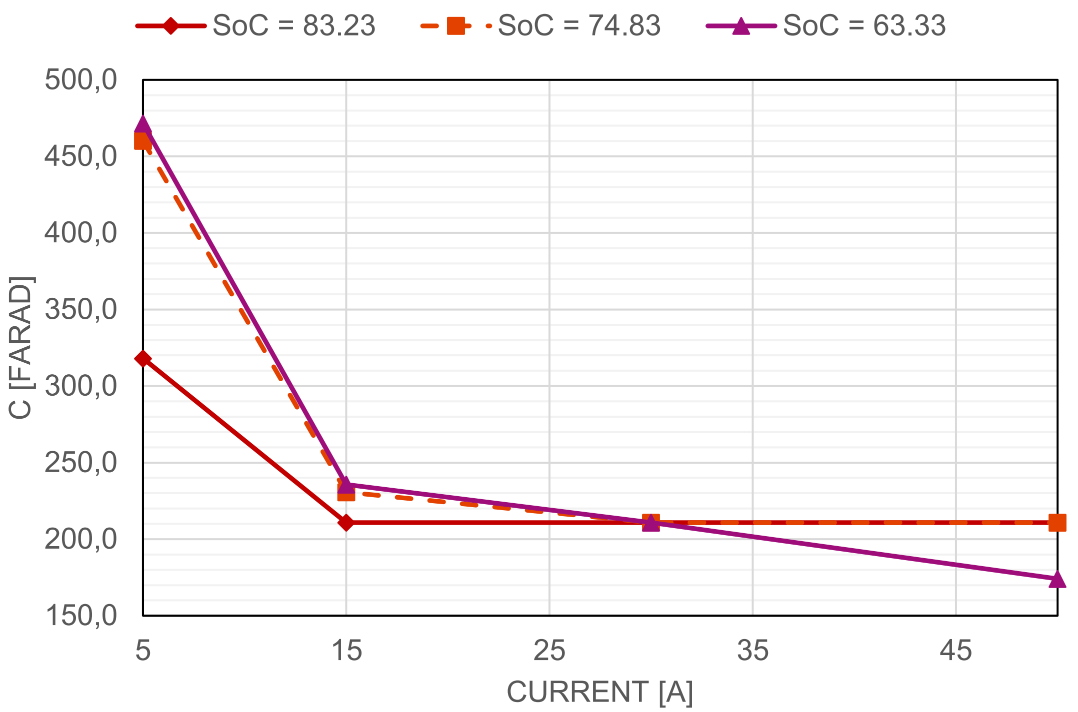

Figure 6.13. C vs current for discharge (SoC estimated from OCV)

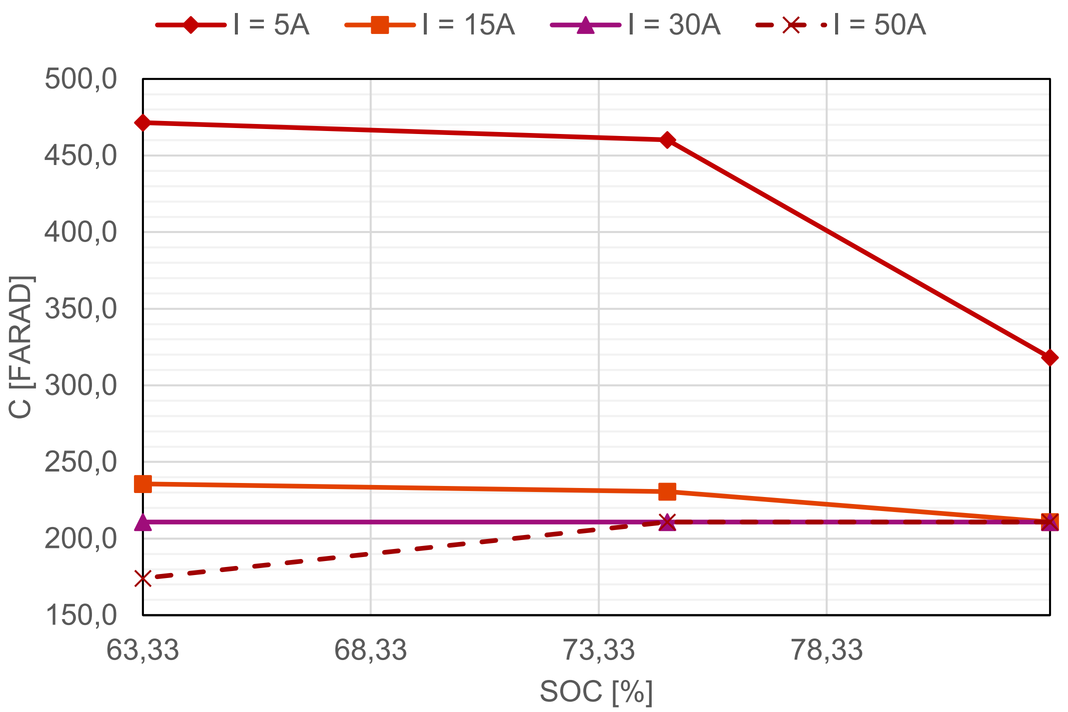

Figure 6.14. C vs SoC for discharge (SoC estimated from OCV)

As an alternative, the values in table 6.2 have been found estimating only the initial SoC of the sequence from the OCV, and the SoC of the individual discharge impulses through Ah count method. As shown in figure 6.16, R_1 variation between the two SoC estimation methods is negligible. For the R_0 variation, the situation is different, a noticeable change is present, both in terms of values and profile. This is due to the strong influence of the SoC estimation on the way the algorithm finds the value of R_0. As stated in paragraph 3.1, in point B it is $V_{model} = OCV + R_0 I_{batt}$. Thus, it is obvious that, considering different SoC, which means different values of the OCV component, the final value of R_0 will be strongly affected.

R_0 [ohm]		State of Charge [%]		
		83 %	74 %	63 %
Current [A]	5	0.01159	0.01021	0.00950
	15	0.01136	0.01119	0.01086
	30	0.00948	0.00953	0.00943
	50	0.00853	0.00861	0.00859
R_1 [ohm]		State of Charge [%]		
		83 %	74 %	63 %
Current [A]	5	0.06011	0.05215	0.04623
	15	0.02478	0.02194	0.02026
	30	0.01352	0.01193	0.01150
	50	0.00826	0.00748	0.00738
C [Farad]		State of Charge [%]		
		83 %	74 %	63 %
Current [A]	5	318.1	460.3	471.5
	15	210.8	226.0	240.7
	30	210.8	210.8	210.8
	50	210.8	210.8	174.1

Table 6.2. R_0 values for discharge (second SoC estimation method)

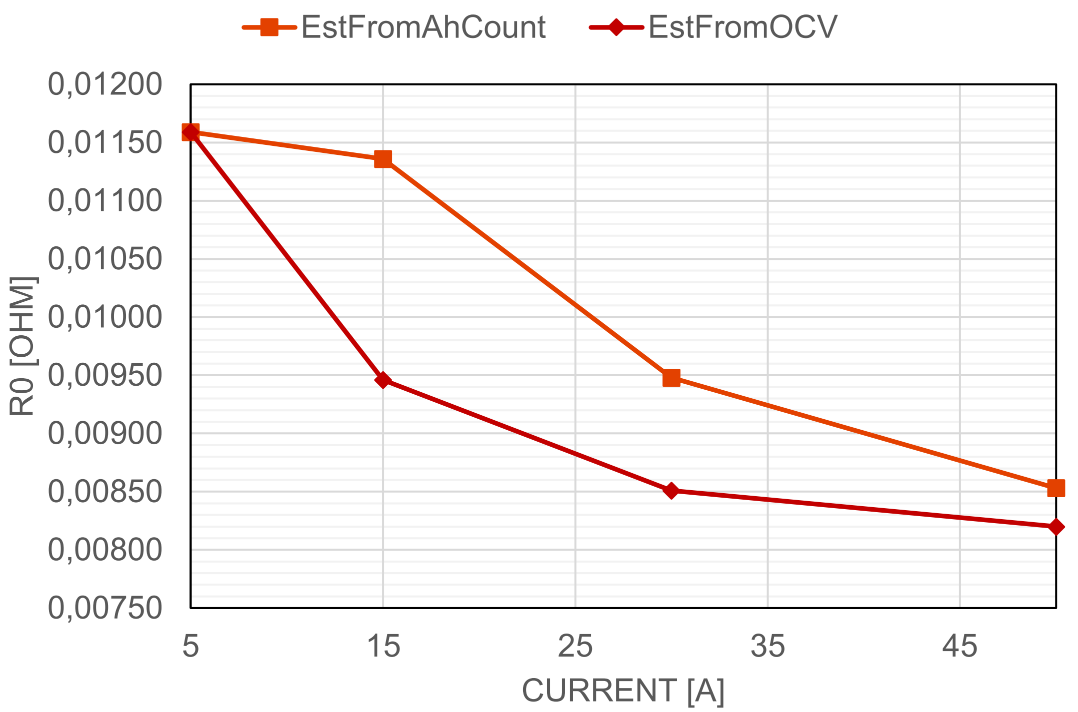

Figure 6.15. R_0 vs current for discharge, SoC estimation methods comparison

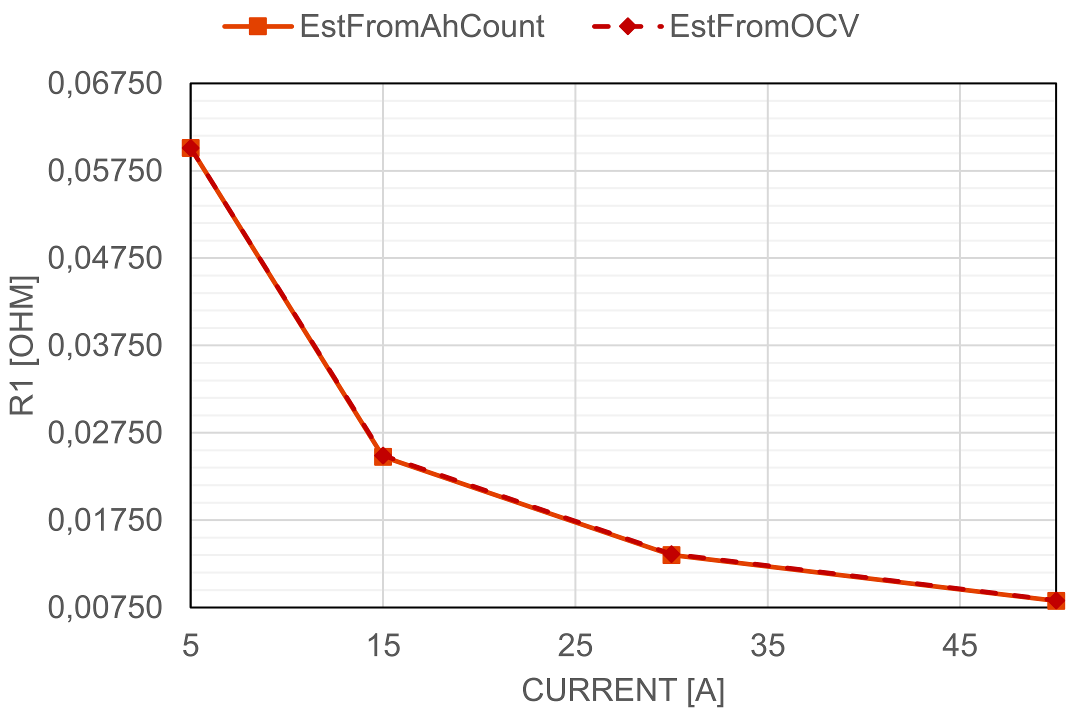

Figure 6.16. R_1 vs current for discharge, SoC estimation methods comparison

b) Charge Parameters

The values in table 6.3 have been found estimating the initial SoC of each discharge impulse from the OCV. As for the discharge parameters, the biggest variation in term of resistance is registered on R_1, and the variation of R_0 is almost negligible by comparison. From figure 6.17 to figure 6.22, the values of the parameters are plotted as a function of current intensity and SoC. From R_1 profiles, it is visible that the results are similar to what has been obtained in discharge but looking at R_0 results, no monotone profile is obtained, neither versus the current nor versus the SoC. The values with * have been estimated due to technical problems during testing.

R_0 [ohm]		State of Charge [%]		
		62 %	74 %	78 %
Current [A]	5	0.01334	0.01052	0.01262
	10	0.01012	0.00902	0.01057
	15	0.01109	0.00920	0.01080*
	20	0.01111	0.00990	0.01080*
R_1 [ohm]		**State of Charge [%]**		
		62 %	74 %	78 %
Current [A]	5	0.10503	0.12110	0.12865
	10	0.06026	0.06995	0.08219
	15	0.04292	0.05083	0.05800*
	20	0.03677	0.04571	0.05100*
C [Farad]		**State of Charge [%]**		
		62 %	74 %	78 %
Current [A]	5	378.3	340.5	334.2
	10	310.6	245.7	250.7
	15	335.7	310.6	260.0*
	20	348.0	310.6	260.0*

Table 6.3. R_0 values for charge (first SoC estimation method)

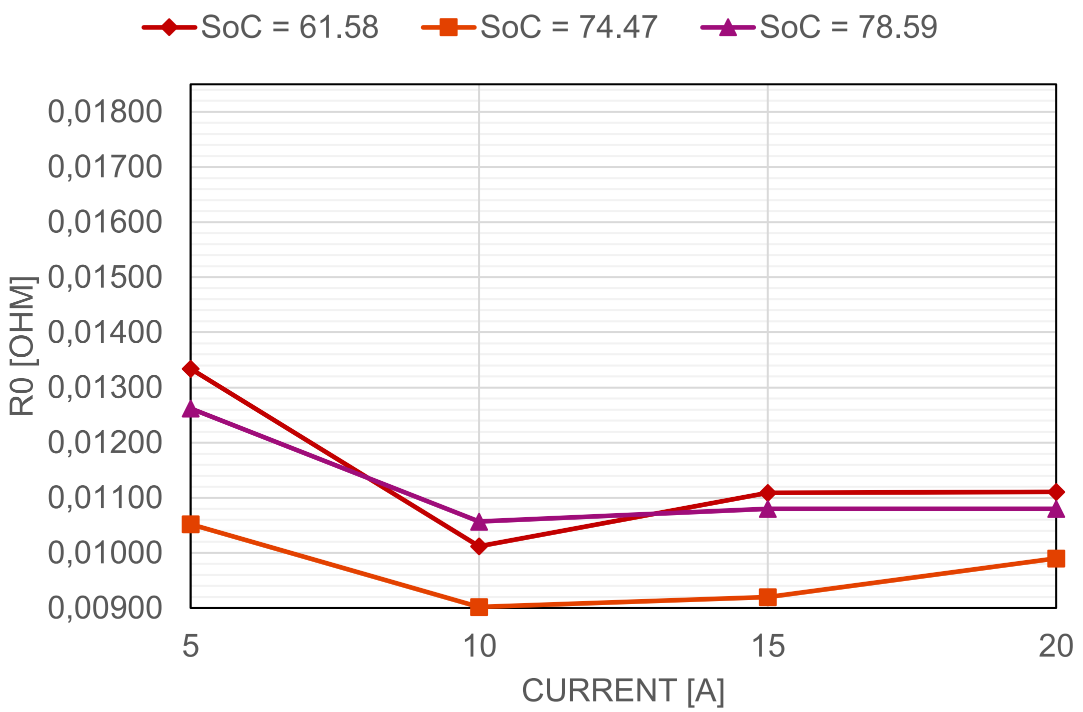

Figure 6.17. R_0 vs current for charge (first SoC estimation method)

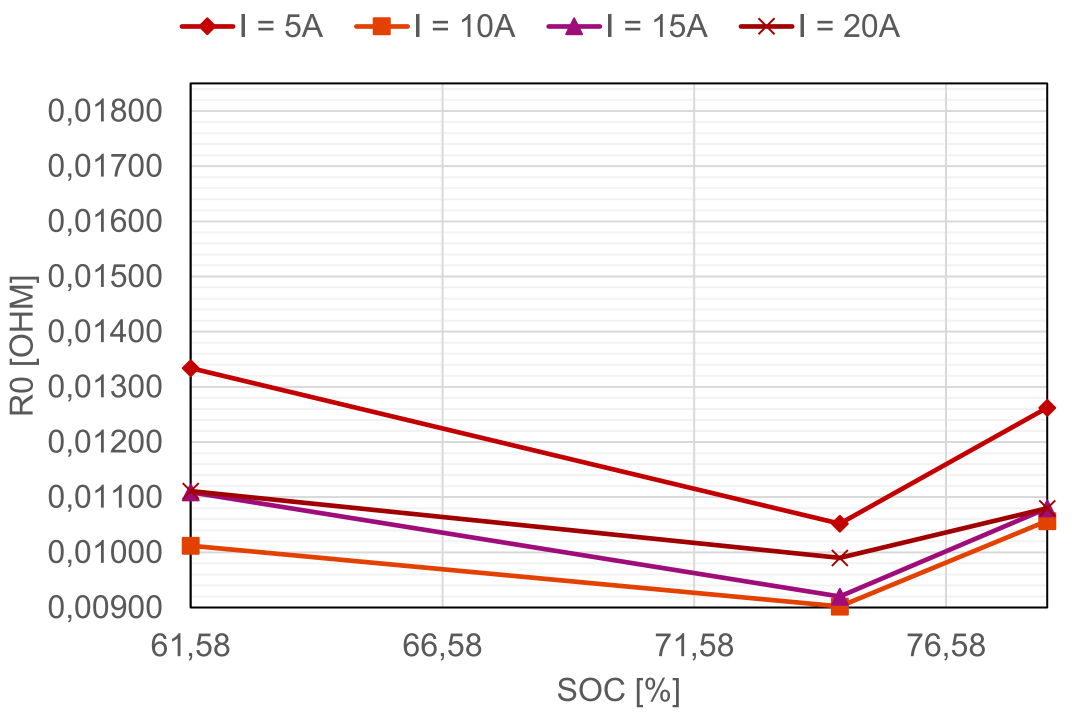

Figure 6.18. R_0 vs SoC for charge (first SoC estimation method)

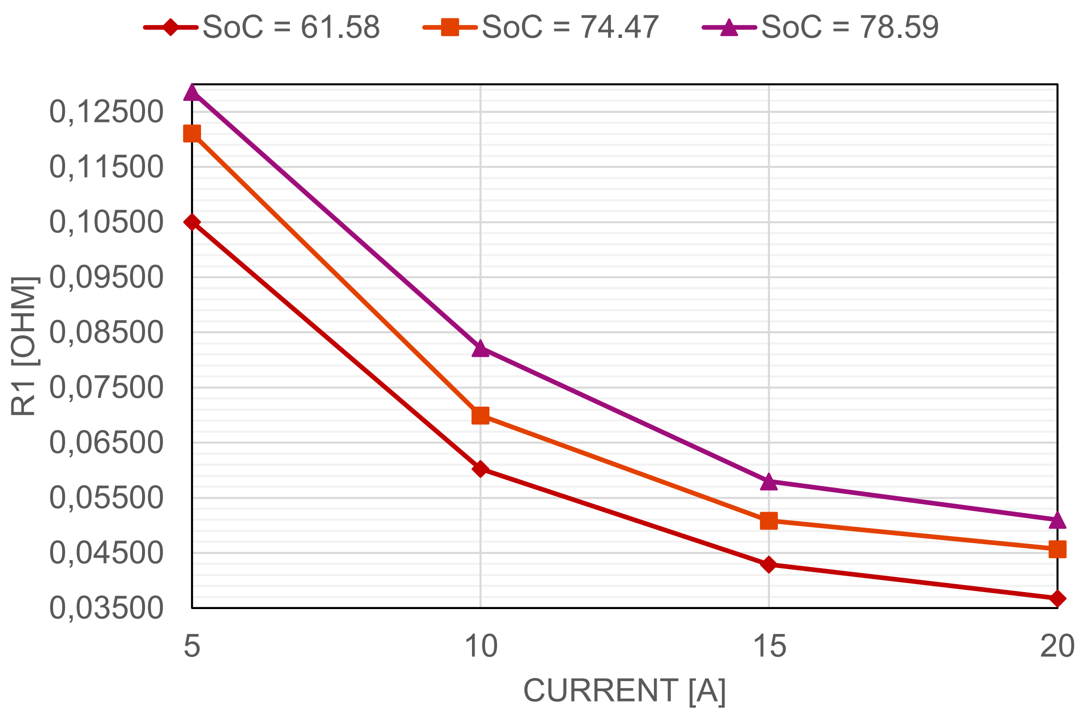

Figure 6.19. R_1 vs current for charge (first SoC estimation method)

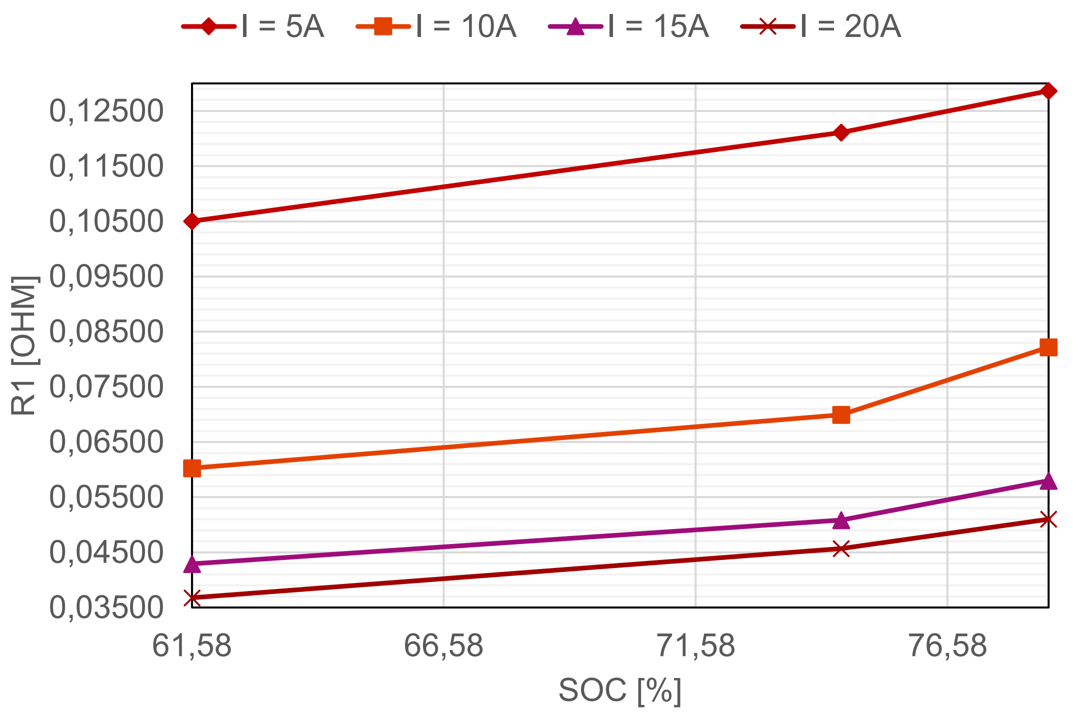

Figure 6.20. R_1 vs SoC for charge (first SoC estimation method)

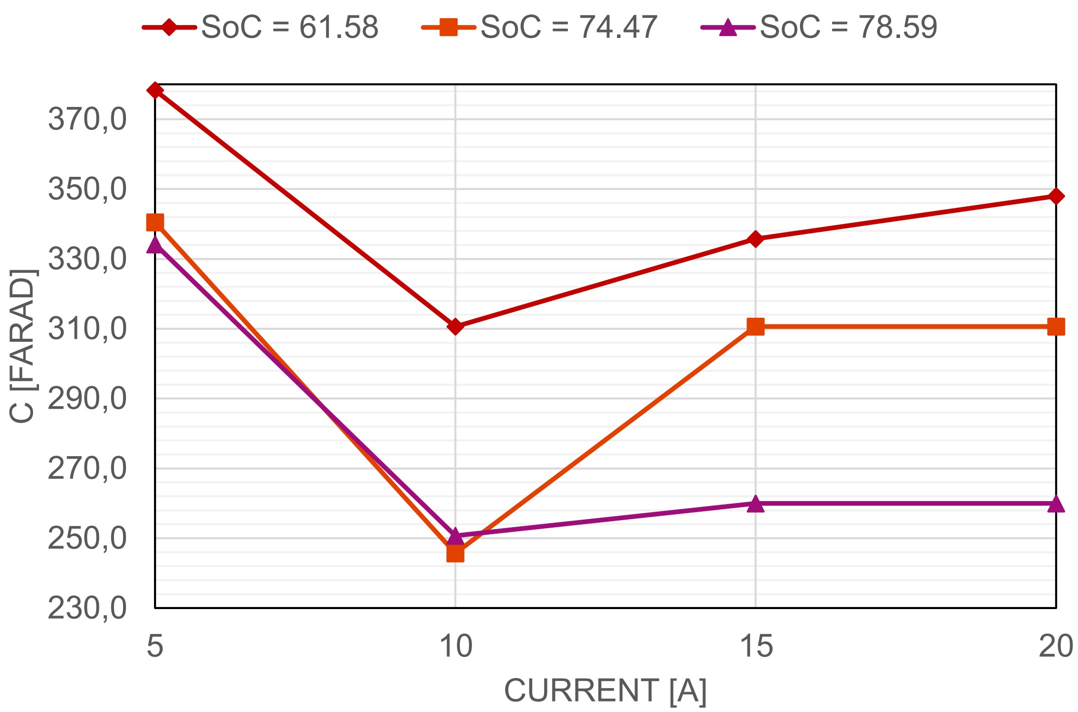

Figure 6.21. C vs current for charge (first SoC estimation method)

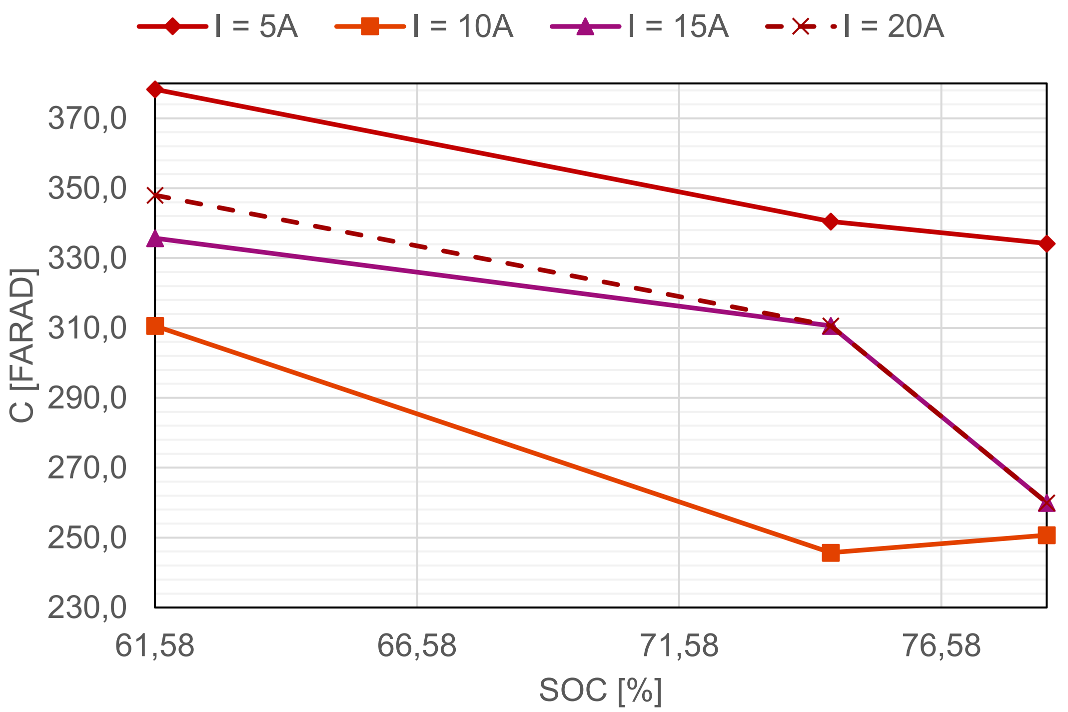

Figure 6.22. C vs SoC for charge (first SoC estimation method)

As an alternative, the values in table 6.4 have been found estimating only the initial SoC of the sequence from the OCV, and the SoC of the individual discharge impulses through Ah count method. As for the discharge results, R_1 variation between the two SoC estimation methods is negligible, as shown in figure 6.24, and R_0 variation shows a noticeable change, as shown in figure 6.23. The reasons are the same presented for the discharge case regarding the way the SoC estimation method influence the R_0 value obtained.

R_0 [ohm]		State of Charge [%]		
		62 %	74 %	78 %
Current [A]	5	0.01334	0.01052	0.01262
	10	0.01592	0.01381	0.01750
	15	0.01827	0.01749	0.01750*
	20	0.01721	0.01723	0.01750*
R_1 [ohm]		State of Charge [%]		
		62 %	74 %	78 %
Current [A]	5	0.10503	0.12110	0.12865
	10	0.06022	0.06992	0.08277
	15	0.04232	0.05084	0.05900*
	20	0.03611	0.04557	0.05200*
C [Farad]		State of Charge [%]		
		62 %	74 %	78 %
Current [A]	5	378.3	340.5	334.2
	10	310.6	245.9	255.7
	15	349.9	312.1	260.0*
	20	364.1	325.6	260.0*

Table 6.4. R_0 values for charge (second SoC estimation method)

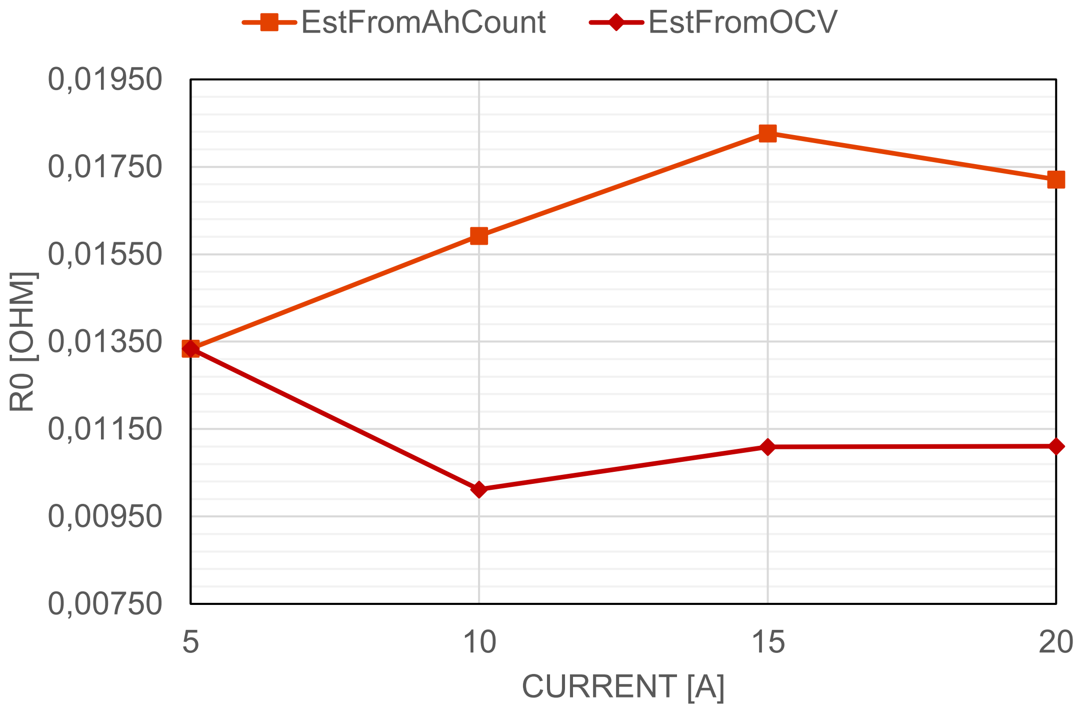

Figure 6.23. R_0 vs current for charge, SoC estimation methods comparison

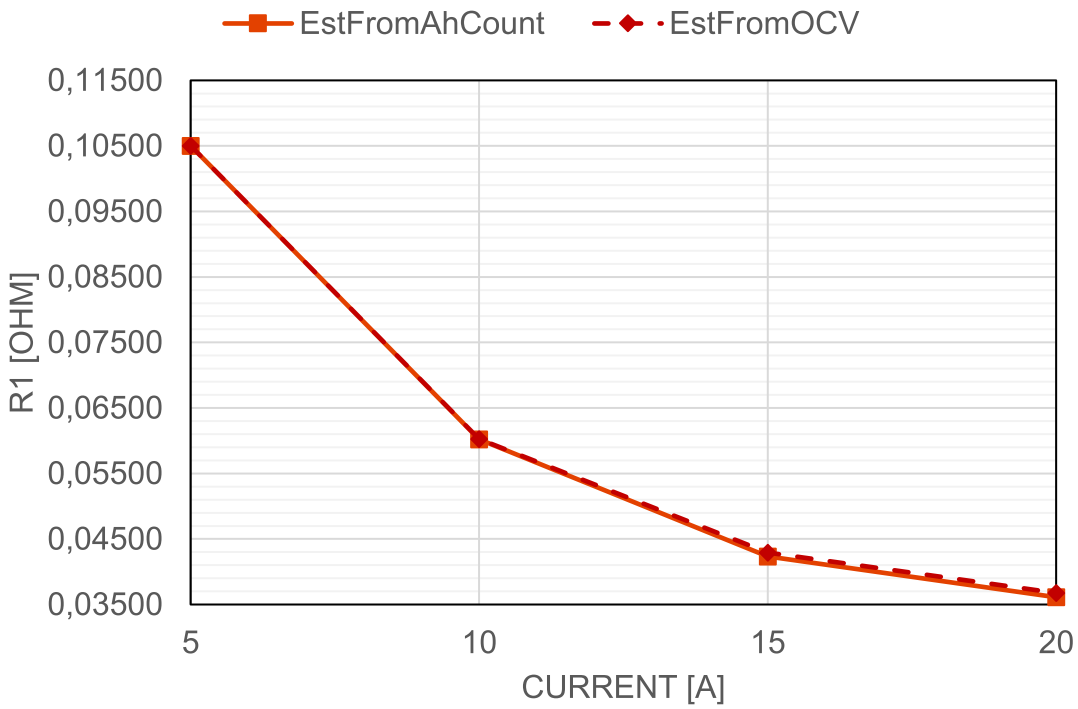

Figure 6.24. R_1 vs current for charge, SoC estimation methods comparison

6.1.3 Final parameters to be implemented

From the results shown, it is possible to make some considerations. In the parametrization, two different approaches have been followed to estimate the SoC during the tests. The second method, which consisted in estimating the initial SoC from the OCV value and the SoC evolution during the test from Ah counting, is considered the most reliable. This choice is made considering the affinity between this method and the actual condition of normal functioning of the model. As already stated, only R_1 has a clear monotone pattern both in charge and discharge, while R_0 and C do not. Thus, the full set of R_1 values depending on current and state of charge will be implemented. At the same time, the complete sets of R_0 and C values are not considered reliable enough to be taken as they are.

In detail, for R_0, during discharge only the influence of the SoC has been considered and during charge a single average value has been implemented. For what concerns the discharge, the R_0 profile versus the SoC is not monotone as shown in figure 6.25. Instead, in figure 6.26 the R_0 average over the current is plotted versus the SoC and its profile is monotone, reason for which it has been implemented in the final model. Regarding the charge, R_0 values do not show any pattern, thus their average value has been implemented.

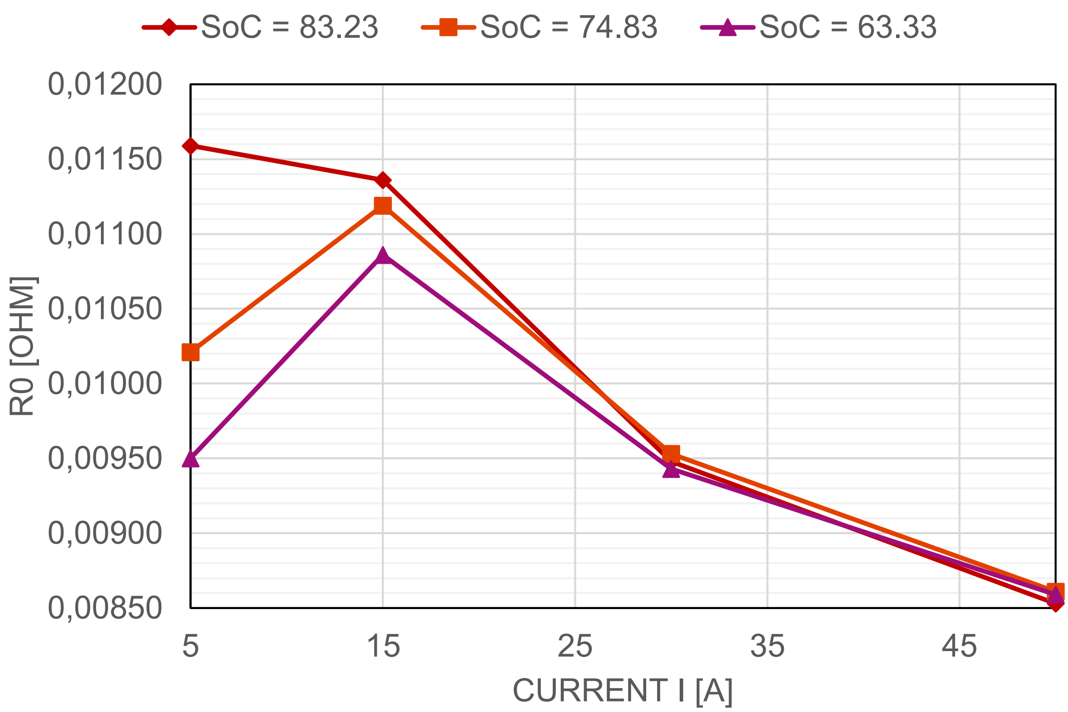

Figure 6.25. Profile of R_0 versus current for discharge

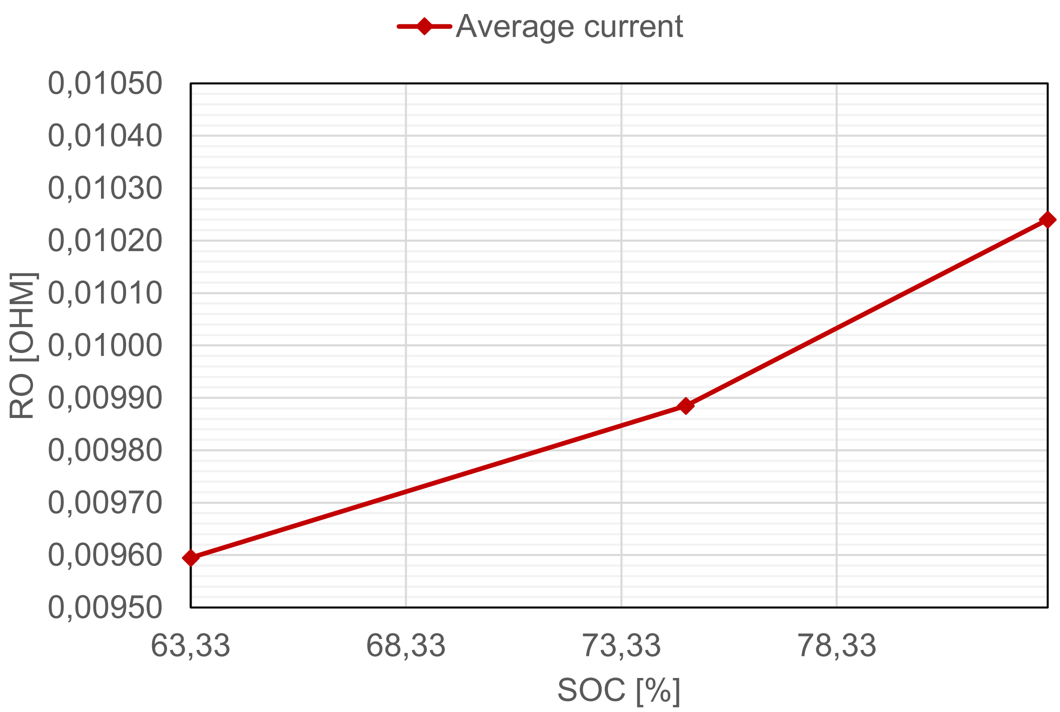

Figure 6.26. Profile of implemented R_0 values versus SoC for discharge

For what concerns C, the values are almost constant, exception made for the values calculated from the 5A impulses, for both the discharge and charge parametrizations. This deviation is due to the bidirectional power supply inaccuracy during the transient phase, shown in figure 6.27. It is possible to notice the presence of a spike before the current reaches the final constant value. This phenomenon occurs only when the bidirectional power supply is required to deliver small currents.

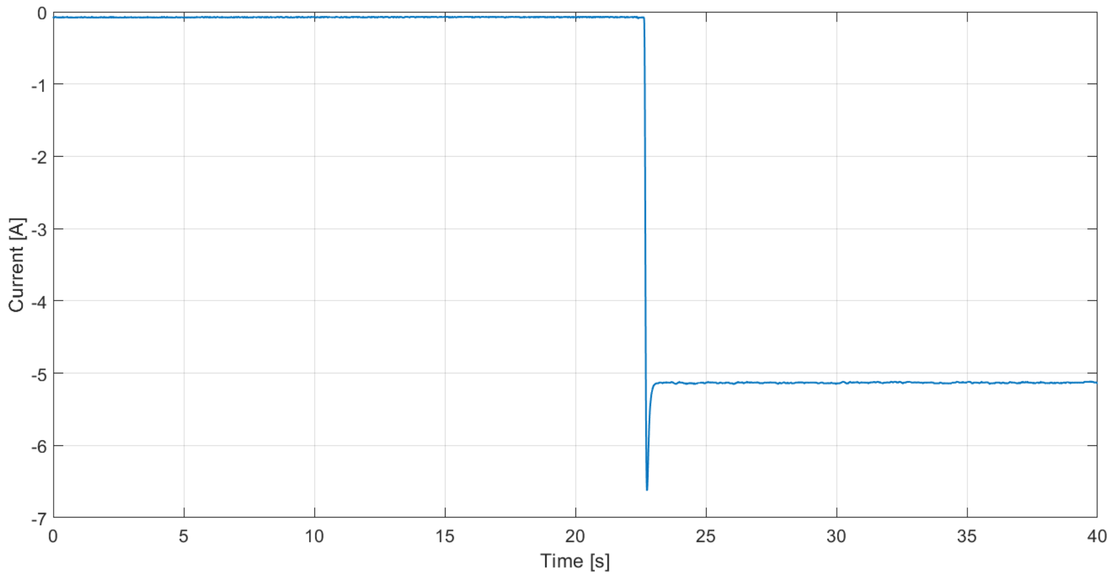

Figure 6.27. Bidirectional power supply behavior when draining a small current

In table 6.5 and table 6.6 the final parameters implemented in the model are shown.

R_0 [ohm]		State of Charge [%]		
		83,23	74,83	63,33
Average		0,01024	0,00989	0,00960
R_1 [ohm]		State of Charge [%]		
		83,23	74,83	63,33
Current [A]	0	0,09562	0,08219	0,07404
	5	0,06011	0,05215	0,04623
	15	0,02478	0,02194	0,02026
	30	0,01352	0,01193	0,01150
	50	0,00826	0,00748	0,00738
C [Farad]		Average		
		215,8		

Table 6.5. Final parameters values for the discharge phase

R_0 [ohm]		Average		
		0,01078		
R_1 [ohm]		State of Charge [%]		
		61,58	74,47	78,59
Current [A]	0	0,21060	0,22650	0,24765
	5	0,10503	0,12110	0,12865
	10	0,06022	0,06992	0,08277
	15	0,04232	0,05084	0,05900
	20	0,03611	0,04557	0,05200
C [Farad]		Average		
		298,2		

Table 6.6. Final parameters values for the recharge phase

6.2 Tests for validation

6.2.1 Validation tests design

For the validation, the same Exide 60Ah600A previously characterized, an Exide 50Ah420A and an Exide 70Ah620A have been tested. The choice to test also the 50Ah and the 70Ah is due to the will to verify the effectiveness of the model for simulating different batteries in use of FCA vehicles. The main difference of the validation tests with respect to the parametrization tests is the absence of relaxations between the several discharge/charge impulses.

On the Exide 60Ah600A three tests in total have been performed. The first test regards the discharge phase and is composed by:

- Complete recharge.
- Fast discharge to $SoC = 80\%$ considering Ah counting method.
- 24-hour relaxation.
- Sequence of several discharge steps of variable length at different current levels. The sequence is shown in figure 6.28

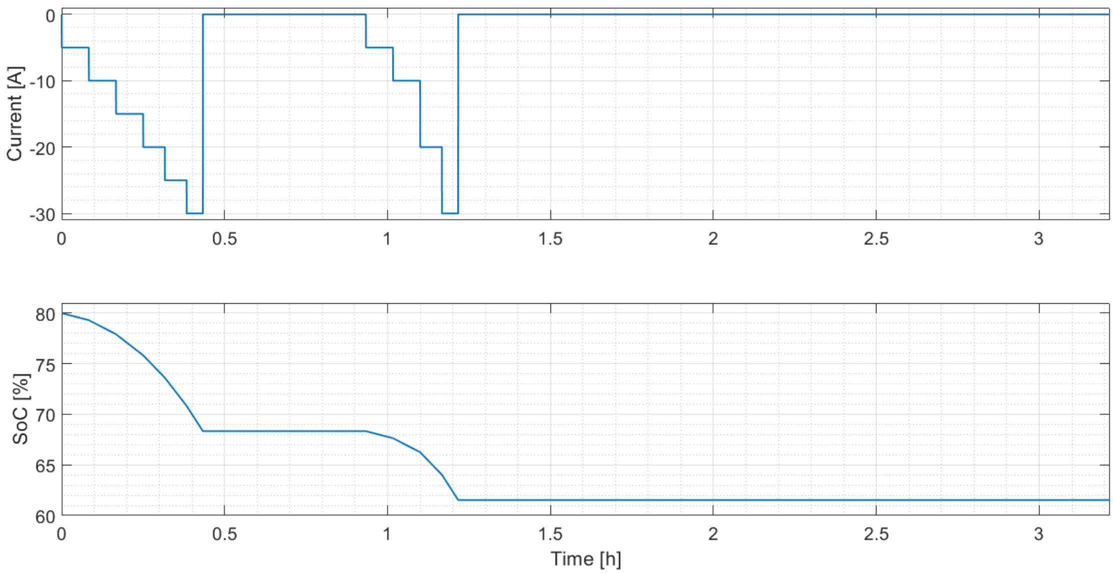

Figure 6.28. Discharge test for validation, Exide 60Ah600A

The second test, regarding the recharge phase, is similar and is performed starting from the final condition of the battery of the previous test after a 24 hours relaxation. Thus, the steps of the test are:

- End of discharge validation tests (figure 6.28).
- 24-hour relaxation.
- Sequence of several charge steps of variable length at different current levels. The sequence is shown in figure 6.29.

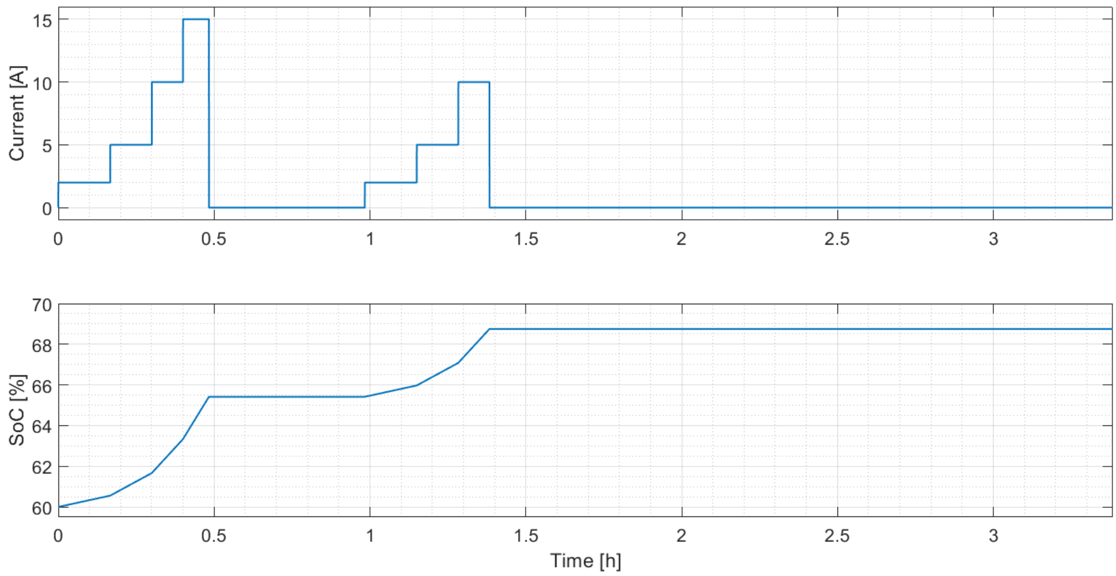

Figure 6.29. Recharge test for validation, Exide 60Ah600A

The third and final test regards both the recharge and discharge phases and is aimed to verify the ability of the model to reproduce the transitions between the two working conditions. For this purpose, strong current transitions have been considered, much steeper than the transitions registered during road tests. In fact during this sequence, the current pass from -50A to 15A in less than 20 minutes. The test is composed by:

- Complete recharge.
- Fast discharge to $SoC = 80\%$ considering Ah counting method.
- 24-hour relaxation.
- Sequence of several charge/discharge steps of variable length at different current levels. The sequence is shown in figure 6.30.

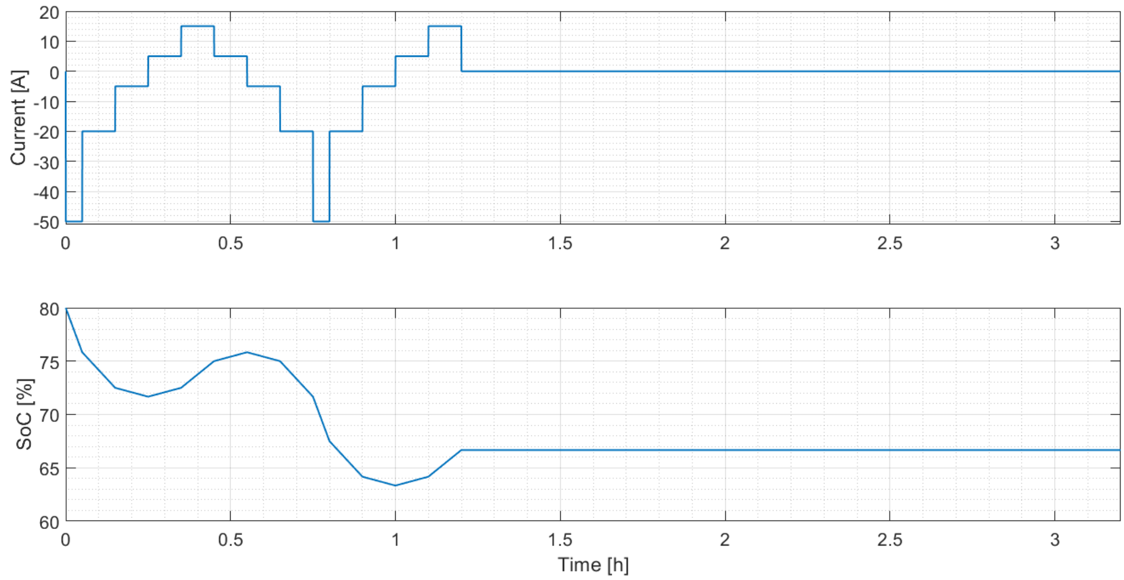

Figure 6.30. Mixed test for validation, Exide 60Ah600A

For what concerns the Exide 50Ah420A and the Exide 70Ah620A tests, the same first two procedures followed for the Exide 60Ah600A have been used.

6.2.2 Validation tests results

In figure 6.31 and figure 6.32, the discharge and recharge tests performed on the Exide 60Ah600A are shown. The battery behavior is the expected one, showing a series of voltage steps corresponding to the current profile.

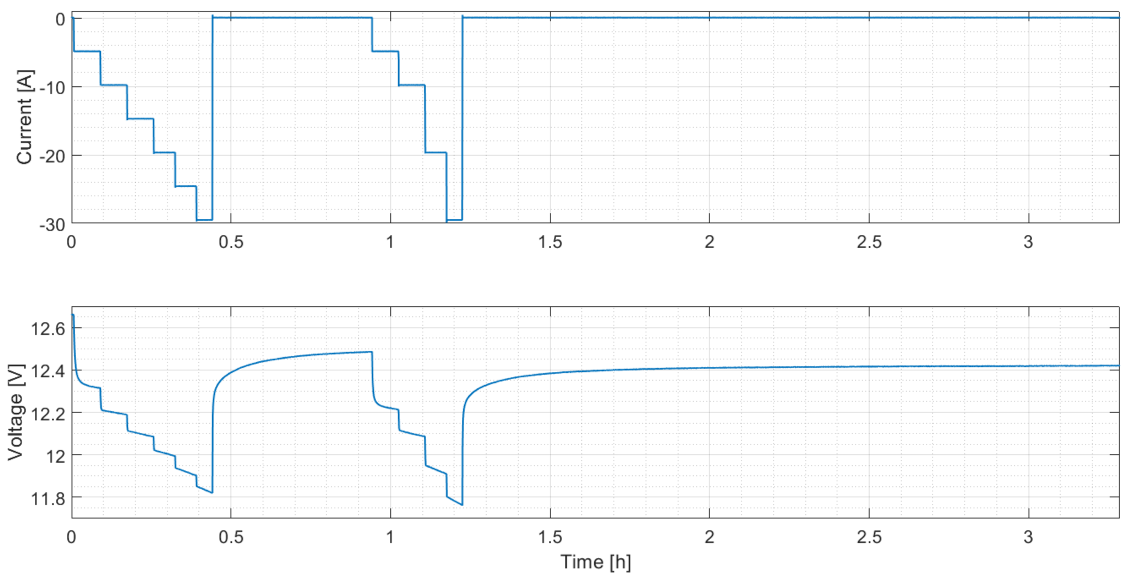

Figure 6.31. Discharge test for validation, Exide 60Ah600A

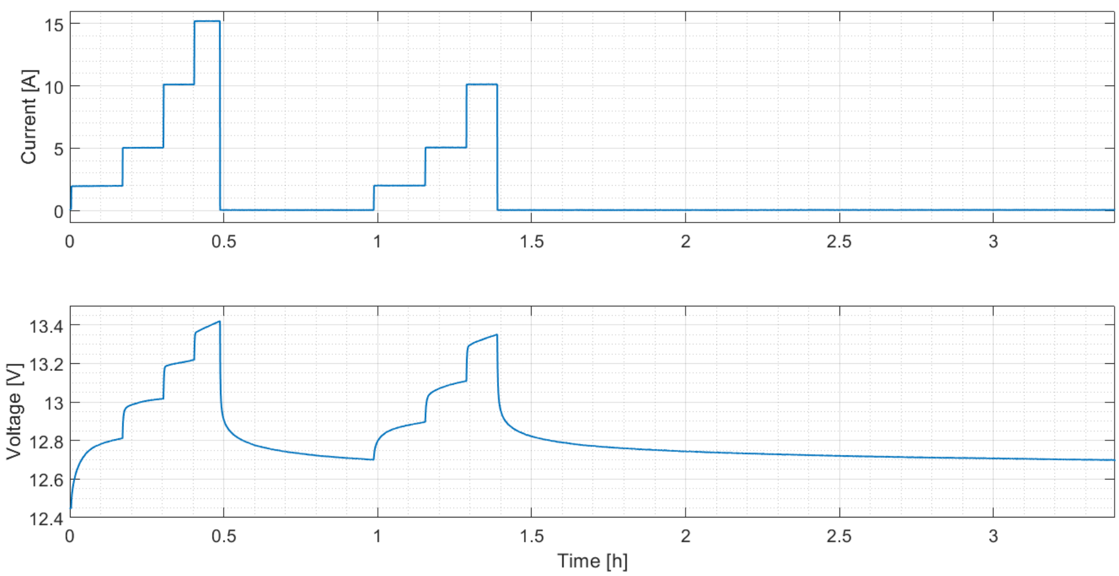

Figure 6.32. Charge test for validation, Exide 60Ah600A

In figure 6.33, the comparison between the two subsequences of the discharge test is shown; the same current is drawn, but the SoC of the battery is different. As expected, the two voltage levels corresponding to the same current intensity are slightly shifted due to the smaller value of the OCV component at lower SoC.

The same observation can be made for the charge test, as shown in figure 6.34. The larger voltage obtained for the higher SoC is due to the larger value of the OCV component and to a slight increase of the internal resistance.

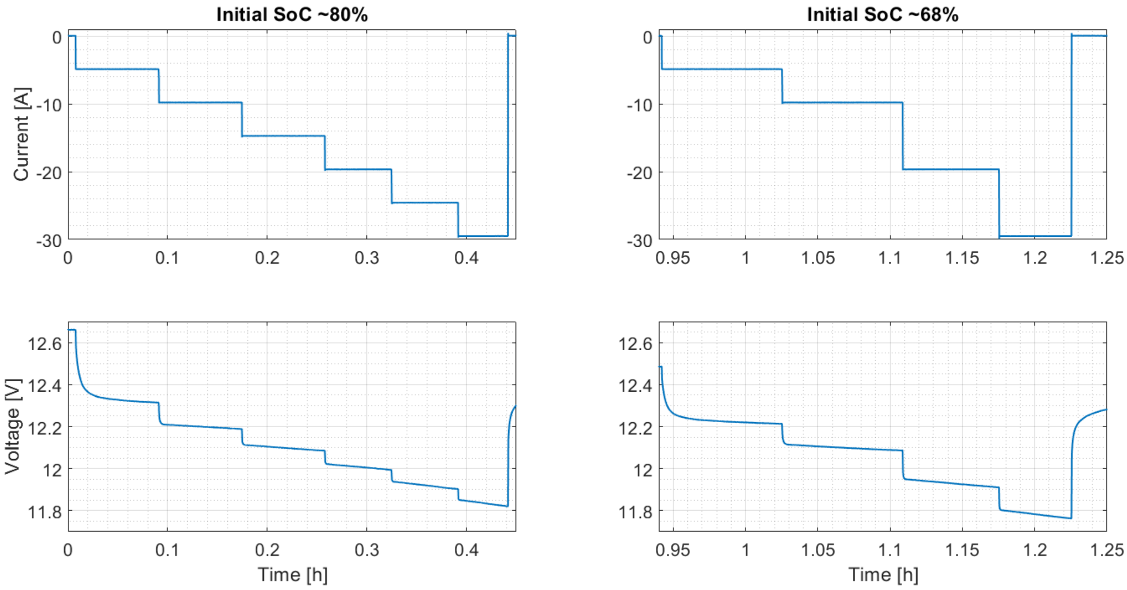

Figure 6.33. Detail of the discharge test, Exide 60Ah600A

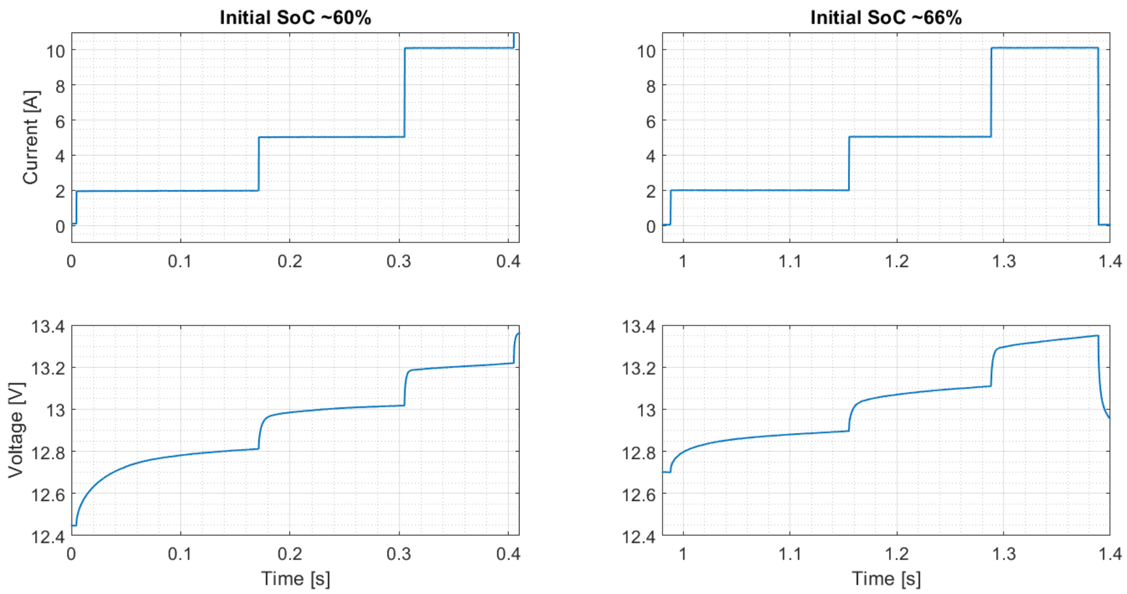

Figure 6.34. Detail of the charge test, Exide 60Ah600A

For what concerns the mixed test, shown in figure 6.35, the battery behavior is similar, but an unexpected feature can be observed. After the transition from charge to discharge at $t \approx 0.55h$ the values and the profile of the voltage are unusual, showing the presence of the effects of concentration polarization.

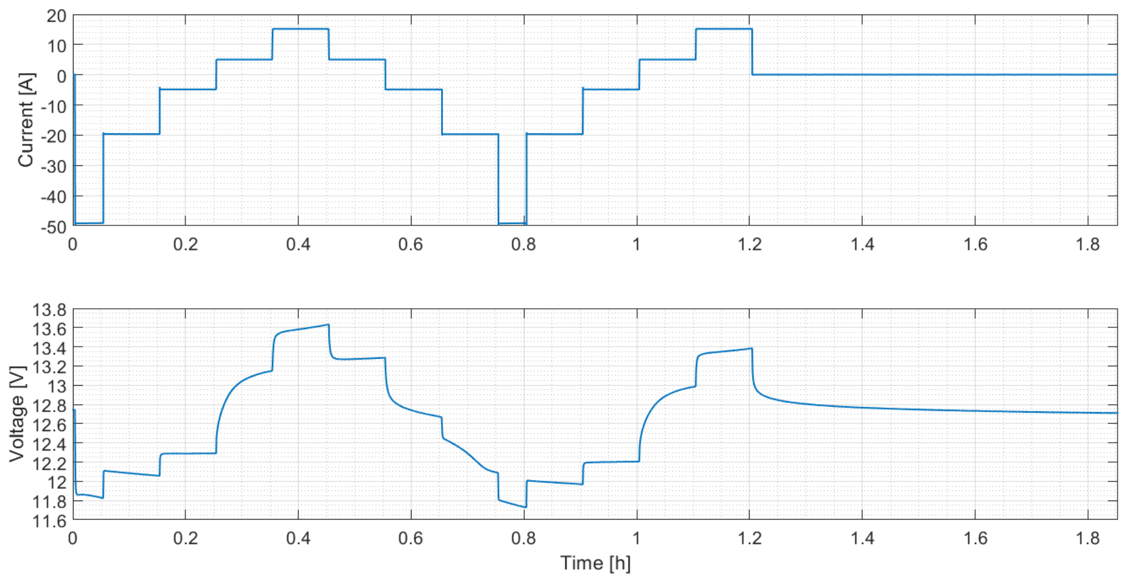

Figure 6.35. Mixed test for validation, Exide 60Ah600A

The unexpected behavior is shown in detail in figure 6.36. Observing the voltage profile, the voltage difference between the two steps where a current of -5A is drawn is ~0.35V. Considering that the difference of SoC between the two points is ~2%, this voltage difference is way higher than expected. In addition, during the discharge step at -10A starting at $t \approx 0.65h$, the voltage shows a particular profile. The presence of these two features is probably due to the insurgence of polarization effects from $t \approx 0.55h$ to $t \approx 0.75h$.

In fact, at $t \approx 0.55h$, the battery comes from a recharge, which implies that the electrolyte concentration is higher near the plates surface compared to the bulk density of the solution. This causes the battery to behave as it has a higher SoC, which implies a higher voltage. Starting to discharge the battery, the first effect is to reduce the concentration of the electrolyte near the plates surface, and thus, to restore the expected value of the electrolyte concentration. This process is reflected on the voltage behavior, and in fact, at $t \approx 0.75h$ the voltage goes back to the expected level.

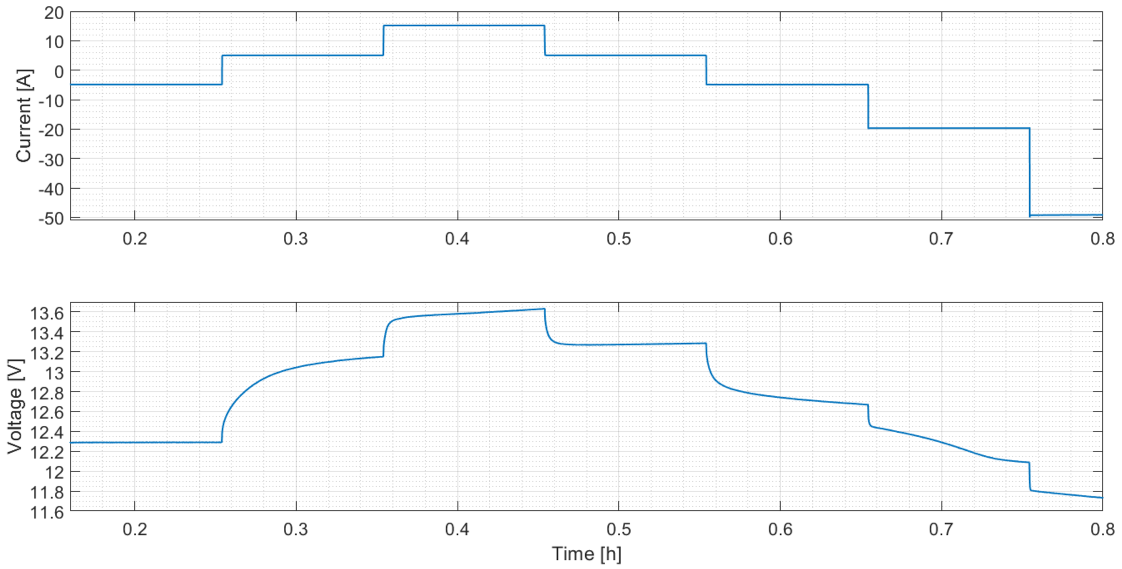

Figure 6.36. Detail of the mixed test, Exide 60Ah600A

From figure 6.37 to figure 6.40 the results of the tests performed on the Exide 50Ah420A and the Exide 70Ah620A are shown. The voltage profiles are similar to the profiles of the tests performed on the Exide 60Ah600A and the same consideration can be done.

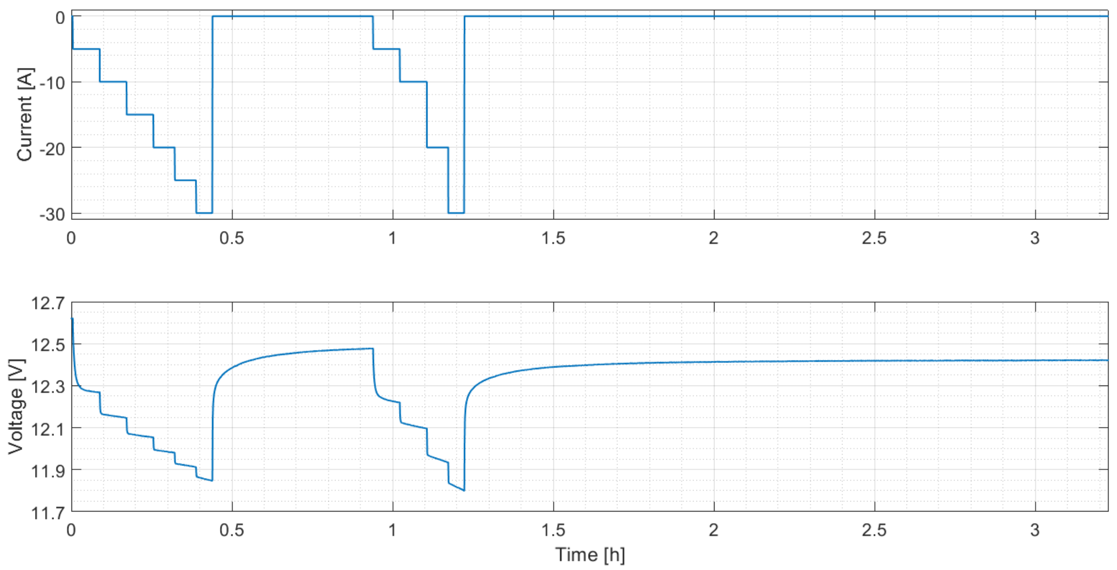

Figure 6.37. Discharge test for validation, Exide 70Ah620A

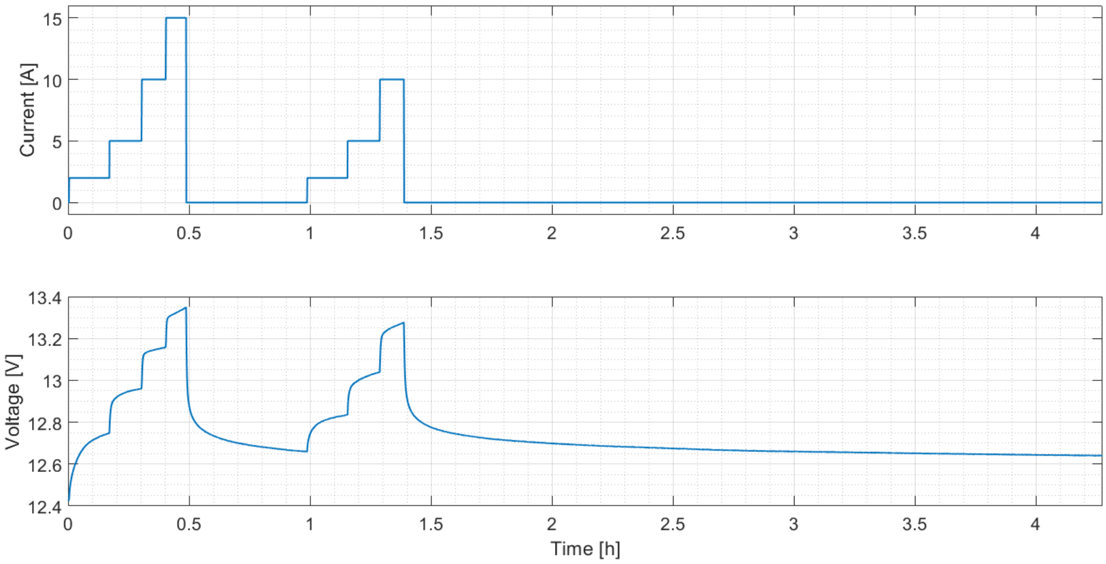

Figure 6.38. Charge test for validation, Exide 70Ah620A

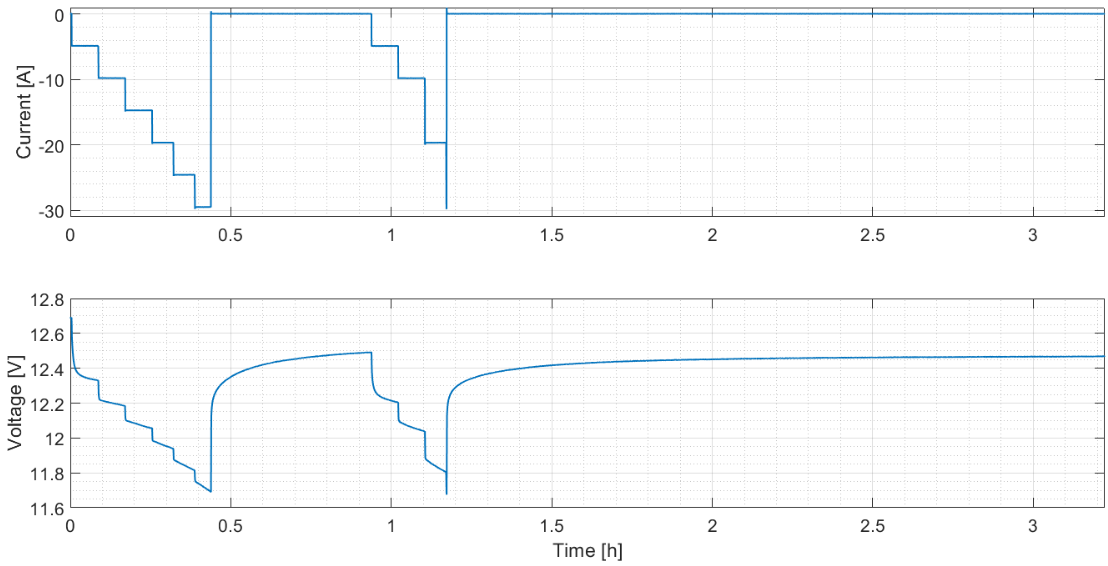

Figure 6.39. Discharge test for validation, Exide 50Ah420A

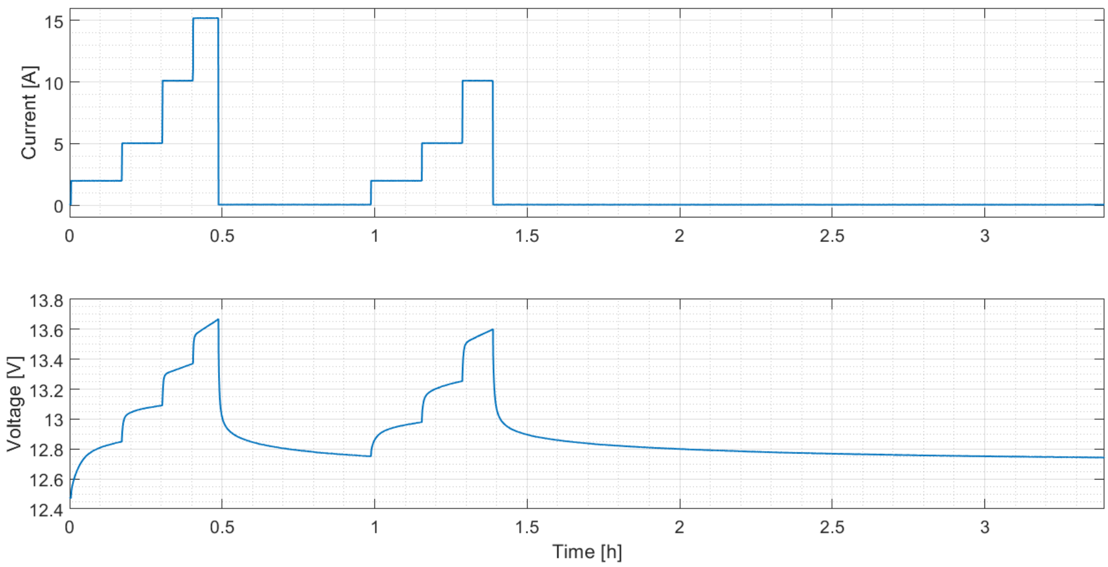

Figure 6.40. Charge test for validation, Exide 50Ah420A

Chapter 7
Model validation

The validation of the model has been made using the experimental tests presented in paragraph 4.2 and a set of in-vehicle acquisitions. The current of the real data is fed to the model as the input for the simulation. The voltage output by the model is then compared with the real voltage. To evaluate the impact of this error in terms of the Ah difference at the end of the test.

7.1 Exide 60Ah600A

In figure 7.1, the comparison between the simulated voltage and the real voltage for the discharge test is shown. The result can be considered satisfactory, exception made when the current drops to zero. Condition that, however, is not representative of the normal operation of the battery and that the model is not intended to reproduce. In fact, as already stated in paragraph 3.1, to simulate the battery relaxation transient, a second order model with a second longer time constant would be needed.

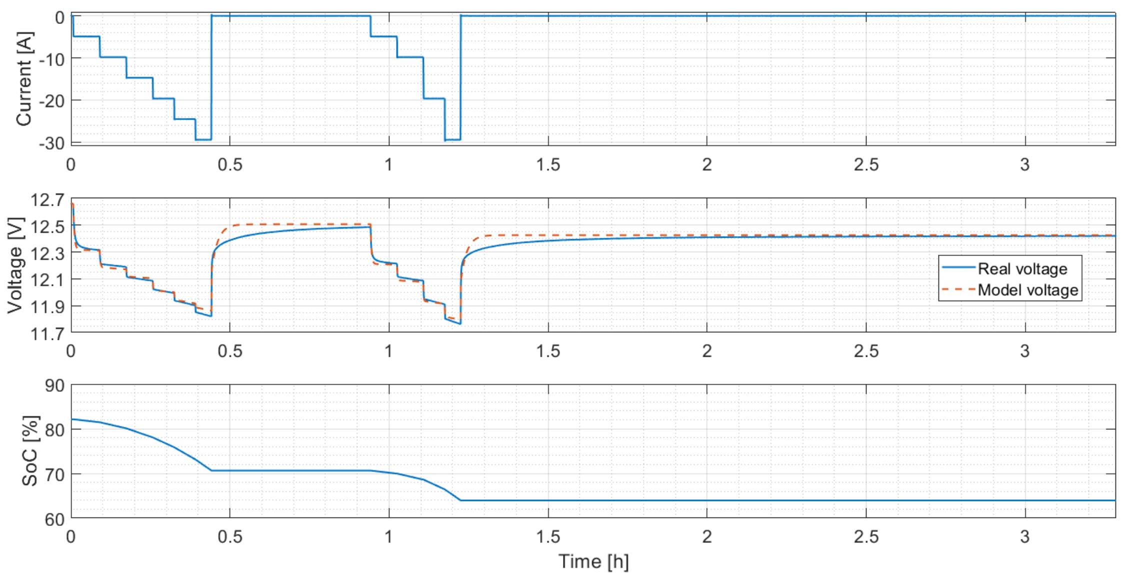

Figure 7.1. Model and real voltages comparison for the discharge test, Exide 60Ah600A

In figure 7.2, the voltage error for the same test is shown. The error generally remains below 0.05 V and reaches ~0.1 V only when $I_{batt} = 0$. Anyway, it can be noticed that, after ~30 minutes, the two voltages are at the same level, which implies the identity between the real SoC and the SoC calculated by the model.

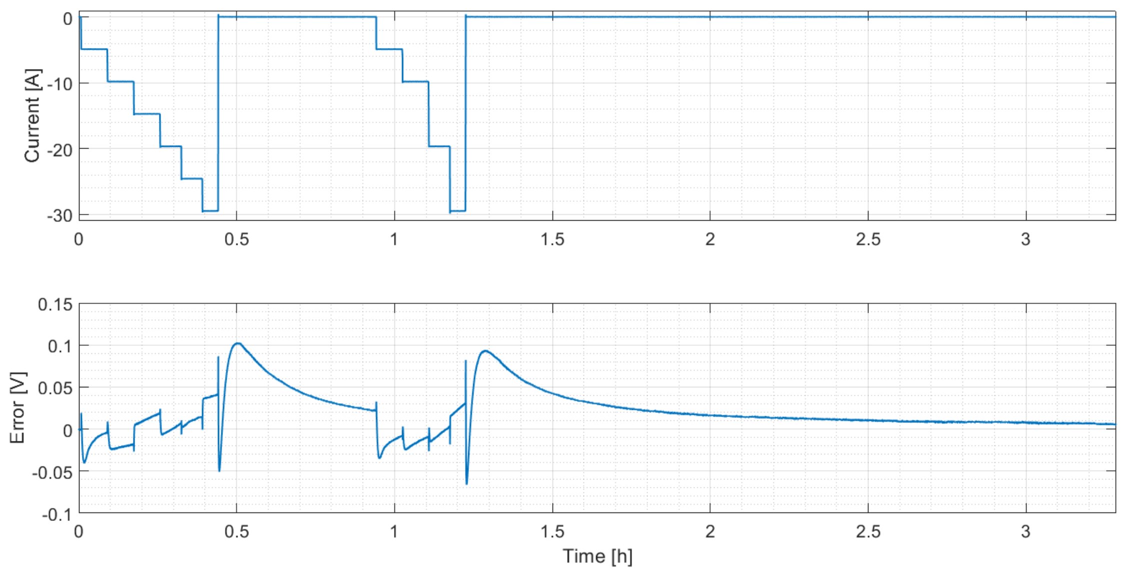

Figure 7.2. Voltage error of the discharge test, Exide 60Ah600A

In figure 7.3, the comparison between the simulated voltage and the real voltage for the charge test is shown. For this test too, the result, exception made for the condition with null current, is satisfactory.

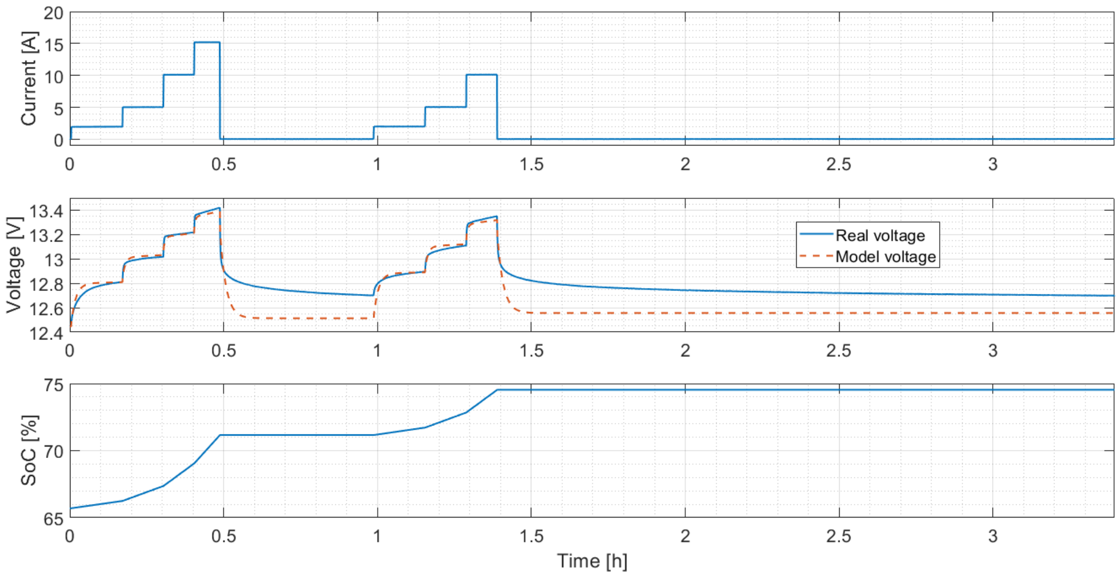

Figure 7.3. Model and real voltages comparison for the charge test, Exide 60Ah600A

The voltage error, shown in figure 7.4, is generally below 0.1 V but reaches ~0.25 V during the battery relaxation. Contrary to the discharge test, after the final 2 hour relaxation the error is still relevant, ~0.15 V, which could be due to a discrepancy between the real SoC and the SoC calculated by the model. However, measuring the OCV the day after the test, the voltage is ~12.7 V, as the final voltage of the simulation, confirming the SoC estimation made by the model. Nevertheless, it draws attention to the longer time required by the battery to relax after a recharge rather than after a discharge.

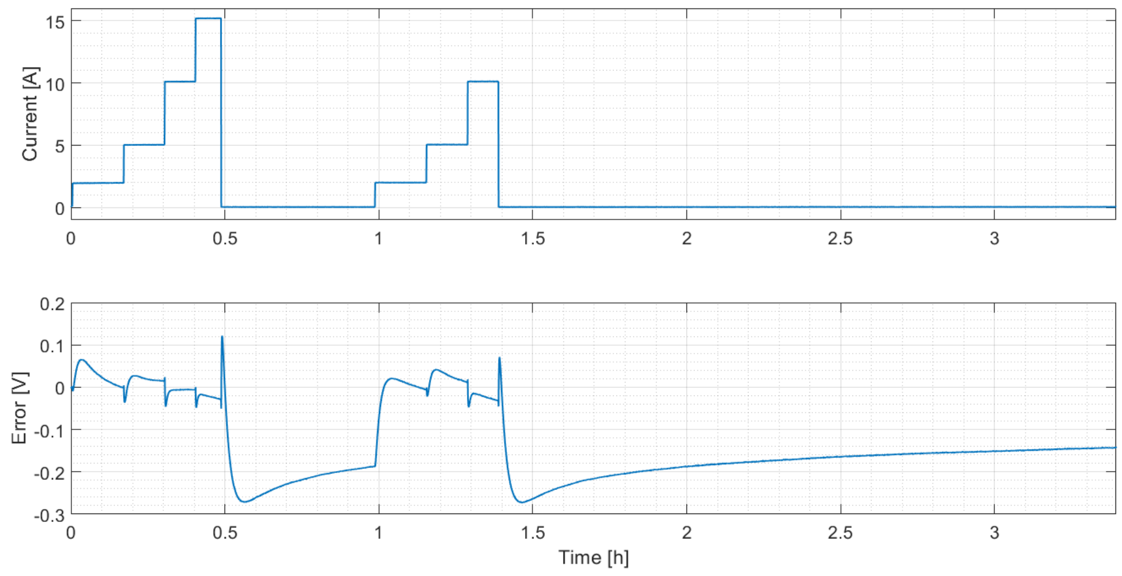

Figure 7.4. Voltage error of the charge test, Exide 60Ah600A

In figure 7.5, the comparison between the real voltage and the simulated voltage for the mixed test is shown. The result is satisfactory, but it is possible to highlight a larger inaccuracy during the transitions between charge and discharge at $t \approx 0.25\ h$, $t \approx 0.55\ h$ and $t \approx 1\ h$. As already stated in paragraph 4.2.2, it is due to the presence of effects of concentration polarization that the model is not able to reproduce.

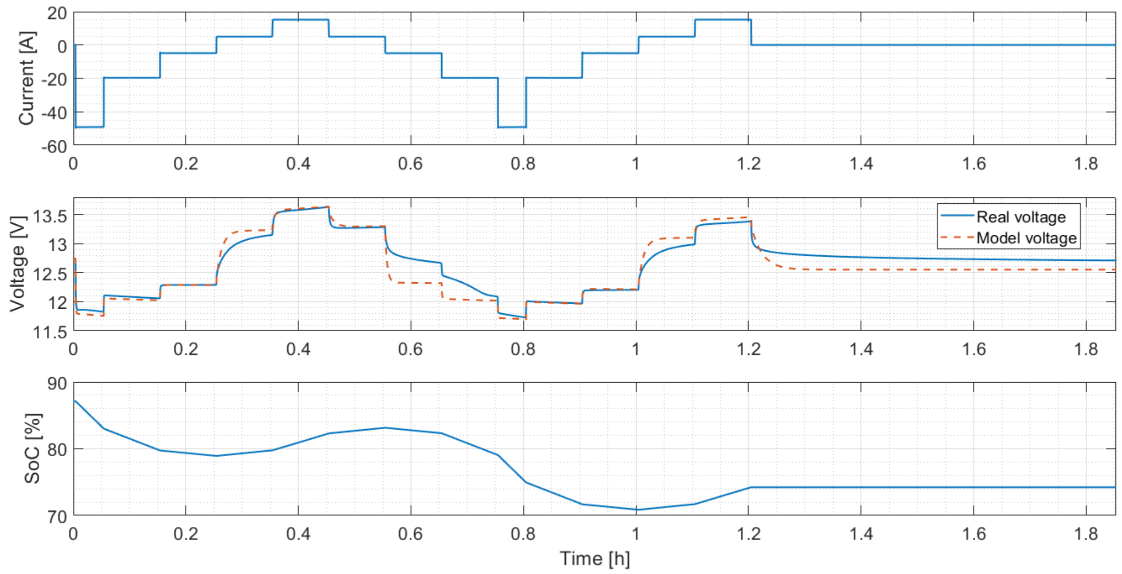

Figure 7.5. Model and real voltages comparison for the mixed test, Exide 60Ah600A

In figure 7.6, the voltage error is shown. The error is above 0.1 V only after the charge/discharge transitions and during the final relaxation of the battery. More in detail, the error after the two transitions from discharge to charge, at $t \approx 0.25\ h$ and $t \approx 1\ h$, has a peak of ~0.25 V but drops to ~0.1 V after 5-6 minutes. The error after the transition from charge to discharge, at $t \approx 0.55\ h$, is more severe. It presents a peak of ~0.5V and drops to ~0.1 V in more than 10 minutes.

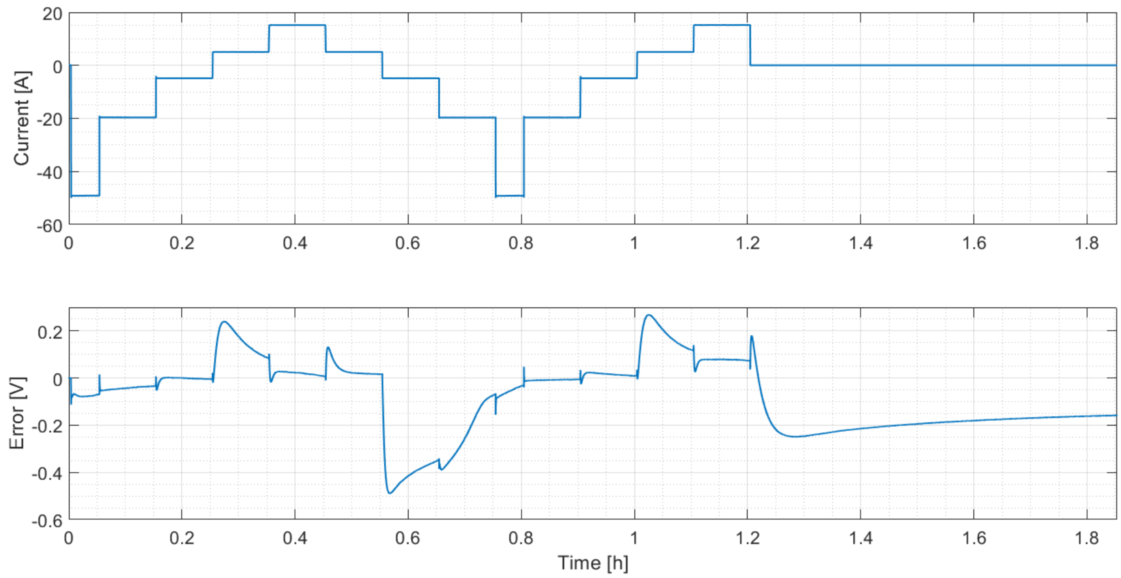

Figure 7.6. Voltage error of the charge test, Exide 60Ah600A

7.2 Exide 50Ah420A and Exide 70Ah620A

For batteries different from the Exide 60Ah600A on which the model has been parametrized, a simple assumption has been made. Considering two batteries of different size discharged with a current of the same intensity, the voltage drop will be larger for the battery with the smaller nominal capacity. For this reason, the actual current fed to the model will not be the real current but:

$$I_{batt,input} = \frac{60}{C_{20}} I_{batt,real}$$

where C_{20} is the nominal capacity of the tested battery and 60 is the nominal capacity of the Exide 60Ah600A used for the parametrization.

In figure 7.7 and figure 7.8, the comparison between the real voltage and the simulated voltage for the discharge and charge tests of the Exide 50Ah420A is shown. The voltage error, exception made for the $I_{batt} = 0$ condition, remains below 0.15 V, which is considered a good result.

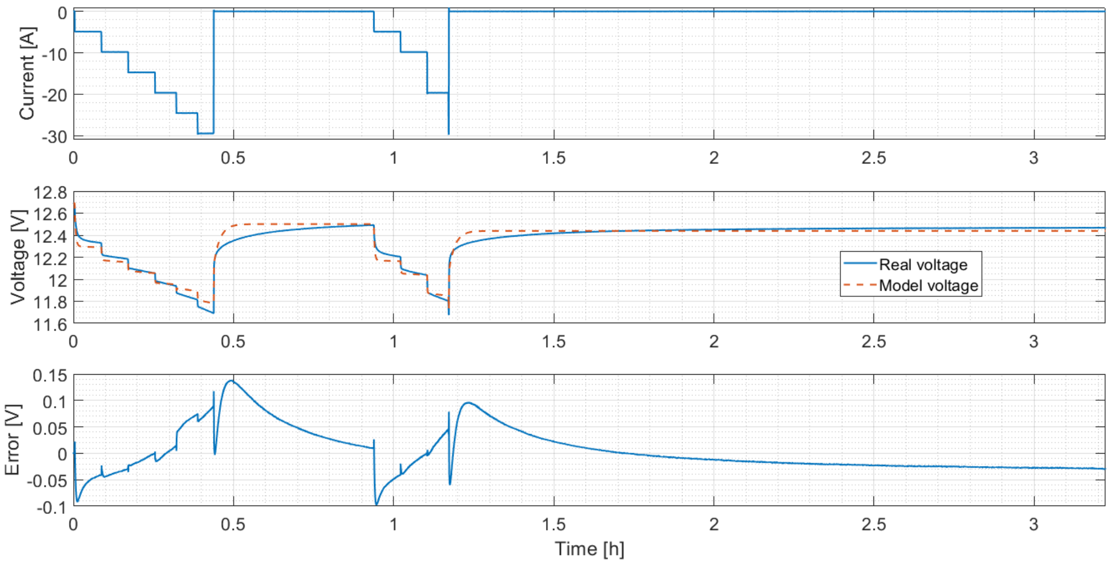

Figure 7.7. Voltage comparison and voltage error for discharge test, Exide 50Ah420A

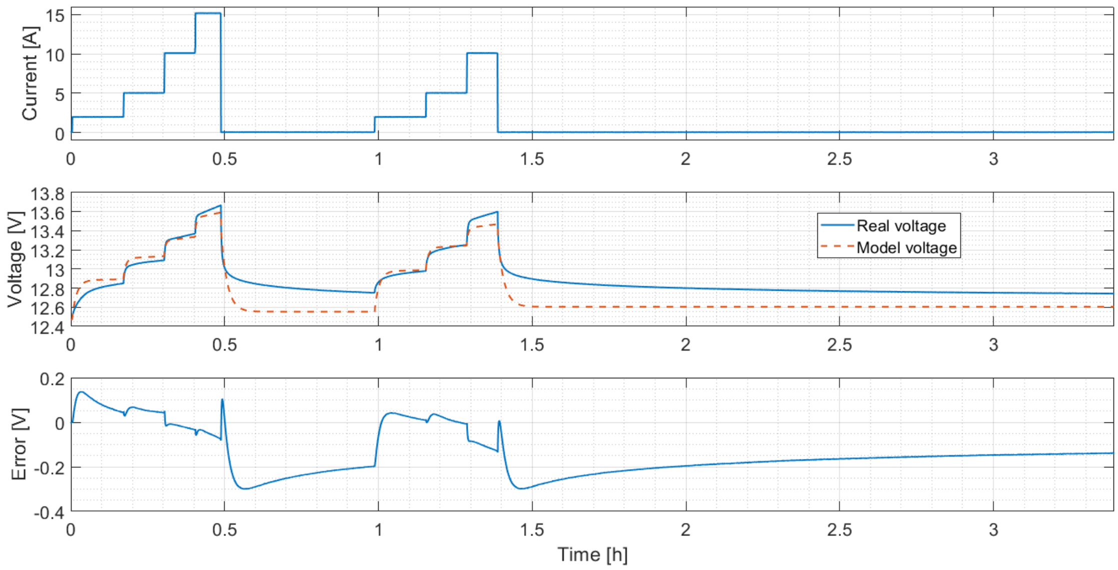

Figure 7.8. Voltage comparison and voltage error for charge test, Exide 50Ah420A

In figure 7.9 and figure 7.10, the comparison between the real voltage and the simulated voltage for the discharge and charge tests of the Exide 70Ah620A is shown. The voltage error, exception made for the $I_{batt} = 0$ condition, remains below 0.1 V, which is considered a good result.

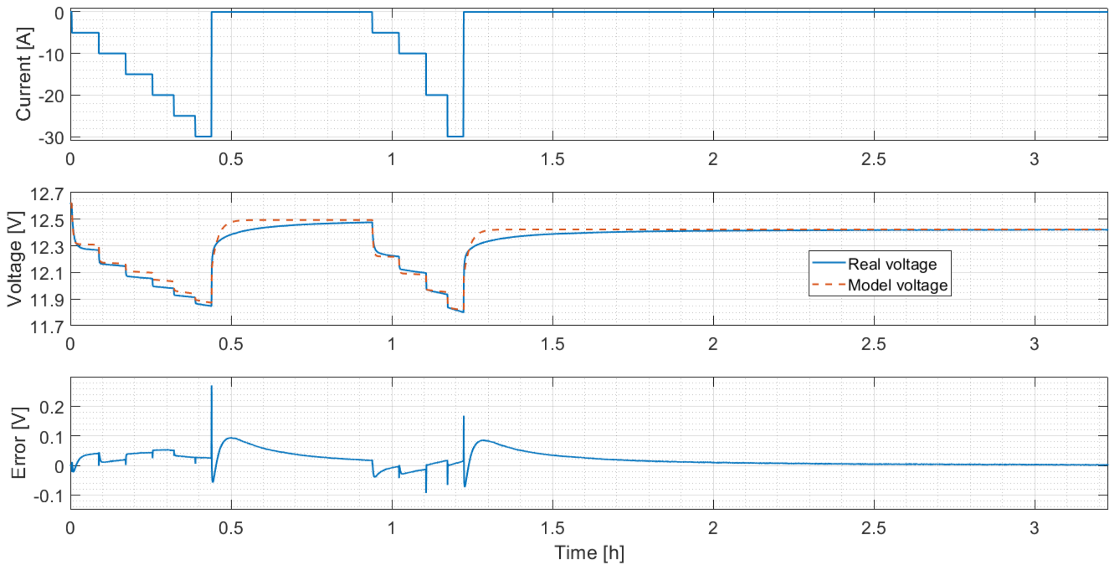

Figure 7.9. Voltage comparison and voltage error for discharge test, Exide 70Ah620A

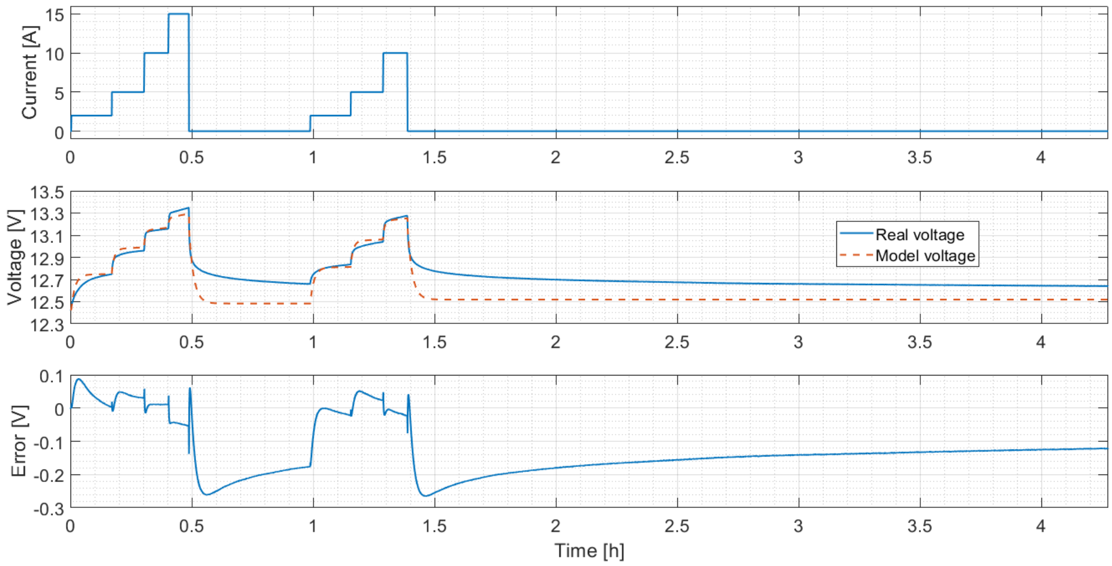

Figure 7.10. Voltage comparison and voltage error for charge test, Exide 70Ah620A

Chapter 8

Conclusions

The objective of this thesis, as already stated in the introduction, was to develop a lead-acid battery model capable to reproduce the car battery behavior when the vehicle is running. This working condition is characterized by specific ranges of current and SoC:

$$I_{batt} \approx -50 \div 20\ A \qquad and \qquad SoC \approx 60 \div 80\%$$

The results of the validation showed the good level of accuracy of the model when simulating the Exide 60Ah600A used for the parametrization but also the capability of the model to reproduce the voltage profiles of EFB batteries of different size, thanks to a simple linear scaling of the input current fed to the model.

Currently, the main limits of the model are the absence of the temperature influence, the need of a validation process for high intensity currents in discharge (required for cranking) and the inability to reproduce the polarization effects. In future, some additions could be made to extend the sensitivity of the model to different working condition.

To introduce the temperature influence, different SoC-OCV curves for different temperatures (they can be easily obtained from the battery manufacturer) should be implemented, and for the effect of the temperature on the battery internal resistance, a new set of experimental tests, much more complex and long to perform have to be done.

For the use of the model with currents of high intensity, the best solution is to design two small sets of experimental tests, one for the parametrization and one for the validation. Procedures similar to the parametrization tests presented in this thesis can be used.

The final improvement should concern the inability of the model to reproduce the polarization effects. The best solution would be to implement a physical sub model able to reproduce the diffusion phenomena inside the electrolyte, giving the instantaneous concentration of the electrolyte at the surface of the battery plates. The concentration of the electrolyte is what really defines the battery SoC, and then, estimating the SoC on the concentration of the electrolyte volume closer to the plates, instead of using the overall battery SoC, would give a much more accurate estimation of the OCV component of the terminal voltage.

For what concerns the large error encountered during the condition with null current, implementing a second RC parallel could improve the final result but in fact, the goodness of this solution is not sure and no real need of the model simulating such condition is present.

Appendix A

The code of the algorithm starts with the definition of all the inputs and the initial values of R_0, R_1 and C. A first simulation is made using these initial parameters.

```
clear all
cd
'D:\users\f63930c\Documents\MATLAB\validation\Parametrizati
on_example'
load '30A90sec.mat';          % Impulse acquisition
load 'OCV_60Ah600A.mat';      % SoC-OCV curve
TimeStep = time(2);
TimeEnd  = round(time(end)/TimeStep)*TimeStep;
NominalCapacity = 60;
% Initial parameters definition
R0_start=0.001;
R0(1)=0.001;
R1_start=0.001;
R1(1)=0.001;
C_start=10;
C(1)=10;
% Initial simulation
R0_sl=R0(end); R1_sl=R1(end); C_sl=C(end);
sim ThesisModel.slx
plot(V_batt_model.time,V_batt_model.signals.values)
```

Now, the times corresponding to point B and point D (shown in figure 5.1) of the real impulse are defined.

```
% Target0: point B time
pointB=18.89; % [sec]
target0=int16((pointB+TimeStep)*(1/TimeStep));
% Target1: point D time
pointD=106.00; % [sec]
target1=int16((pointD+TimeStep)*(1/TimeStep));
% TargetC: from point B to point D
target_start=target0;
target_end=target1;
```

The main for-cycle is defined, and R_0, R_1 and C are calculated as described in paragraph 5.2. Every time a parameter is calculated, it is compared with its value found during the previous step of the for-cycle, and if they are equal the *check* variable is incremented of one unity, else it is defined equal to 0. When the *check* value is equal to 3, the for-cycle is interrupted.

```
for_length=100;
check=0;
for j=1:20

% R0 calculation
    clear multi1 multi2 multi3
    R0_sl=R0_start; R1_sl=R1(end); C_sl=C(end);
    sim ThesisModel.slx;
    R0(j+1)=round((err.signals.values(target0)/...
    ...abs(I_batt(target0))+R0_start),5);

    if R0(j+1)==R0(j)
        check=check+1;
    else
        check=0;
    end
    if check>=3
        break
    end

% R1 calculation
    clear multi1 multi2 multi3
    R0_sl=R0(end); R1_sl=R1_start; C_sl=C(end);
    sim ThesisModel.slx;
    R1(j+1)=round((err.signals.values(target1)/...
    ...abs(I_batt(target1))+R1_start),5);

    if R1(j+1)==R1(j)
        check=check+1;
    else
        check=0;
    end
    if check>=3
        break
    end

% C calculation
    clear multi1 multi2 multi3
    R0_sl=R0(end); R1_sl=R1(end); C_sl=C_start;
    sim ThesisModel.slx;

    multi1(1)=1;
```

```
int(1)=0;
area(1)=sum(Error.signals.values(target_start:...
...target_end))+1;
prop=0.01;
for i=2:for_length
    area(i)=sum(Error.signals.values(target_start:...
    ...target_end));
    if area(i)<area(i-1)
        int(i)=(int(i-1)+1)*1.5;
    else
        break
    end
    int_coeff=(prop/10)*int(i);
    multi1(i)=multi1(i-1)+prop+int_coeff
    C_sl=C_start*multi1(i);
    sim ThesisModel.slx;
end

multi1_delta=multi1(end)-multi1(end-1);
multi2(1)=multi1(end-1);
prop=multi1_delta/(for_length/5);
C_sl=C_start*multi1(end-1);
sim ThesisModel.slx;
for i=2:((for_length/5)+2)
    area(i)=sum(Error.signals.values(target_start:...
    ...target_end));
    if area(i)>area(i-1)
        break
    end
    multi2(i)=multi2(i-1)+prop
    C_sl=C_start*multi2(i);
    sim ThesisModel.slx;
end

multi2_delta=multi2(end)-multi2(end-1);
multi3(1)=multi2(end-1);
prop=multi2_delta/(for_length/5);
C_sl=C_start*multi2(end-1);
sim ThesisModel.slx;
for i=2:((for_length/5)+2)
    area(i)=sum(Error.signals.values(target_start:...
    ...target_end));
    if area(i)>area(i-1)
        break
    end
    multi3(i)=multi3(i-1)+prop
    C_sl=C_start*multi3(i);
    sim ThesisModel.slx;
end

multi3(end-1)
C(j+1)=round(C_start*multi3(end-1),1);
```

```
    if C(j+1)==C(j)
        check=check+1;
    else
        check=0;
    end
    if check>=3
        break
    end
end
```

When the for-cycle is interrupted, the final set of R_0, R_1 and C is showed in the command window.

```
text0=['R0 = ',num2str(R0(end))];
text1=['R1 = ',num2str(R1(end))];
textC=[' C = ',num2str(C(end))];
disp(text0); disp(text1); disp(textC);
```

Appendix B

The so-called Coup the Fouet is a phenomenon due to slow electrolyte diffusion. When the battery delivers a discharge current from open circuit condition, the local electrolyte concentration in proximity of electrodes decrease more sharply than the in the rest of the volume of the electrolyte. This generates a voltage decrease larger than expected and when electrolyte diffusion rate goes back to usual values, the voltage increases instead of decreasing. When the effect has terminated the voltage start again to decrease. In figure B.1 typical curves showing this phenomenon for different discharge intensities. The same effect, reflected, can occur during charge too.

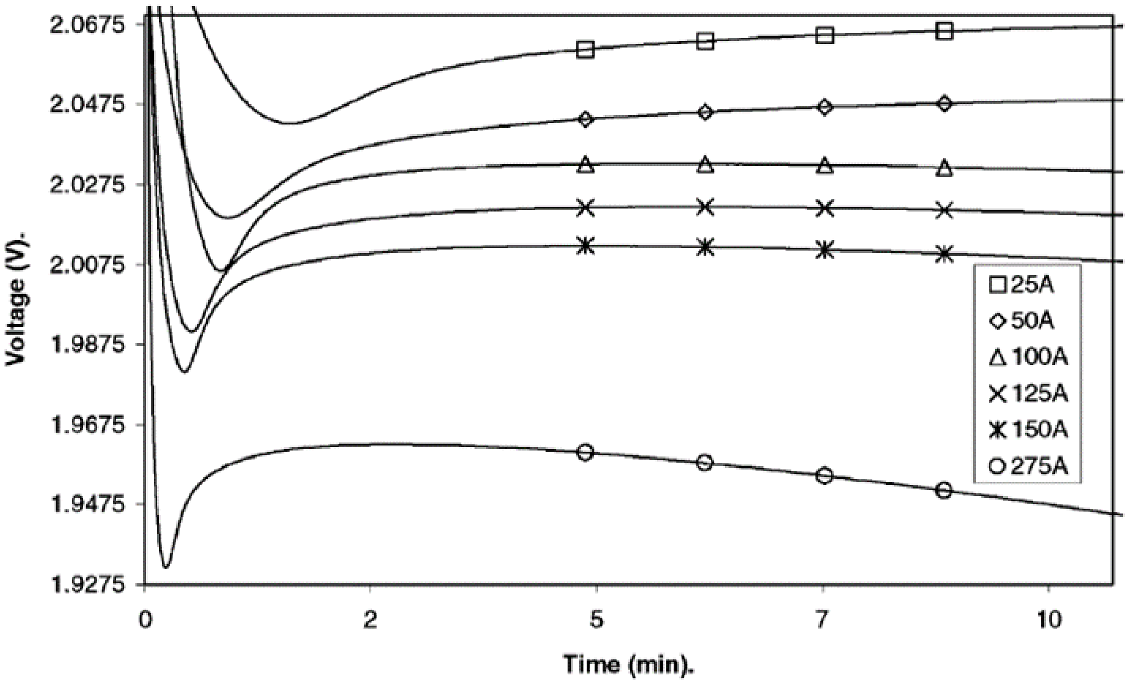

Figure B.1. Typical Coup de Fouet voltage profile [8]

References

[1] M. Ceraolo, "New dynamical models of lead-acid batteries" in *IEEE Transactions on Power Systems*, vol. 15, no. 4, pp. 1184-1190, November 2000.

[2] S. Barsali and M. Ceraolo, "Dynamical models of lead-acid batteries: implementation issues" in *IEEE Transactions on Energy Conversion*, vol. 17, no. 1, pp. 16-23, March 2002.

[3] Thomas Reddy (2010). *Linden's Handbook Of Batteries, 4th Edition.* New York: McGraw-Hill.

[4] Robert Bosch GmbH (2014). *Bosch Automotive Electrics and Automotive Electronics, 5th Edition.* Wiesbaden: Springer Vieweg.

[5] P. S. Crovetti, “Lecture Notes” from course of *Electric and electronic systems in vehicles*, Politecnico di Torino, Torino, 2017.

[6] S. Piller, M. Perrin and A. Jossen, "Methods for state-of-charge determination and their applications" in *Journal of Power Sources*, vol. 96, Issue 1, pp. 113-120, 1 June 2001.

[7] K. Ng, C. Moo, Yi-Ping Chen and Y. Hsieh, "State-of-charge estimation for lead-acid batteries based on dynamic open-circuit voltage" in *2008 IEEE 2nd International Power and Energy Conference*, Johor Bahru, 2008, pp. 972-976.

[8] P. E. Pascoe and A. H. Anbuky, "The behaviour of the coup de fouet of valve-regulated lead–acid batteries" in *Journal of Power Sources*, vol. 111, Issue 2, pp. 304-319, 23 September 2002.

[9] A. Delaille, M. Perrin, F. Huet and L. Hernout, "Study of the “coup de fouet” of lead-acid cells as a function of their state-of-charge and state-of-health" in *Journal of Power Sources*, vol. 158, Issue 2, pp. 1019-1028, 25 August 2006.

[10] S. Lee, J. Cherry, M. Safoutin and J. McDonald, "Modeling and Validation of 12V Lead-Acid Battery for Stop-Start Technology” in *SAE Technical Paper 2017-01-1211,* 2017.